The *Chandra* Survey of the SMC "Bar": II. Optical counterparts of X-ray sources

V. Antoniou[1,2], A. Zezas[1], D. Hatzidimitriou[2], J. C. McDowell[1]

ABSTRACT

We present the most likely optical counterparts of 113 X-ray sources detected in our *Chandra* survey of the central region of the Small Magellanic Cloud (SMC) based on the OGLE-II and MCPS catalogs. We estimate that the foreground contamination and chance coincidence probability are minimal for the bright optical counterparts (corresponding to OB type stars; 35 in total). We propose here for the first time 13 High-Mass X-ray Binaries (HMXBs), of which 4 are Be X-ray binaries (Be-XRBs), and we confirm the previous classification of 18 Be-XRBs. We estimate that the new candidate Be-XRBs have an age of $\sim 15-85$ Myr, consistent with the age of Be stars. We also examine the "overabundance" of Be-XRBs in the SMC fields covered by *Chandra*, in comparison with the Galaxy. In luminosities down to $\sim 10^{34}$ erg s^{-1}, we find that SMC Be-XRBs are ~ 1.5 times more common when compared to the Milky Way even after taking into account the difference in the formation rates of OB stars. This residual excess can be attributed to the lower metallicity of the SMC. Finally, we find that the mixing of Be-XRBs with other than their natal stellar population is not an issue in our comparisons of Be-XRBs and stellar populations in the SMC. Instead, we find indication for variation of the SMC XRB populations on kiloparsec scales, related to local variations of the formation rate of OB stars and slight variation of their age, which results in different relative numbers of Be stars and therefore XRBs.

Subject headings: Magellanic Clouds—stars: early-type—stars: emission-line, Be—stars: formation—pulsars: general—X-rays: binaries

[1]Harvard-Smithsonian Center for Astrophysics, 60 Garden Street, Cambridge, MA 02138; vantoniou@head.cfa.harvard.edu

[2]Physics Department, University of Crete, P.O. Box 2208, GR-710 03, Heraklion, Crete, Greece

1. Introduction

X-ray binaries (XRBs) are stellar systems consisting of a compact object (neutron star, black hole, white dwarf) accreting material from a close companion star. They are the end points of stellar evolution, and thus by studying them we can set constraints on stellar evolution and compact object formation models. They constitute a numerous class of X-ray bright objects, with typical luminosities of $\sim 10^{36} - 10^{38}$ erg s^{-1} when in outburst. They are divided into two classes depending on the mass of the donor star, with M $\leq$ 1 M$_{\odot}$ for the Low-Mass XRBs (LMXBs), and M $\geq$ 10 M$_{\odot}$ for the High-Mass XRBs (HMXBs).

The companion star in HMXBs is of O or B spectral type, with optical bolometric luminosity usually exceeding that of the accretion disk (e.g. van Paradijs & McClintock 1995). HMXBs can further be divided into two groups, the supergiant X-ray binaries (hereafter SG-XRBs), and the Be/X-ray binaries (hereafter Be-XRBs). In the SG-XRBs the primary is a supergiant of spectral type earlier than B2, or an Of star, and it has evolved away from the main sequence (MS), while in the Be-XRBs, the primary is an Oe or Be star lying close to the MS. The optical spectra of Be-XRBs are characterized by emission lines (mostly of the Balmer series of hydrogen; for a review of HMXBs and their properties see for example van Paradijs & McClintock 1995).

Different mechanisms are believed to be responsible for the mass transfer in these two groups of HMXBs. The most luminous SG-XRBs usually have an accretion disk fueled via Roche-lobe overflow, while the less luminous systems may be fed by a supersonic stellar wind. In the Be-XRBs, Be stars are characterized by a low velocity, high density equatorial wind, resulting in periodic accretion episodes during the passage of the compact object through the decretion disk of the donor.

Be-XRBs show pulsations and have hard 1-10 keV spectra (i.e. with a power-law energy index of $\Gamma \sim 0 - 1$; e.g. White, Nagase & Parmar 1995, Yokogawa et al. 2003), which are signatures of accretion onto strongly magnetized neutron stars. In contrast, SG-XRBs have generally softer spectra, and do not always have a pulsar as the compact object.

Be-XRBs are the most numerous sub-class of HMXBs. In the Milky Way as well as in the Large Magellanic Cloud (LMC), they constitute 60-70% of all HMXBs (Sasaki, Pietsch & Haberl 2003), while in the Small Magellanic Cloud (SMC) only one out of 92 known or probable HMXBs (Liu, van Paradijs & van den Heuvel 2005) is a supergiant system.

The SMC is an excellent laboratory to study the Be-XRB populations. It is the second nearest star-forming galaxy, and it has a large number of Be-XRBs seen through moderate Galactic foreground absorption ($N_H \simeq 6 \times 10^{20} cm^{-2}$; Dickey & Lockman 1990), and well mapped extinction (Zaritsky et al. 2002). In addition, its well measured distance (60 kpc;

e.g. van den Bergh 2000, Hilditch, Howarth & Harries 2005), small line-of-sight depth of the young populations at its main body (<10 kpc; e.g. Crowl et al. 2001; Harries, Hilditch & Howarth 2003), well studied recent star-formation (SF) history (Harris & Zaritsky 2004), and generally uniform metallicity of the young populations facilitate the interpretation of the results. Therefore, one can study in great detail and in an homogeneous way the faint end of the XRB populations.

Several studies of the optical characteristics of the XRB systems in the SMC, have been published in the last few years. Haberl & Sasaki (2000), based on the ROSAT surveys of the SMC, identified 25 X-ray sources as new Be-XRBs. Haberl & Pietsch (2004) extended this work presenting 65 SMC HMXBs, of which 45 are associated with an emission-line object indicating that they are Be-XRBs. In the latest census of HMXBs by Liu et al. (2005) 62 Be-XRBs are listed (for 92 confirmed or proposed HMXBs). In addition out of the 38 currently known X-ray pulsars in the SMC, 34 have identified optical counterparts (Coe et al. 2005a).

In this paper we study in a systematic way the young SMC XRB populations. The SMC ROSAT survey reached a non-uniform detection limit of $\sim 5 \times 10^{34} - 10^{35}$ erg s^{-1} (e.g. Kahabka & Pietsch 1996, Haberl et al. 2000, Sasaki et al. 2000). Here we are using data down to $\sim 4 \times 10^{33}$ erg s^{-1} from the *Chandra* survey of the SMC (Zezas et al. 2003) that allow to investigate the faintest of the HMXB populations.

1.1. The *Chandra* survey of the SMC

The SMC as a prime target to study the faint end of the XRB populations (with typical $L_x < 10^{34}$ erg s^{-1}), overcoming in this way the inherent problems of observations in the Milky Way (e.g. distance determination, and obscuration). For this reason we initiated a *Chandra* survey, consisting of five observations of the central part of the SMC performed between May and October 2002 with the *Chandra* ACIS-I detector (Advanced CCD Imaging Spectrometer; Garmire et al. 2003). The survey covers an area of $1280\,arcmin^2$ along the central, most actively star forming, region of the SMC (also referred to as the SMC "Bar", although it bears no relation to a dynamical bar; van den Bergh, 2000). In Figure 1 we plot the footprints of the *Chandra* and OGLE-II fields (for the latter see §2) overlaid on a Digitized Sky Survey (DSS) optical image of the main body of the SMC.

The survey yielded a total of 158 sources, detected on the ACIS-I CCDs, down to a limiting luminosity of $\sim 4 \times 10^{33}$ erg s^{-1}, which is within the luminosity range of quiescent HMXBs (typical $L_x \sim 10^{32} - 10^{34}$ erg s^{-1}; van Paradijs & McClintock 1995). Each of the 5

fields contained between 8 and 16 sources with fluxes at least of 3σ significance (assuming Gehrels statistics; Gehrels 1986) above their local background. A brief description of the survey and the first results are presented in Zezas et al. (2003). The final source-list (including the X-ray luminosity functions) and the spectral properties of the sources are presented in Zezas et al. (2008, in prep.). Because of the large off-axis angle (and therefore large positional uncertainty) of sources on the ACIS-S3 and ACIS-S4 CCDs we do not include them in the present work.

The absolute astrometric accuracy of on-axis sources is dominated by the boresight error of *Chandra* ($< 0.6''$ at the 90% confidence level[1]). However, at larger off-axis angles the Point Spread Function (PSF) becomes broader and asymmetric, resulting in larger positional uncertainties (see *Chandra* POG, 2005). To estimate the positional errors of the off-axis sources, we used the empirical formula of Kim et al. (2004), which gives positional uncertainties for sources with 20 and 100 counts as a function of their off-axis angle (up to a maximum of $10'$). For sources with net number of counts within the range we linearly interpolated between these two estimates, while for sources with less than 20 or more than 100 counts we used the appropriate branch of the equation.

Five sources out of the 158, which were at large off-axis angles ($\mathrm{D_{off-axis}} > 10'$), yielded high positional errors and were discarded from further consideration in this paper. The *Chandra* field IDs, and the coordinates of their centers are listed in Table 1 (Columns (1)-(3)). In Column (4) we present the number of all detected X-ray sources in each *Chandra* field, while in parenthesis we give the number of sources with fluxes at 3σ or greater level above their local background. In Column (5) we give the number of *Chandra* sources for which we searched for counterparts (i.e. detected in $\mathrm{D_{off-axis}} < 10'$).

The identification and classification of the optical counterpart of an X-ray source allow us to identify the interlopers, while it is the only way to confirm the different types of XRBs (e.g. Be-XRBs, SG-XRBs, LMXBs). Although the classification of the counterparts is only secure via optical spectroscopic observations, color-magnitude and/or color-color diagrams (hereafter CMDs and 2-CDs, respectively) can be used to obtain rough classifications for the optical counterparts, and at least identify HMXBs. From the appropriate isochrones and the stellar tracks we can also obtain a feel for the mass and the age of the donor star, if it dominates the optical emission of the X-ray sources.

In this paper we have used the *Chandra* survey of the SMC (Zezas et al. 2003), and searched for optical counterparts of the X-ray sources included in this survey. In particular, we confirm or suggest new counterparts of the above X-ray sources, based on their optical

[1]http://cxc.harvard.edu/cal/docs/cal_present_status.html#abs_spat_pos

properties, and when possible we give a tentative classification. In Section 2 we present the optical catalogs used in this study, and in Section 3 the counterparts of the X-ray sources. We also present their finding charts (Section 4), and we examine the photometry of the optical data (Section 5). In Section 6 we describe the data used in the construction of the V, $B-V$ CMD for the classification of the sources, and we estimate the expected contamination by foreground stars, while in Section 7 we estimate the chance coincidence probability. In the discussion (Section 8) we present the criteria used to classify the X-ray sources, and distinguish among multiple matches the most likely counterpart. We also discuss the properties of the optical counterparts, and the relative numbers of Be-XRBs in the SMC, LMC and Milky Way. In the Appendix we present notes on individual sources.

2. Optical data

The SMC has been surveyed extensively in the optical and in the near infrared. In the past decade, several photometric catalogs have become available, with varying photometric and astrometric accuracy, limiting magnitudes, completeness and spatial coverage. The most extensive of these are the US Naval Observatory USNO-B1.0 (Monet et al. 2003), the USNO CCD Astrograph Catalog (UCAC2, 2nd release; Zacharias et al. 2004), the Massive Compact Halo Objects database (MACHO, Alcock et al. 1997), the Optical Gravitational Lensing Experiment survey (OGLE-II; Udalski et al. 1998a)[2], the $UBVR$ CCD Survey by Massey (2002), and the Magellanic Clouds Photometric Survey (MCPS; Zaritsky et al. 2002). We also mention, for completeness, the Two Micron All Sky Survey (2MASS; Skrutskie et al. 2006), which is sensitive to red stars, and thus it is not used in the present work (see §8.2).

Taking into consideration the photometric and astrometric accuracy of each of these surveys, and their spatial coverage of the *Chandra* fields, we selected the OGLE-II and MCPS surveys, as the main optical catalogs for the present work. We also looked for additional possible counterparts of the X-ray sources within the SIMBAD Astronomical Database[3], and for previously identified optical counterparts of known X-ray sources within the NASA's Astrophysics Data System[4](ADS) (for more details see §3.2).

[2]http://ogle.astrouw.edu.pl/ogle2/smc_maps.html

[3]http://simbad.u-strasbg.fr/Simbad/

[4]http://www.adsabs.harvard.edu

2.1. OGLE-II catalog

The second release of the OGLE survey (hereafter OGLE-II) is a *BVI* survey of the SMC, carried out with the 1.3m Warsaw telescope at Las Campanas Observatory (Udalski et al. 1998a). The survey provides photometric (in B, V and I band) and astrometric data for about 2.2 million stars in the dense central regions of the SMC "Bar", down to $B \sim 20.0$ mag, $V \sim 20.5$ mag, and $I \sim 20.0$ mag, with typical completeness $\sim 75\%$, 80% and 85%, respectively, down to these limits. In the densest fields (e.g. corresponding to *Chandra* field 6), the completeness is reduced almost by half. The vast majority of observations was performed in the I band (because of the microlensing observing strategy of this survey). However meticulous photometry was also performed in both B and V bands (Udalski et al., 1998a). For these reasons, and because of its small astrometric error ($\sim 0.7''$), matching well the positional uncertainty of the *Chandra* detections (see §1.1), the small pixel size ($0.417''$), and the good average seeing (as good as $0.8''$ with typical median value of $1.25''$) during the survey, we opted to use the OGLE-II catalog in order to identify optical counterparts for the X-ray sources detected in our *Chandra* fields. However, due to incomplete coverage of our *Chandra* fields by the OGLE-II survey ($\sim 72\%$ of the area of our *Chandra* survey), we were able to search for optical counterparts for only 102 ($\sim 66.7\%$) of our sources. Four of our fields are partially covered by OGLE-II, and only field 4 is fully covered. However, due to the distribution of the X-ray sources in our *Chandra* fields, we were able to search for counterparts for all our sources also in field 6. For the remaining fields, we searched for counterparts in the OGLE-II catalog for $\sim 22\%$, $\sim 28\%$ and $\sim 86\%$ of the detected sources in *Chandra* fields 3, 5 and 7, respectively.

2.2. MCPS catalog

Because of the incomplete coverage of the *Chandra* fields by the OGLE-II survey, we supplemented the optical data with the MCPS catalog (Zaritsky et al. 2002). The MCPS survey is based on drift-scan images of the SMC in the Johnson U, B and V and Gunn I filters obtained with the Las Campanas Swope telescope (1m). The MCPS catalog contains stellar photometry for more than 5 million stars in the central 18 deg^2 area of the SMC, which fully covers our *Chandra* survey. Only for one of our X-ray sources we were not able to look for counterparts in the MCPS catalog, because it falls in the gap between the different subscans of this survey. The final MCPS catalog includes only stars with both B and V detections, while there are not always measurements in the U band. The incompleteness is significant below $V \sim 20$ mag, while the typical seeing for this survey is $\sim 1.5''$, and the pixel size $0.7''$.

In general the two catalogs have consistent photometry: Evans et al. (2004) reported a difference of $\delta B_{(\mathrm{MCPS-OGLEII})} = +0.02$ mag for stars in their 2dF spectroscopic sample. Zaritsky et al. (2002), in their comparison between MCPS and OGLE-II magnitudes, found mean photometric offsets of $\delta B = 0.011$, $\delta V = 0.038$, and $\delta I = 0.002$ mag. However, in crowded fields, actual photometric (as well astrometric) uncertainties can be larger, due to source confusion (see also Zaritsky et al. 2002), which we consider to be more severe in the MCPS catalog, due to the larger pixel size, and worse overall seeing. In addition, observations were not repeated in the MCPS survey, which makes it more likely to contain a higher percentage of stars with less reliable photometry, especially in the faint end, and crowded regions.

3. Cross-correlation analysis

3.1. OGLE-II and MCPS

In order to identify the optical counterparts of the *Chandra* sources we have first cross-correlated their coordinates with the OGLE-II, and the MCPS catalogs. The search radius for each X-ray source was calculated from the combination, in quadrature, of the astrometric uncertainty of the corresponding optical catalog, and the positional uncertainty for each X-ray source (including the absolute astrometric uncertainty of *Chandra*). When the resulting search radius was less than $1.5''$ we enforced a conservative minimum of $1.5''$ ($\sim 48\%$ of our sources). The maximum resulting radius was $5.29''$ with the average search radius being $1.99''$.

The optical counterparts of the X-ray sources are presented in Tables 2-6 (one for each *Chandra* field). In Columns (1) and (2) we give the *Chandra* source ID and the search radius (in arcseconds), respectively. The X-ray sources (Column (1)) are named as F_NN, where F is the *Chandra* field number, and NN is the source ID in this field (from Zezas et al. 2008, in prep.). In Column (3) we give the proposed counterparts, following a similar notation: OGLE-II sources are named as O_F_NNNNNN, where F and NNNNNN are the field and optical source number, respectively (from Udalski et al. 1998a), while MCPS sources are named as Z_NNNNNN where NNNNNN is the line number of the source in Table 1 of Zaritsky et al. (2002). In Columns (4) and (5) we present the right ascension and declination (J2000.0) of the counterparts from their respective catalogs. The distance (in arcseconds) of the counterpart to the *Chandra* source is given in Column (6). The photometric data of the sources are presented in Columns (7) to (12) (these data are taken directly from the original catalogs without applying any reddening or zero-point correction): apparent magnitude in the V band (Column (7)), the B - V and U - B colors (Columns (9) and (11)), and their

errors (Columns (8), (10) and (12), respectively). Non detections in a band are indicated by 99.99, while three dots indicate that an entry was not available at the original catalog. In Column (13) we give notes on individual sources: "n" indicates a new candidate counterpart for the X-ray source, "c" denotes that there are additional comments for this source in Table 8, while "u" indicates sources for which we were not able to uniquely identify an optical counterpart.

Matched sources between the OGLE-II and MCPS catalogs are grouped together, with different source groups separated by blank lines, while single horizontal lines separate the counterparts of different X-ray sources (see §1.1). When we were not able to uniquely identify a MCPS source with an OGLE-II source, we list all possible matches (because of source confusion, in several cases, two or more OGLE-II sources are detected as a single brighter source in MCPS). In cases of unclear matches between the two catalogs, we show the MCPS sources in parenthesis. The matched pairs are based on positional coincidence, visual inspection of the OGLE-II I band images, and comparison of the magnitudes and colors of the sources. MCPS sources that may be associated with OGLE-II sources but lie just outside the search radius of each X-ray source are marked with an "o" (e.g. Z_2132222 for X-ray source 4_36).

We indicate in bold face the most likely counterpart. In all but one case (*Chandra* source 3_19, which is discussed in §8.3), this is the brightest OGLE-II match, or, when there is no OGLE-II match the brightest MCPS source. For sources with more than one stars with the same or very similar magnitudes we indicate all of them in bold face. There are 3 such cases (*Chandra* sources 4_6, 7_16, and 7_17), for which even if we apply additional criteria (see §8.2) we cannot identify the true counterpart, and classify the sources.

From the total of 102 X-ray sources covered by the OGLE-II fields, we found that 34% have a unique candidate optical counterpart, 23% have two, and 29% have three or more matches. In total, we identified 229 optical matches for 87 X-ray sources.

Since the MCPS survey covers the entire area of the *Chandra* survey, we were able to search for counterparts for all X-ray sources apart from source 7_12, which falls on the gap between two scans of the MCPS survey (we identified a unique counterpart for this source from the OGLE-II survey). We found that 45% of the 152 X-ray sources have a unique candidate optical counterpart, 13% have two and 6% have three or more, resulting in a total of 138 matches. Fifty five X-ray sources do not have any match in the MCPS catalog; from them, 22 have match(es) in the deeper OGLE-II catalog.

In Table 7 we summarize the above results. In Column (1) we give the field ID, while in Column (2) we indicate the complete or partial coverage of these fields by the OGLE-II

survey. In Column (3) we specify the optical catalog used for the cross correlation (O for OGLE-II, Z for MCPS and "combined" for the results of the matched lists of OGLE-II and MCPS sources presented in Tables 2-6). In Columns (4), (5), (6) and (7) we give the number of sources with no counterparts, and with 1, 2 or more matches, respectively. Only in four cases (sources 4_23, 4_36, 5_34 and 7_5) we found two separate OGLE-II and MCPS matches within the search radius (derived as described in §3.1). The coordinates and photometry of these stars indicate that they are distinct objects, and thus we consider them as two individual sources. Because, in many cases, the MCPS sources are resolved into two or more OGLE-II stars, and because of the cases of non-matched associations just mentioned, the number of counterparts in the "combined" entry is always smaller than the numbers corresponding to individual catalogs.

In total, out of the 153 *Chandra* sources, 34% have unique candidate optical counterparts, 22% have two, and 23% have three or more optical matches. There are also 33 X-ray sources with no matches.

3.2. Other bibliographic sources

For all detected sources we performed an extensive (but by no means complete) literature search for previously published identification and classifications. In Table 8 we present (when available) information on the X-ray sources and/or the optical sources detected within 1.5″, based on a search of the ADS and SIMBAD Astronomical Databases (see also §2). In particular, in Column (1) we give the X-ray source ID (same as in Tables 2-6). In columns (2) and (4) we give any reported classification for the X-ray source[5] and previously identified optical counterparts (the relevant references are given in Columns (3) and (5)). In the last 2 columns we present any other sources encompassed by the minimum search radius of 1.5″ around each X-ray source. In Column (6) we present the source ID, and in Column (7) its reference.

We note that we have made no attempt to match the sources given in Columns (2), (4), and (6) since they are produced from several different surveys, with different areal coverage and positional accuracy. However, for completeness we present them all.

Summarizing the above results, within the search radius, we find 2 AGN (Dobrzycki et al. 2003a, 2003b; [DMS03] and [DSM03], respectively), 1 foreground star (Sasaki et al. 2000;

[5]Comparison with previously published X-ray catalogs is based on positional coincidence and the spectral and timing properties of the sources (Zezas et al. 2008, in prep.)

[SHP00]), 16 confirmed pulsars (e.g. Edge et al. 2004, [EHI04]; Haberl et al. 2004, [HPS04]), 1 eclipsing binary (Wyrzykowski et al. 2004; [WUK04]), 1 planetary nebula (Murphy & Bessell 2000; [MB00]), 4 variable stars from the OGLE-II survey (one of which is also a candidate HMXB; Ita et al. 2004, Zebrun et al. 2001), 5 stars with spectral classification (using the 2dF spectrograph on AAT; 3 by Evans et al. 2004, and 2 by Antoniou et al. 2008), 1 B[e] star (Massey & Duffy 2001; reported here for the first time as single counterpart of an XRB), 11 optical matches within OB stellar associations (Oey et al. 2004), and 10 candidate Be stars (Mennickent et al. 2002; see §8.3 for more details).

4. Finding charts

For the *Chandra* sources which are covered by the OGLE-II survey, we created optical finding charts, presented in the on-line Figures 2 - 6. These charts are created from the I band OGLE-II fields (Udalski et al. 1998a), they are $\sim 15'' \times 13''$ in size and they are centered on the position of the X-ray source, which is indicated by a cross-hair (each bar of the cross-hair is $0.8''$ long). The positional uncertainty of the finding charts is $\sim 0.7''$, based on the astrometry of the OGLE-II images. The search radius used in the cross-correlation is shown by a circle centered on the X-ray source, and is also given (in arcseconds) at the bottom right corner of each chart. All optical sources from the OGLE-II survey are indicated with an X symbol, while those from the MCPS survey are indicated with a cross. In addition, we present with a diamond the eclipsing binary star identified for *Chandra* source 4_1 (source No.550 in Udalski et al. 1998b). For the X-ray sources which fall on two neighboring OGLE-II fields we only show the finding chart with the largest coverage. We note here that we present finding charts only for those sources with OGLE-II coverage, as the MCPS images are not publicly available.

5. Photometric data

The photometric parameters of the optical matches of the X-ray sources in the OGLE-II and MCPS catalogs are from the second OGLE release (Udalski et al. 1998a), and the catalog of Zaritsky et al. (2002), respectively. These parameters are presented in Columns (7) to (12) of Tables 2-6 (see §3).

Although there are no known significant photometric offsets between the OGLE-II and MCPS catalogs (see §2.2), we look for photometric discrepancies specific to the objects found in our cross correlation by comparing the V and B band magnitudes, and

B-V colors of the 18 stars identified as unique counterparts in both OGLE-II and MCPS. We find $\delta V_{(\mathrm{OGLEII-MCPS})} = 0.00 \pm 0.30$ mag, $\delta B_{(\mathrm{OGLEII-MCPS})} = -0.06 \pm 0.30$ mag and $\delta BV_{(\mathrm{OGLEII-MCPS})} = -0.06 \pm 0.27$ mag (error is the standard deviation). The zero-point differences are comparable to the corresponding errors quoted in the two catalogs. The relatively large scatter (0.30) is mainly caused by the large photometric errors of faint sources, close to the detection limit (particularly of the MCPS catalog), and partly by actual source variability.

6. Color-Magnitude Diagram

CMDs and 2-CDs are a standard tool for the characterization of stars (e.g. Johnson 1966). In this study, we use the V, $B-V$ CMD in order to classify the X-ray sources. An important parameter in CMD studies is the extinction correction. Several different values have been proposed for the SMC reddening. For this work, we use reddening values based on the red clump stars (Udalski et al. 1999) in regions as close as possible to the *Chandra* fields. The mean color excess is $E(B-V) = 0.09 \pm 0.02$ mag. Similar results ($E(B-V) \sim 0.09 \pm 0.07$) have been obtained by the spectroscopic study of Massey et al. (1995). Larsen et al. (2000) derived somewhat higher values of ($E(B-V) \sim 0.21 \pm 0.10$ intrinsic to the SMC and $\sim 0.07 \pm 0.02$ due to the foreground dust), although generally compatible with the previously mentioned values, within the combined errors. In conclusion, we adopt the value of $E(B-V) = 0.09$ for the entire area covered by the *Chandra* fields.

To derive the reddening correction for V, A_V ($= R_V E(B-V)$), we use the standard Galactic value of $R_V = 3.24$ (Schlegel et al. 1998), which was also used in previous published photometric catalogs of the SMC. A lower value of $R_V = 2.74 \pm 0.13$, which has been recently proposed for the SMC (Gordon et al. 2003), would result in a negligible difference of 0.04 mag in A_V. The adopted $R_V = 3.24$, gives a mean reddening value for the 5 OGLE-II fields of $A_V = 0.29$ mag. Based on the extinction curve of Cardelli et al. (1989), we estimate A_B and A_U of 0.39 mag and 0.46 mag, respectively. We correct the original data presented in Tables 2-6 for the extinction to the SMC ($E(B-V) = 0.09$ and A_V=0.29) and we use these corrected numbers for all the plots described below.

Throughout this study we adopt a distance modulus of $(m-M)_V = 18.89 \pm 0.11$ mag (derived from eclipsing O, B-type binaries in the SMC; Harries et al. 2003). The small depth of the young populations (<10 kpc; e.g. Crowl et al. 2001, Harries et al. 2003) results in a difference in the above distance modulus of < 0.2 mag, while the corresponding difference in the X-ray luminosity is $\sim 5.9 \times 10^{34}$ erg s^{-1}.

In Figure 7 we present the extinction corrected M_{V_o} vs. $(B-V)_o$ CMD diagram (absolute V magnitude vs. $B-V$ color) for all single and the brightest of multiple matches of our sources (which are indicated in bold face in Tables 2-6). Whenever both OGLE-II and MCPS photometric data exist we use the OGLE-II data. The identifier of each point is the X-ray source number (see §3.1), while we plot in the same color sources from the same *Chandra* field. On the same diagram we overlay with small dots the stars from the OGLE-II catalog in the area common with the *Chandra* field 4 (after having corrected the magnitudes and colors for reddening and distance as described above).

In order to identify on the CMD the locus of stars of different spectral types, we use data from the 2dF spectroscopic survey of SMC stars (the most extended such catalog available; Evans et al. 2004). This survey provides spectroscopic classification for 4161 stars in the SMC[6], covering spectral types from O to FG, and sampling the MS to ∼mid-B. However, the Be stars are generally redder than B-type stars (e.g. McSwain & Gies 2005). Mennickent et al. (2002), studying the light curves of the OGLE-II data for the SMC, identified ∼ 1000 candidate Be stars. We have identified 10 of our proposed counterparts with their type-4 stars (objects with light curves similar to Galactic Be stars) from this catalog (shown in Figure 7 as black squares). For the classification of the *Chandra* sources we used the combined locus (blue curve) of early-type stars (O and B, including the Be stars) identified in the 2dF spectroscopic survey of Evans et al. (2004) and the candidate Be stars of Mennickent et al. (2002). This choice is in agreement with the $B-V$ color range of O and B spectral-type stars from Massey (2002), and is confirmed by follow-up spectroscopy of selected targets from our survey (Antoniou et al. 2008). Even a difference of ∼0.2 mag in the distance modulus (due to the depth of the young populations discussed above) does not affect the classification of a bright source. On the other hand, faint counterparts do not "contaminate" the locus of OB stars even if we adopted the lower value of the distance modulus (∼ 18.7 mag).

For stars brighter than $M_{V_o} \sim -0.25$ the majority of the candidate optical counterparts (either single or brightest of the multiple) lie within the loci of OB and Be stars. Fainter objects are mainly found in regions of higher spatial density, and they populate the high density regions of the CMD (lower MS and red clump), clearly indicating high incidence of chance coincidences in these dense regions. This issue is discussed in detail in §7.

Isochrones and stellar evolutionary tracks can give further insight on the properties of the companion star. In Figure 7, we overplot the isochrones from the Geneva database (Lejeune & Schaerer 2001) for the metallicity of the young SMC stars ([Fe/H] $= -0.68 \pm 0.13$

[6]In this paper we only utilized photometric catalogs, as we found only 3 matches of our *Chandra* sources with the 2dF catalog; see below Table 8.

dex, equivalent to Z = 0.004[7]; Luck et al. 1998), for ages of 8.7 Myr to 275.4 Myr and initial stellar masses from 12 $M_\odot$ to 3 $M_\odot$, respectively. The age of the OB stars, as they are defined based on their locus in the CMD, is estimated to range from $\sim$ 15.5 to $\sim$ 85 Myr.

Given the large area covered by the *Chandra* survey, we expect a significant contamination by Galactic foreground stars. Based on the tables of Ratnatunga & Bahcall (1985), the fraction of Galactic stars at the locus of early-type stars is very small ($< 3.6\%$), and thus, the foreground contamination can be safely considered negligible. Exception to the above is the region of the CMD between $-6 < M_{V_o} < -4$ and $(B-V)_o > 0.75$, in which the contamination is more significant ($\sim$11%). However, there are no counterparts identified in this range (see Figure 7), except for *Chandra* source 7_9 that has been previously identified as a foreground star (Sasaki et al. 2000). These estimates are consistent with those of Massey (2002), although direct comparison is difficult because of the different detection limits of the two surveys.

7. Chance coincidence probability

To estimate the number of possible chance associations between the X-ray sources and the stars in the OGLE-II and MCPS catalogs, we followed a Monte-Carlo procedure similar to that in Zezas et al. (2002). We simulated 1000 random samples of X-ray sources by applying to the position of each source a random offset in R.A. and Dec.. The offsets were drawn from a uniform distribution, taking care that the new position is outside the search radius of each source but within the boundaries of the OGLE-II fields (the latter constraint does not apply to the MCPS catalog since in that case the overlap is complete). However the maximum offset was restricted so a source does not fall in a region of different stellar density. Each of these samples was cross-correlated with the optical catalogs in the same way as the observed data.

We calculated the chance coincidence probability for detecting *(a)* unique, and *(b)* any number of multiple optical matches (one or more) for various search radii. We note that our minimum search radius is 1.5″ (see §3.1), while only 20% of the *Chandra* sources have search radii larger than 2.5″. In addition, we estimated the expected chance coincidence probability for matches with optical sources of different spectral types (O, B, and later, following Binney & Merrifield 1998) depending on their position on the CMD:

[7]For the conversion, we use the relation [Fe/H] $\equiv \log(Z/Z_\odot)$, with $Z_\odot$=0.02 for the solar metallicity of [Fe/H] = 0; Russell & Dopita (1992).

(i) MS and post-MS O-type stars ($(B-V)_{\rm o} \leq -0.31$ and $(B-V)_{\rm o} > -0.31$, respectively, for $M_{V_o} \leq -4.5$)

(ii) MS and post-MS B-type stars ($(B-V)_{\rm o} \leq -0.11$ and $(B-V)_{\rm o} > -0.11$, respectively, for $-4.5 < M_{V_o} \leq -0.25$)

(iii) later type stars ($M_{V_o} > -0.25$, with no restriction in the color range),

where M_{V_o} denotes the absolute V magnitude. The photometric data used here (both in B and V band) are corrected for extinction (see §6).

In Figure 8, we plot the expected chance coincidence probability per X-ray source (i.e. the normalized probability and not the additive) as a function of the search radius for the cases of single, and multiple matches. The errors are estimated from the variance of the combined simulations of the 5 fields, and reflect field to field stellar density variations. These values are the average for all the *Chandra* fields (weighted by the number of sources in each field; a quantile-quantile plot of the distribution of the simulated chance associations shows that they follow approximately a Gaussian distribution). It is clear from Figure 8 that for the same search radius the OGLE-II data result in fewer spurious matches for single associations than the data from the MCPS catalog. This is mainly due to the smaller pixel size and better overall seeing of the OGLE-II catalog resulting in better positions, especially in crowded fields. On the other hand, we find no difference between the two catalogs for the case of one or more (multiple) matches.

The (normalized) chance coincidence probability for OGLE-II and MCPS sources of different spectral types is presented in Tables 9 and 10, respectively. In Column (1) we give the magnitude range (M_{V_o}) of the stars in the optical catalog, and in Column (2) their color range ($(B-V)_o$). In Columns (3) and (4) we present the estimated chance coincidence probability for the single counterparts for $1.5''$ and $2.5''$ search radius, respectively, while in Columns (5) and (6) we present the corresponding results for sources with one or more optical matches.

These results indicate that $\leq 19\%$ of the bright blue ($M_{V_o} \leq -0.25$ and $(B-V)_o \leq -0.11$) counterparts can be considered spurious matches. Therefore for sources with multiple matches, the brightest blue object is the most likely counterpart. On the other hand, the high chance coincidence probability for the fainter optical sources does not allow us to securely identify an optical counterpart.

8. DISCUSSION

In the previous sections we described the results from the cross-correlation of the sources detected in our *Chandra* survey of the SMC with the OGLE-II and MCPS optical catalogs. We find 52 sources with a single counterpart, 68 sources with two or more matches, while for 33 sources we do not find any matches, within an average search radius of 1.99″ (see §3.1). We also find that the chance coincidence probability and foreground contamination are minimal for early-type (O, B) stars. Here, we will use the optical photometric data (discussed in §5 and §6), and the X-ray properties of the *Chandra* sources with early-type optical counterparts (from Zezas et al. 2008, in prep.) in order to set constraints on their nature. We do not attempt to classify X-ray sources with faint optical matches ($M_{V_o} > -0.25$), because of their large photometric errors and high chance coincidence probability.

8.1. Classification criteria

In order to classify the X-ray sources we use a scheme involving the position of the counterparts on the CMD and their spectral and timing X-ray properties:

(i) The broad spectral types of the optical counterparts of the X-ray sources are determined on the basis of their position on the CMD. In this work we focus on OB stars (see §6). It should be noted that the contribution of the accretion disk in the optical band is not expected to be significant for early-type stars, while it becomes dominant for the later spectral types (e.g. van Paradijs & McClintock 1995). On the other hand, it is expected a substantial contribution from the decretion disk of any Be star, which gets redder in B-V than the Be star itself (e.g. Janot-Pacheco, Motch & Mouchet 1987).

(ii) A hard ($\Gamma < 1.6$) X-ray spectrum or hardness ratio is indicative of a pulsar binary (e.g. Yokogawa et al. 2003). Sources with softer spectra could be either background AGN, black-hole binaries or neutron stars with weak magnetic fields. Although a subset of AGN have hard X-ray spectra (Compton thick AGN; e.g. Matt et al. 2000), the identification of a hard X-ray source with an early-type star would strongly suggest that it is a HMXB pulsar.

(iii) The X-ray to optical "color index", $\xi = B_o + 2.5log(F_X)$ (where B_o is the reddening corrected apparent B magnitude, and F_X is the 2.0-10.0 keV X-ray flux in μJy) introduced by van Paradijs & McClintock (1995), is another standard means of classifying X-ray sources, as HMXBs have lower values of ξ than the LMXBs. Since many of our optical counterparts do not have B band photometry, we define ξ in terms of the extinction corrected V band magnitude, and we calibrate it for different types of XRBs based on the HMXBs and LMXBs catalogs of Liu et al. (2005 for the SMC and LMC HMXBs, 2006 for the Galactic HMXBs,

and 2007 for the Galactic and LMC LMXBs). From these catalogs we only used data for sources which have X-ray fluxes in the 2.0-10.0 keV band, V band photometry, and reported $E(B-V)$ reddening correction (used to calculate V_o assuming $R_V = 3.24$). However, for the Magellanic Clouds (MCs) HMXBs we included even sources without reported $E(B-V)$, since we opted to correct all of them for extinction of $A_V = 0.29$ mag and $A_V \sim 0.55$ mag (mean value for the hot SMC and LMC populations, respectively; Zaritsky et al. 2002, 2004). So far, no LMXBs have been detected in the SMC, while for the LMC there is only one source listed in Liu et al. (2007).

The histogram of the ξ parameter values for previously identified HMXBs and LMXBs (using data from the above catalogs), and for HMXBs and AGN using data from this study, is presented in Figure 9 (bottom and top panel, respectively). In particular, in the bottom panel we present the ξ values for 17 SMC Be-XRBs (shown in red), the only SMC SG-XRB (in green), 8 LMC Be-XRBs (in yellow), 1 LMC LMXB (in cyan), 29 Galactic Be-XRBs (in black), and 44 Galactic LMXBs (in blue), using data from the catalogs of Liu et al. (2005, 2006, 2007). In the top panel, we present the ξ values for the brightest counterparts of all *Chandra* sources (indicated in bold face in Tables 2-6 and shown with an open blue histogram). Previously known Be-XRBs and XRB pulsars (hereafter XBPs), which have been detected in our *Chandra* survey, are shown in black. We note that the majority of these sources is included in the SMC Be-XRB sample of Liu et al. (2005), thus in the bottom panel. However, for the ξ parameter shown in the top panel we used their fluxes from the *Chandra* survey of the SMC (Zezas et al. 2008, in prep.; also presented below in Table 11). Two *Chandra* sources previously identified as AGN are also included (shown in green; for *Chandra* source 3_1 we show both counterparts). Finally, newly identified HMXBs from this study are shown in red. The flux limits of the Be-XRBs samples from the work of Liu et al. used here are 1.2×10^{-13} erg cm^{-2} s^{-1} for the SMC, 2.2×10^{-13} erg cm^{-2} s^{-1} for the LMC, and 1.2×10^{-10} erg cm^{-2} s^{-1} for the Milky Way (in the 2.0-10.0 keV energy band)[8]. The identified AGN with $\xi \sim 11$ (top panel), which coincides with the locus of known Be-XRBs and Be-XBPs, is associated to *Chandra* source 5_15 and is discussed in detail in §A.1.

HMXBs and LMXBs are well separated in the ξ parameter space, with only exception the value range between $\sim 16-17$, for which there is overlap among the two types of XRBs and small number of sources, as it is shown in Figure 9. Regarding the Galactic Be-XRBs, we find two populations that could be considered as the "outbursting" and "in

[8]Using a flat power-law (Γ=1), and $N_H = 6.0 \times 10^{21}$cm^{-2} and 6.0×10^{20}cm^{-2} for the SMC and the LMC, respectively. For the Milky Way sample, N_H appropriate for each source has been used (using http://heasarc.gsfc.nasa.gov/cgi-bin/Tools/w3nh/w3nh.pl).

quiescence" sources with ξ parameter values >11 and <11, respectively. Sources with ξ values around 11 most probably represent the low tail of active Be-XRBs, and can be considered as HMXBs being in an intermediate state, e.g. soon after outburst. From Figure 9, it is also confirmed the classification of HMXBs derived in this work. Using this plot as an interpretation tool, the classification of the above sources as candidate new Be-XRBs is suggested, given that they all fall well within the locus of known Be-XRBs. In addition, all but one of the identified HMXBs and candidate Be-XRBs from this work have ξ values <11, thus suggesting a quiescent nature, or at least that there is small probability these detected sources to be in outburst. Thus, although for the classification of an X-ray source, the ξ parameter is not as sensitive as the position of the optical counterparts on the CMD and the X-ray spectral properties, nevertheless, this criterion can be used in order to confirm the classification derived using the first two criteria and as a way to distinguish between outbursting and less active HMXBs.

Given the large area covered by the Chandra survey, we expect a significant number of background AGN. However, we cannot use the F_x/F_{opt} ratio in order to identify them, since its range ($0.1 \leq F_x/F_{opt} \leq 10$; e.g. Silverman et al. 2005) also covers the bona fide Be-XRBs. Therefore, we do not attempt to identify any AGN, but we note that the majority of the unclassified *Chandra* sources (see below Table 11) could be background AGN. In addition, this work is focused on the early-type counterparts of the *Chandra* sources, for which the chance coincidence probability and the photometric errors are small, thus we do not attempt to classify any source as a LMXB. On the other hand, this work is not sensitive on identifying black-hole XRBs (BH-XRBs; with either an early or a later type counterpart). A tell-tale signature of BH-XRBs is the detection of periodic modulations in their X-ray lightcurves, which then requires their detailed optical spectroscopic follow-up in order to identify them as such.

A more detailed presentation of these classification criteria will be presented in a forthcoming paper.

8.2. Sources with multiple optical matches

For 61 X-ray sources in our survey with more than one optical match (out of the 68 in total), we tentatively identify them with the brightest optical source in the region of low chance coincidence within their error circle (§7). Whenever possible, we confirm this identification with the spectral properties of the X-ray source: a hard ($\Gamma < 1.6$) spectrum and/or detection of pulsations are tell-tale signatures of pulsar binaries. For example, we suggest that the counterpart of *Chandra* source 5_7 is the early-type star O_7_70829 from

the OGLE-II catalog, and not one of the three fainter stars within its error circle, which do not lie on the locus of OB stars, in agreement with the same identification by Sasaki et al. (2003), and also supported by its optical variability (Zebrun et al. 2001). We also classify this X-ray source as Be-XRB pulsar (in agreement with Haberl & Sasaki 2000), due to its possibly hard spectrum (for details see below §8.3), and its detected pulsations (Marshall et al. 1998). For the few (4 out of the 68) X-ray sources which do not have optical counterparts in the region of low chance coincidence, we cannot propose a likely counterpart (discussed in §8.3).

8.3. Properties of the optical counterparts and implications for the nature of the X-ray sources

Following the above approach, out of the 120 X-ray sources with optical matches, we were able to identify 35 with early-type counterparts. The locus of O and B spectral-type sources (as defined in §6) consists of objects with $-5.75 \leq M_{V_o} \leq -0.75$ and $-0.45 \leq (B-V)_o \leq 0.2$.

In Table 11 we summarize the optical and X-ray properties of the *Chandra* sources with optical counterparts brighter than $M_{V_o} \leq -0.25$, which have low chance coincidence probability (as discussed in §7). We also present sources with counterparts fainter than $M_{V_o} > -0.25$, only in cases of reliable public classification (*Chandra* sources 3_1, 3_2, and 5_15). In total there are 54 *Chandra* sources for which we present their optical and X-ray properties in Table 11. In Column (1) we give the *Chandra* source ID, in Column (2) the optical counterpart ID, and in Columns (3), (5) and (7) their V magnitude, $B-V$ and $U-B$ colors, respectively (along with their errors in Columns (4), (6), and (8)). In Column (9) is given the offset from the X-ray source (in arcseconds). In Column (10) we indicate if the X-ray source has a hard ($\Gamma < 1.6$) or soft ($\Gamma > 1.6$) spectrum, and whether this is based on spectral fits (S) (Zezas et al. 2008, in prep.) or X-ray colors (HR; calculated using the Bayesian method of Park et al. 2006). The X-ray color derived parameters are based on color-color diagrams involving X-ray colors defined as Col1=log(S/M) and Col2=log(M/H), where S, M and H correspond to the soft (0.5-1.0 keV), medium (1.0-2.5 keV), and hard (2.5-7.0 keV) band, respectively. A "possibly" hard or soft X-ray spectrum is used in order to indicate some uncertainty due to the small number of source counts, thus large errors in the X-ray colors. In Column (11) we indicate if the X-ray source has detected pulsations or not and its reference, while in Column (12) we give its observed flux in the 2.0-10.0 keV energy

band[9]. In Column (13) we give the ξ parameter value, and in Column (14) the identified emission-line object from the catalog of Meyssonnier & Azzopardi (1993; hereafter [MA93]) and its distance from the X-ray source (given in parenthesis). Finally, in Column (15) we present a tentative classification for the X-ray sources derived in this study. New HMXBs are proposed on the basis of early-type counterparts and hard (or possibly hard) X-ray spectrum and/or pulsations (listed as "new HMXBs" in Table 11), while as new candidate HMXBs (listed as "new HMXBs ?") we consider those sources with early-type counterparts but no X-ray spectral information available (due to their small number of source counts). Sources with a soft X-ray spectrum, unavailable X-ray spectral information and/or sources without an early-type optical counterpart cannot be classified without further information (e.g. optical spectroscopy, X-ray timing or spectroscopic analysis). We note that in Column (15) we list as unclassified sources, some few previously classified for which we did not identify an OB counterpart in this work and they do not have hard X-ray spectra or pulsations. However, we mention that we agree with the previous classification in all such cases. In Column (16) we present any previous classification of *Chandra* sources (including those with fainter than $M_{V_o} \sim -0.25$ counterparts). We note here that since all but one known SMC HMXBs are Be-XRBs (there is only one spectroscopically confirmed SG-XRB), a classification of a source as a "new HMXB" may well suggest that this source could be a new candidate Be-XRB. This is also in agreement with the ξ parameter values of the newly identified HMXBs, which coincide with those of previously known Be-XRBs (as discussed in detail in §8.1).

We mention here that in the above table we included *Chandra* sources 4_19 and 5_35 for which there is a bright optical match in the 2σ search radius (also discussed in §A.7, and §A.6, respectively). Source 5_35 does not have any counterpart in the 1σ radius, while source 4_19 has a single faint match in the 1σ radius.

In this paper we present classifications for 34 sources of which 13 are previously unclassified. *Chandra* source 4_3, which has been previously listed as a candidate Be-XRB (Haberl & Pietsch 2004), is further classified at the present work as a new candidate Be-XBP, for which it remains to be confirmed the X-ray pulse period (found by Laycock, Zezas & Hong 2008). Our results are consistent with previous classifications in all cases of overlap (21 sources in total all of which are Be-XRBs). There are 20 additional sources with bright optical counterparts which remain unclassified: 4 with OB spectral type counterparts and soft X-ray spectra (discussed below), and 16 sources with bright optical counterparts ($M_{V_o} \leq -0.25$), but not within the locus of OB stars. Nine out of these 16 sources do not

[9]Using the unabsorbed flux values in the 0.5-7.0 keV band (Zezas et al. 2008, in prep.), and assuming $\Gamma = 1.7$ and $N_H = 5.94 \times 10^{20} cm^{-2}$, $4.69 \times 10^{20} cm^{-2}$, $6.33 \times 10^{20} cm^{-2}$, $6.33 \times 10^{20} cm^{-2}$, $6.19 \times 10^{20} cm^{-2}$ for *Chandra* fields 3, 4, 5, 6, and 7, respectively.

have X-ray spectral information, 6 have soft spectra and 1 has a possibly hard spectrum (*Chandra* source 4_11, discussed below). For 2 sources (out of the 54 in total presented in Table 11), we cannot confirm the previously published classification based on the data we used (1 AGN, and 1 Quasar), thus we list them as unclassified in this work. The 13 sources with new classification (excluding *Chandra* source 4_3) have a mean value of $\xi = 8.90 \pm 1.15$, which is in the range of quiescent HMXBs (as discussed in §8.1). We mention here that for the ξ value of *Chandra* sources 4_8 and 4_13, for which we find 2 optical counterparts within the locus of OB stars, we used the V magnitude of the brightest of the two objects. In addition, these 13 X-ray sources have low luminosities ($L_x \sim 5 \times 10^{33}$-$10^{35}$ erg s^{-1}), and all but 2 (for which we cannot derive spectral information) have hard or possibly hard X-ray spectra, which together with the intermediate value of the ξ parameter are indicative of residual accretion. Therefore, these 13 sources can be considered as HMXBs being in an intermediate state, e.g. soon after outburst.

Four *Chandra* sources (sources 4_10, 5_6, 5_32, and 6_3) have optical matches within the locus of OB stars, but have a soft or possibly soft X-ray spectrum. These sources could be XBPs with a weak accretion component (e.g. XBPs close to quiescence), possibly as a result of the propeller effect (Illarionov & Sunyaev 1975). This interpretation is consistent with their typical low X-ray luminosity ($L_x \sim 5 \times 10^{33}$-$10^{34}$ erg s^{-1}), and mean value of the ξ parameter (9.79 ± 2.29) characteristic of intermediate state XRBs.

Chandra source 4_11 is not classified in the current work, although it has a hard X-ray spectrum and a bright single optical counterpart. The latter is located just below the locus of OB stars in the CMD (see also §A.4 for more details). Thus, optical spectroscopy is needed in order to unambiguously identify it as a new Be-XRB. The same holds for the optical counterpart of *Chandra* source 5_35 (MCPS source Z_2438540), for which there is no optical match in the 1σ search radius and no X-ray spectral information. On the other hand, *Chandra* source 7_9 is classified as a foreground star (in agreement with previous studies), because its brightest optical counterpart (source O_5_316703) has $M_{V_o} \sim -6$ and $(B-V)_o \sim 1.5$ (following the discussion in §6). Furthermore, we classify *Chandra* source 6_11 as a new HMXB. Its brightest counterpart (MCPS source Z_2657679) does not have an OGLE-II match within the 1σ search radius. However, it is associated with OGLE-II source O_7_57270 (≡O_6_320020) just outside this radius, which is an OB-type star (with $V = 17.14$, and $B - V = 0.25$). The early-type counterpart coupled with the possibly hard X-ray spectrum of this source, make *Chandra* source 6_11 a new HMXB.

Moreover, there are 8 sources with more than one optical match for which it is not possible to select the most likely counterpart. The optical matches of *Chandra* sources 3_1, 3_2, 4_6 and 7_16 are very faint, and because of their large photometric errors and high chance

coincidence probability, we cannot select one of the two counterparts (*Chandra* source 3_1 is discussed in §A.4). This is also the case for *Chandra* source 4_23, for which we find two optical matches, one in each of the studied optical catalogs. The O_5_101577 source has only been detected in the I band (i.e. no B, V photometric data available for it), while the Z_2029266 source is also faint ($V > 19$ mag). Likewise, for *Chandra* sources 7_4 and 7_17 we cannot choose the most likely counterpart without optical spectroscopic or variability information, as the 2 brightest sources within the search radius have similar V magnitudes. In particular, for *Chandra* source 7_4 we do not have X-ray spectral information, while source 7_17 has possibly a soft spectrum (also discussed in the Appendix, §A.1). However, the blue object of the bright identified counterparts is the best choice since it results in smaller chance coincidence probability. In the case of *Chandra* source 3_19 the brightest counterpart (source Z_3050592) is not an OB star, but it lies in the area between the red giant branch and the MS. Instead, we find that a fainter source (Z_3049033) is located in the OB star locus. For completeness, we present the optical properties of both sources in Table 11. However, the low X-ray luminosity of source 3_19 indicates that the compact object does not accrete via Roche-lobe overflow as would be expected in the case of an evolved donor (most probably this is a wind-fed system). Furthermore, the hard X-ray spectrum of this source, that is indicative of a pulsar, suggests a younger system, possibly a Be-XRB. Thus, we propose the OB star candidate Z_3049033 as the most likely counterpart of *Chandra* source 3_19.

Chandra sources 5_4 and 5_12 have early-type counterparts and hard (or possibly hard) X-ray spectra. Following the above classification scheme, they would be classified here as new HMXBs. However, optical spectra for these sources have been recently published (Antoniou et al. 2008), revealing their Be nature, thus in Table 11 they are listed as new Be-XRBs. We mention that *Chandra* source 5_4 is identified with the emission-line object [MA93]798, while *Chandra* source 5_12 has no match in the latter catalog (within a search radius of 5″). Although it is difficult to estimate the incompleteness of the [MA93] catalog, the fact that there are Be-XRBs confirmed spectroscopically for which there is not a match in this catalog, implies that if a source does not have a [MA93] counterpart it does not necessarily mean that the source does not exhibit any Hα emission (typical of Be-XRBs). Actually, from the cross-correlation of MCPS stars within our *Chandra* fields with the [MA93] catalog, we find that the vast majority of the matches have $V < 16.6$ mag. This suggests that sources with early (O, B) type counterparts but fainter magnitudes may have Hα emission, but not a [MA93] counterpart. *Chandra* source 5_12 has a bright optical counterpart ($V \sim 14.9$ mag), thus revealing that even brighter sources may have remained undetected in the [MA93] work. Other sources which are previously known Be-XBPs and do not have [MA93] counterparts[10]

[10]This problem is not limited to the present work. Previous works on Be-XRBs (e.g. by Haberl & Pietsch

include *Chandra* sources 4_2, 4_8, 5_16, 6_1, and 7_1.

In total, we identify 35 sources with early-type counterparts, 27 of which have hard X-ray spectra, strongly suggesting that they are XBPs. All but one pulsars (i.e. 14) that have been identified as X-ray sources within our *Chandra* fields have hard spectra and early-type counterparts (for completeness in our *Chandra* fields lie 22 confirmed and 11 candidate pulsars[11], however only 16 have been detected in our survey). The only exceptions are *Chandra* sources 3_18 and 5_24: although their optical counterparts are OB spectral-type star, their small number of counts does not provide us the necessary spectral information.

Ten of the candidate Be stars of Mennickent et al. (2002) have been identified as counterparts to our *Chandra* sources. One of those is proposed as counterpart to *Chandra* source 4_17 for the first time, while for the remaining 9 X-ray sources (3_3, 4_2, 4_8, 5_3, 5_7, 5_15, 6_1, 6_4, and 7_1) there is a known counterpart in the literature (see Table 8 for more details). An extensive presentation of these 10 sources is given in §A.3. This supports our classification of the aforementioned source as new Be-XRB, given also its possibly hard X-ray spectrum and the emission-line object [MA93]396 within its search radius.

From the finding charts we see that a few sources have brighter counterparts that fall outside the 1σ search radius. Thus, we extended the search radius to twice the one used in the original search and we cross-correlated again the coordinates of the *Chandra* sources with the OGLE-II and MCPS catalogs. We find that out of the 33 X-ray sources without an optical counterpart identified in the 1σ search radius, there are 7 X-ray sources with bright optical matches ($M_{V_o} \leq -0.25$ mag) between the 1σ and 2σ search radii. None of these matches lie in the locus of OB stars, while we ignore fainter sources. In addition there are 33 *Chandra* sources with optical matches between the 1σ and 2σ search radii, which are brighter than those found within the 1σ search radius. In particular, for 10 of these *Chandra* sources their optical matches lie in the locus of OB stars, and 3 of them have hard or possibly hard X-ray spectrum (sources 3_2, 4_13, 4_19). *Chandra* source 3_2 is a known pulsar, possibly Be-XRB (Edge et al. 2004), while sources 4_13 and 4_19 have not been previously identified. The hard spectrum of these sources and the early-type counterpart make them candidate XBPs (see §A.7 in the Appendix). We note that although the chance coincidence probability for the bright optical matches within the 2σ search radius is very high (∼70%; see Tables 9 and 10 for more details), the identification of a hard X-ray source with an optical source within the locus of OB stars makes it a HMXB (these additional 3 sources are included

2004), were not successful in identifying a [MA93] counterpart even for confirmed Be-XRBs.

[11]The confirmed systems are taken from http://www.astro.soton.ac.uk/∼mjc/ (as of 08/22/2008), while the candidate XBPs are from the work of Laycock et al. (2008).

in Table 11 and in our census of confirmed and candidate Be-XRBs in the SMC). For the remaining sources we do not propose any of their optical matches as a counterpart, and we only present them for completeness (Tables 12 and 13 in the Appendix, §A.6).

8.4. Comparison with the Galactic and LMC Be-XRBs

In order to understand the HMXB population of the SMC, several studies have compared the number of Be-XRBs in the MCs and the Milky Way (e.g. Haberl & Sasaki 2000, Majid, Lamb & Macomb 2004, Coe et al. 2005a, Haberl & Pietsch 2004; hereafter [HP04]). One approach is to compare the ratios of Be-XRBs to normal (i.e. non-emission line) OB stars. By studying the Be-XRB population with respect to their related stellar populations, we minimize age effects or variations due to SF rate differences for populations of different ages, allowing us to probe for intrinsic differences in the XRB formation efficiency. For the same reason, we do not compare the ratio of Be-XRBs to SG-XRBs, since this is sensitive to the age of these systems, and therefore to variations of the SF rate over these time scales. We note that because of the transient nature of the Be-XRBs, their numbers can be considered only as lower limits. This has been demonstrated by the increasing number of Be-XRBs detected in long term monitoring surveys of the SMC (e.g. Laycock et al. 2005). So far, various studies have confirmed 21 Be-XRBs in the SMC ([HP04], Raguzova & Popov 2005; hereafter [RP05]) and only 1 supergiant, which is located in the SMC Wing (SMC X-1, Webster et al. 1972). In the compilation of [HP04], 17 (out of the 21) Be-XRBs are X-ray pulsars, while for another 8 pulsars the identification with a Be star is suggested (see [HP04] and references therein). There are also 23 proposed Be-XRBs without detected pulsations, and one suggested Be-XRB with uncertain pulse period ([HP04]). Since the detection of pulsations requires high S/N X-ray data, in our study, we include all Be-XRBs, and not only those with detected X-ray pulsations. In total, there are 44 confirmed and candidate Be-XRBs in the 5 *Chandra* fields: 19 listed in [HP04] (with 4 of those not detected in the *Chandra* survey), 12 listed in more recent works (such as by Liu et al. 2005, and Antoniou et al. 2008), 2 newly identified Be-XRBs (*Chandra* sources 4_17 and 7_19), and 11 HMXBs from this work, which can be considered as new candidate Be-XRBs (see also the discussion in §8.3).

At this point, we revisit the relation between Be-XRBs and OB stars, taking into account the latest census of XRBs, and comparing it with the corresponding ratios for the LMC and Milky Way. The numbers of Be-XRBs in the 3 galaxies are based on the compilations of Liu et al. (2005, 2006). Since these compilations consist of different samples of sources detected in various surveys with different sensitivities, we use a subset of Be-XRBs down to the same

detection limit of 10^{34} erg s^{-1} (in the 2.0-10.0 keV band; equivalent to $\sim 1.1 \times 10^{34}$ erg s^{-1} in the 0.7-10.0 keV band). This cut-off X-ray luminosity was chosen in order to assemble uniform samples of sources detected in surveys of the SMC and the Milky Way, given also that this is the detection limit of the *Chandra* survey used in this work (Zezas et al. 2008, in prep.). From those catalogs we used all sources with available spectral types for their counterparts. We also converted their flux densities from the various energy bands to the 2.0-10.0 keV band, assuming a flat power-law spectrum of $\Gamma = 1$.

In the catalog of Liu et al. (2006) we find 31 Galactic Be-XRBs located within 10 kpc from the Sun (based on distances from [RP05][12]) with $L_x \geq 10^{34}$ erg s^{-1} (Liu et al. 2006) and 17 confirmed Be-XRBs in the SMC area covered by our *Chandra* survey (Liu et al. 2005). Including 7 Be-XRBs[13] from the present work with an X-ray luminosity of $\sim 10^{34}$ erg s^{-1}, results in a total of 24 SMC Be-XRBs within our *Chandra* fields. In this comparison (down to $L_x \geq 10^{34}$ erg s^{-1}) we do not consider LMC sources since the LMC has not been surveyed as extensively and in the same depth as the Milky Way or the SMC.

We then estimate the number of OB stars using their locus on the CMD defined in §6. Based on the MCPS catalog (Zaritsky et al. 2002) we find $\sim$ 13720 OB stars within our *Chandra* fields ($\sim$2220, $\sim$4060, $\sim$2730, $\sim$3040, and $\sim$1670 OB stars for *Chandra* field 3, 4, 5, 6, and 7, respectively). The photometric data of these sources have been reddening corrected as described in §6. In the case of the Milky Way, Reed (2001) estimated that there are $\sim$ 25800 OB stars within 10 kpc of the Sun. Based on the above numbers we find that the Be-XRBs with $L_x \geq 10^{34}$ erg s^{-1} are $\sim$ 1.5 times more common in the SMC when compared to the Milky Way, with respect to its populations of young stars, thus confirming the notion that the SMC has a large number of Be-XRBs (e.g. Liu et al. 2005; Coe et al. 2005b).

For completeness, we extend this comparison to the LMC, considering only sources with $L_x \geq 10^{36}$ erg s^{-1}, which is the average completeness level of the ROSAT observations of LMC fields. In this case we find 6 Be-XRBs in the LMC (Liu et al. 2005), 10 in the SMC, and 29 in the Milky Way (in the case of the LMC we find $\sim$ 42200 OB stars, in the area covered by the ROSAT fields where the 6 Be-XRBs were detected, based on the MCPS catalog of Zaritsky et al. (2004) and assuming $A_V \sim 0.55$ mag as in §8.1). Hence, the Be-XRBs are $\sim$ 5.5 times more common in the SMC, with respect to the LMC, while when compared to the Milky Way we find almost equal ratios of Be-XRBs to OB stars. However, one caveat

[12]http://xray.sai.msu.ru/$\sim$raguzova/BeXcat/ as of 08/25/2006 for the Milky Way.

[13]These systems are: 3 Be-XRBs not listed in Liu et al. (2005; *Chandra* sources 3_2, 5_7, and 6_1), one newly identified system (*Chandra* source 5_4), and 3 HMXBs from this work (*Chandra* sources 3_7, 4_4, and 7_4 which are candidate Be-XRBs).

in the case of the LMC, is that its small number of Be-XRBs may be due to the fact that it has not been monitored as extensively and in the same depth as the SMC or the Milky Way.

The high number of Be-XRBs in the SMC could simply be the result of enhanced star forming activity in the SMC $\sim$ 30 Myr ago (e.g. Majid et al. 2004). In particular, the formation and lifetimes of wind-fed HMXBs are driven by the stellar evolution of the donor. Be stars, which are the most common type of donor in wind-fed XRBs, develop their decretion disks at ages of $25 - 80$ Myr (McSwain & Gies 2005), with a peak at $\sim$ 35 Myr. Indeed, using the isochrones presented in §6, we determine that bright counterparts of the X-ray sources in our fields (of OB spectral type) have ages ranging from $\sim$ 15.5 to $\sim$ 85 Myr. Based on the SF history of the SMC (Harris & Zaritsky 2004),and for Z=0.008, we find that the most recent major burst occurred $\sim$ 42 Myr ago. The only exceptions are *Chandra* field 6, where a similarly strong burst occurred somewhat earlier ($\sim$ 27 Myr ago), and *Chandra* field 4 which shows an additional burst only $\sim$ 7 Myr ago. The duration of the major bursts is $\sim$ 40 Myr. In addition, there were older SF episodes ($\sim$ 0.4 Gyr ago) with lower intensity but longer duration. However, we do not expect a population of Be-XRBs associated with either the relatively old ($\sim$ 0.4 Gyr) widespread star forming activity, or the most recent episode ($\sim$ 7 Myr) at the current time. Therefore, the large number of Be-XRBs in the SMC is most likely due to its enhanced star-forming activity $\sim$ 42 Myr ago. OB stars formed during this episode are expected to reach now the maximum rate of decretion disk formation. Even in smaller spatial scales the excess of Be-XRBs in fields 4 and 5 is consistent with their higher SF rate $\sim$ 42 Myr ago, in comparison to the other fields, and with the fact that the age of their stellar populations is in the range of maximum Be-star formation.

However, the comparison of the ratios of Be-XRBs over OB stars in the SMC, and the Milky Way indicates that there is still a residual excess of a factor of $\sim$ 1.5 that cannot be accounted for by SF and age differences. This residual excess can be attributed to the different metallicity of the two galaxies. Population synthesis models predict a factor of $\sim$ 3 higher numbers of HMXBs in galaxies with metallicities similar to that of the SMC, when compared to the Milky Way (Dray 2006). In addition, there is observational evidence for higher proportion of Be stars in lower metallicity environments (at least in the case of younger systems). Wisniewski & Bjorkman (2006) found a ratio of $\sim$ 2 for the numbers of Be stars in SMC and Galactic metallicities, while Martayan et al. (2007) found that the B and Be stars rotate faster in the SMC than in the LMC and faster in the LMC than in the Milky Way. This could also explain the residual excess of binaries in the SMC, since only a fraction of the B stars that reach the zero-age MS with a sufficiently high initial rotational velocity can become Be stars (Martayan et al. 2006). Moreover, by noticing the lack of massive Be stars in the Milky Way at ages for which Be stars are found in the MCs, Martayan et al. (2007) suggested that the Be star phase can last longer in low metallicity

environments, such as in the MCs, than in the Milky Way.

8.5. Local variations of the Be-XRB populations

When we compare the number of SMC HMXBs (or equivalently the number of Be-XRBs, since all but one of the confirmed HMXBs is a SG-XRB) in the different *Chandra* fields we find an excess of these objects in fields 4 and 5. In particular, these two fields have 14 and 15 HMXBs, respectively, versus an average of 5 HMXBs in each of the other 3 fields. Field 5 also has the largest number of identified pulsars (8; fields 3, 4, 6, and 7 have 3, 6, 3, and 2 confirmed pulsars, respectively). Although given the small numbers of sources this excess is only marginally statistically significant, it is intriguing that fields 4 and 5 had the highest SF rate at the age of maximum Be-star production ($\sim$ 42 Myr ago). In Figure 10 (lower panel), we present the height of the SF rate at the age of $\sim$ 42 Myr versus the number of HMXBs in each *Chandra* field. In the upper panel of Figure 10 we present the SF rate versus the ratio of the number of HMXBs to the number of OB stars in each field. In this plot we include all HMXBs detected in our *Chandra* fields (based on our survey and the census of Liu et al. 2005; 44 in total), and the OB stars in each field (selected as described in §8.4) from the MCPS catalog. Predominantly, field 5 which has the most intense SF peak at the peak age of Be-star formation ($\sim$ 2 times more intense when compared to that of the other fields) appears to have almost double ratio of HMXBs to OB stars than the other fields.

The direct comparison between the XRB populations and the SF history of different regions, may be complicated by kicks imparted on the compact object during the supernova explosion (e.g. van den Heuvel et al. 2000). The result of these kicks is that the XRBs may be spread over a larger volume with respect to their parent stellar population, and thus complicating the study of their connections. In the case of the SMC, and given a typical projected runaway velocity of 15 ± 6 km s^{-1} (van den Heuvel et al. 2000), we estimate that a Be-XRB would have traveled a maximum distance of $\sim$ 640 pc from the time it was formed (i.e. $\sim$ 42 Myr ago, given the SF history of the SMC). This distance is an upper limit, since the age of 42 Myr is only based on the formation time-scale of Be binaries, and it does not include the formation time-scale of the pulsar, which is a few Myr. For a distance of 60 kpc this translates to a projected angular distance of $\sim 36.7'$, roughly twice the dimension of the *Chandra* fields. However, the scales of the star-forming regions at the age ranges of interest (<20 Myr, $20 - 60$ Myr, >60 Myr) are much larger than the size of the *Chandra* fields. Therefore, our fields across the SMC "Bar" provide a representative picture of the Be-XRB population in its main body. Moreover, the excess of Be-XRBs at fields 4 and 5 which have the highest SF rates in ages of $\sim$ 42 Myr (which corresponds to the age of maximum

production of Be stars) gives further confidence that the kick velocities are small enough not to smear the correlation between X-ray sources and their parent stellar populations.

9. Conclusions

In this paper we report the results for the optical counterparts of 153 X-ray sources detected in the *Chandra* survey of the central region of the SMC. For 120 sources we find optical matches in the OGLE-II and/or MCPS catalogs. Using these photometric data, we propose the most likely optical counterpart for 113 *Chandra* sources, while for 7 sources the candidate counterparts are equally likely. By combining their optical and X-ray properties (i.e. spectral and timing properties), we classify 34 *Chandra* sources of which 13 were previously unclassified. In particular:

1. We find that 52 X-ray sources have a single counterpart, 68 have two or more matches, while 33 sources do not have counterparts in either OGLE-II or MCPS catalog within the 1σ search radius (7 out of these 33 sources have bright optical matches ($M_{V_o} \leq -0.25$) between the 1σ and 2σ search radii, but none of them is associated with an OB star).

2. Early-type counterparts (of OB spectral type) have been identified for 35 X-ray sources (with a chance coincidence probability $\leq 19\%$). Based on spectroscopic observations of stars in the SMC we define the photometric locus of early-type (OB) stars in the M_{V_o} vs. $(B-V)_o$ CMD. Based on the position on the CMD and their X-ray spectral properties, we propose: (a) 4 new Be-XRBs, and (b) 7 new HMXBs, and 2 new candidate HMXBs. Two of the new HMXBs have hard X-ray spectra and early-type (OB) counterparts within their 2σ search radius.

3. Based on the isochrones of Lejeune & Schaerer (2001), we estimate the age of the 13 new (confirmed and candidate Be-XRBs and HMXBs) to be $\sim 15 - 85$ Myr, in agreement with the age of Be stars.

4. Twenty X-ray sources with bright counterparts ($M_{V_o} \leq -0.25$) could not be classified, because we do not have X-ray spectral information for them and/or they have other than OB spectral-type counterparts.

5. We find that the mixing of Be-XRBs with other than their natal stellar population is not an issue in our comparisons of Be-XRBs and stellar populations in the SMC, because the SF activity across the SMC "Bar" is generally uniform in scales larger

than the size of the *Chandra* fields. Instead we find indication for variation in the XRB populations across the "Bar" and in scales of ~ 1 kpc: fields with higher SF rate at ages which are more prone to produce Be stars show increased number of Be-XRBs.

6. Using the catalogs of Liu et al. (2005, 2006) we find that for luminosities down to $L_x \sim 10^{34}$ erg s^{-1} (chosen as a moderate minimum cut-off between different SMC and Galactic X-ray surveys) the *Chandra* SMC fields contain ~ 1.5 times more Be-XRBs in comparison to the Milky Way (including the new confirmed and candidate Be-XRBs from this study), even after taking into account the different OB star formation rates in the two galaxies. This residual excess can be explained when we account for the different metallicity of the SMC and the Milky Way. This is in good agreement with theoretical predictions derived from population synthesis studies (Dray 2006), and previous observational (both photometric and spectroscopic) works (e.g. Wisniewski & Bjorkman 2006; Martayan et al. 2006, 2007).

We would like to thank the anonymous referee for helpful comments which have improved this paper. We would also like to thank Dr. A. Udalski for providing unpublished light curves of the OGLE-II stars used in this paper. This research has made use of the SIMBAD database, operated at CDS, Strasbourg, France. This work was supported by NASA LTSA grant NAG5-13056, and NASA grant G02-3117X.

A. Notes on individual sources

A.1. Sources with uncertain nature

Most of the sources that remain unclassified in this work have soft (or possibly soft) X-ray spectra or no X-ray spectral information (because of their small number of source counts in the 0.5-7.0 keV energy band; Zezas et al. 2008, in prep.).

Chandra **source 3_1:** One of the two optical counterparts of this source has been identified as a variable star. More details of source 3_1 are presented below in §A.4.

Chandra **source 3_4:** A single optical match was identified in both OGLE-II and MCPS catalogs. However, its $V = 18.19$ magnitude and $B-V = 0.37$ color are not indicative of the nature of the companion star. Its soft X-ray spectrum (Zezas et al. 2008, in prep.) possibly suggests an AGN.

Chandra **sources 5_9 & 6_8:** These sources have possibly a soft X-ray spectrum and multiple optical matches within their search radius. The brightest matches of 5_9 and 6_8 are not O or B-type stars ($B-V$ color ~ 0.59 and ~ 1.12 mag, respectively). Recently, Laycock et al. (2008) detected source 5_9 as a candidate quiescent X-ray pulsar (SXP7.83).

Chandra **source 5_15:** Within the search radius of this source we identified 5 matches, all of them fainter than V$\sim$19 mag. Its possibly soft X-ray spectrum suggests an AGN. However, Laycock et al. (2008) detected this source as a candidate quiescent X-ray pulsar, while the brightest of its matches has been identified as a Be candidate star (Mennickent et al. 2002). See also the discussion in §A.3.

Chandra **source 5_23:** We identify MCPS source Z_2288276 (no OGLE-II overlap) as the optical counterpart of X-ray source 5_23. Based on its V magnitude and B-V color, this is an O or B-type star. Thus, we classify this source as a new candidate HMXB. The small number of net counts of source 5_23 ($\sim$ 10 counts in the 0.5-7.0 keV energy band; Zezas et al. 2008, in prep.) does not allow us to derive its X-ray spectral information, thus prohibiting us to classify it further as a new candidate Be-XRB.

Chandra **sources 4_10, 5_6, 5_32, 6_3, 7_17:** The soft X-ray spectrum of these sources (HR method, more details in Table 11 and its description in §8.3) and their early-type counterparts could be indicative of a candidate black-hole X-ray binary (BH-XRB) nature. However, only X-ray spectral fits and optical spectroscopy of the companion stars could possibly identify their true nature.

Chandra **source 6_20:** The small number of net counts of this source (<10 counts in the 0.5-7.0 keV energy band; Zezas et al. 2008, in prep.) does not allow us to derive spectral information for it. Its $V=13.71$ magnitude and $B-V=0.39$ color are not indicative of the nature of the companion star, thus this source remains unclassified in this work. More details on this source are presented to §A.5.

Chandra **source 7_17:** This source has possibly a soft X-ray spectrum. The large search radius of it ($5.29''$, maximum search radius used in this study because of the large off-axis angle) resulted in the identification of multiple matches. However, only 2 sources are bright ($V\sim 18.4$ mag, thus resulting in smaller chance coincidence probability). One of the two sources lies on the red giant branch, while the other one (O_5_140992) falls just outside the locus of OB spectral type stars. Source 7_17 remains unclassified in this work.

Chandra **source 7_19:** Due to the small number of counts (<10 counts in the 0.5-7.0 keV energy band; Zezas et al. 2008, in prep.) we do not have X-ray spectral information for this source. However, there is an emission-line object within $\sim 2\sigma$ of the search radius (source [MA93]316; Meyssonier & Azzopardi 1993). Actually this source is located in the star

cluster SMC-N32 (Bica & Schmitt 1995), a crowded region surrounded by a diffuse emission (HII region). The detection algorithm in this case resulted in many spurious sources that they were not deblended (see also the on-line finding chart for this source). We note here that the brightest of the 5 matches within the search radius of this source is located just to the right border of the ellipse of OB stars in the V, B-V CMD. Its large error in B-V color could place it within the ellipse, thus suggesting that it could be another new HMXB.

Chandra **sources 4_32, 4_36, 5_18, 5_25, 6_23, 7_9:** All but two of the brightest counterparts of these sources lie on the red giant branch in the V, B-V CMD (Fig. 7), while that of source 5_18 lies on the right of the MS (most probably in the giant branch). The counterpart of source 7_9 has $M_{V_o} = -5.7$ and $(B-V)_o > 0.75$, thus it lies on the locus of foreground stars (for more details see §6). In addition, these sources do not have X-ray spectral information (because of their small number of counts), except from source 7_9 which has possibly a hard X-ray spectrum.

A.2. Point sources associated with known SNRs

In *Chandra* field 4 there are three known supernova remnants (SNRs). Below are given details for the point sources associated with two of them. The third SNR (*Chandra* source 4_38) is located in a large off-axis angle ($D_{off-axis} > 10'$), thus not considered in this study.

Chandra **source 4_16:** This is a point source associated with the previously known SNR 0047-735 (Mathewson et al. 1984). For this source it has been found one single optical match (O_5_27768), while it has been recently classified as a new candidate quiescent X-ray pulsar (CXO J004905.1-731411≡SXP8.94; Laycock et al. 2008).

Chandra **source 4_20:** This point source is associated with the previously known SNR 0049-73.6 (Mathewson et al. 1984). We identify source O_5_262679 as the optical counterpart of source 4_2. CXO J005059.0-732055 (SXP9.39; Laycock et al. 2008) has been classified as a candidate quiescent X-ray pulsar.

Chandra **source 4_21:** This point source is also associated with the SNR 0049-73.6 (Mathewson et al. 1984; Sasaki et al. 2000). There are 3 bright counterparts ($M_{V_o} < -0.25$) within its search radius, while one of those (O_5_256826) is an early-type star (O or B).

A.3. Candidate Be nature of identified counterparts

All sources that are presented below have been classified as type-4 stars (light curves similar to Galactic Be stars) in the compilation of Be candidate stars by Mennickent et al. 2002 (hereafter [MPG02]).

Chandra **source 3_3:** The identified counterpart O_8_49531 (single match) of X-ray source 3_3 is a Be candidate star ([MPG02]No.494), in agreement with the identification of Sasaki et al. (2003).

Chandra **source 4_2:** We find two matches for X-ray source 4_2. Although none of them is located within the locus of OB stars (criterion (i)), we identify source O_5_111490 as the counterpart for 4_2, because of its Be nature ([MPG02]No.206), while it was also found to be a variable star (Ita et al. 2004). This is in agreement with the identification of Coe et al. (2005a).

Chandra **source 4_17:** Source O_5_180008 is identified as the optical counterpart of X-ray source 4_17, while it is also identified as a Be candidate star ([MPG02]No.265). This source coincides with the emission-line object [MA93]396. In combination with the possibly hard X-ray spectrum, we classify this source as a new Be-XRB.

Chandra **source 5_3:** The identified optical counterpart O_6_85614 (in agreement with Schmidtke & Cowley 2006) is a Be candidate star [MPG02]No.321. It is of B0-5 spectral type (source [2dF]No.0828; see below §A.5), and it has been found to coincide with the emission-line object [MA93]No.506 (in agreement with Haberl & Sasaki 2000).

Chandra **source 5_7:** The identified optical counterpart of X-ray source 5_7 is source O_7_70829. It is identified as a Be candidate star ([MPG02]No.426), while Sasaki et al. (2003) presented the same counterpart, identified also as the emission-line object [MA93]No.810.

Chandra **source 5_15:** We identify source O_7_71429 as the optical counterpart of X-ray source 5_15 (see also §A.1). This is also reported as a Be candidate star ([MPG02]No.423). However, Dobrzycki et al. (2003a) identified this object as a quasar ($z = 1.79$) located behind the SMC (based on a spectroscopic study).

Chandra **source 6_1:** The identified counterpart O_6_77228 of source 6_1 is a candidate Be star ([MPG02]No.341; see also §A.5).

Chandra **source 6_4:** Source O_6_147662 is identified as the optical counterpart of X-ray source 6_4. This optical source is also reported as a candidate Be star ([MPG02]No.364), and it is located $\sim 0.57''$ away from the emission-line object [MA93]618 (in agreement with Haberl & Sasaki 2000).

Chandra **source 7_1:** We identify source O_5_65517 as the optical counterpart of X-ray source 7_1. This is star 1 of Stevens et al. (1999), and it is also in agreement with the identification of Coe & Orosz (2000). This OGLE source is identified as a Be candidate star ([MPG02]No.199).

A.4. Sources identified with OGLE-II variable stars

The following OGLE-II optical counterparts have been identified as variable stars in the catalogs of Zebrun et al. (2001) or Ita et al. (2004).

Chandra **source 3_1:** We identify source O_7_267163 as the optical counterpart of X-ray source 3_1. From visual inspection of the finding chart, from comparison of the V magnitude for sources O_7_267163 and O_7_267132, and taking into account the $\sim 0.7''$ astrometric accuracy of OGLE, we believe these stars are a single source. Although none of the identified matches is an early-type star, and the parameter ξ cannot distinguish in this case the right counterpart, source O_7_267163 is identified as a variable star (OGLE00571981-72253375) in the study of Zebrun et al. (2001). Sasaki et al. (2003) identified the same object, while they also associated it with star USNOA2.0 0150-00625436. The soft X-ray spectrum of 3_1 and the identification of the optical counterpart as a background quasar (Dobrzycki et al. 2003b), suggest that this is possibly an AGN (in agreement with Sasaki et al. 2003).

Chandra **source 4_2**: Source O_5_111490 is also identified as a variable star in the analysis of Ita et al. (2004; see also §A.3.

Chandra **source 4_5:** The optical counterpart of X-ray source 4_5 is the variable star O_5_111500 (single optical match; $P_{pulse,opt} = 89.835$ days, Ita et al. 2004). Haberl, Eger & Pietsch (2008) have recently confirmed the Be-XRB nature of this source, while no significant pulsations have been found in their study. In a later work, Laycock et al. (2008) identified *Chandra* source 4_5 as the X-ray pulsar SXP892.

Chandra **source 4_11:** Source O_4_164855 is the single match of *Chandra* source 4_11 within the search radius with V magnitude and $B-V$ color which place it just below the locus of OB stars in the CMD. We mention here that in $\sim 2\sigma$ from the X-ray source position there is a bright variable star (O_4_163513≡OGLE 004802.55-731659.8; Ita et al. 2004). However, the B-V color of this optical source is not indicative of an O or B-type star, thus even if its X-ray spectrum is possibly hard this source remains unclassified.

A.5. Sources with available spectral classification for their counterparts

The sources presented here (with the exception of *Chandra* source 5_16) have been identified spectroscopically in the 2dF survey of the SMC by Evans et al. (2004; hereafter [2dF]) and/or are reported in the emission-line object compilation of Meyssonnier & Azzopardi (1993; hereafter [MA93]). The luminosity classes shown in parenthesis indicate an hybrid photometric/spectroscopic approach and are not true, MK-process, morphological types (for more details see Evans et al. 2004).

Chandra **source 5_1:** The identified optical counterpart in this case is MCPS source Z_2311496, in agreement with Coe et al. (2005). This source is also defined as a B0-5(II)e star in the 2dF spectroscopic catalog of Evans et al. (2004; source [2dF]No.0839).

Chandra **source 5_3:** The optical counterpart O_6_85614 of source 5_3 is identified as a B0-5(II) spectral-type source ([2dF]No.0828).

Chandra **source 5_16:** A single match (source Z_2573354) is identified as the optical counterpart of this source in the MCPS catalog (no OGLE-II overlap), in agreement with Coe et al. (2005a). Buckley et al. (2001) identified source 5_16 as a transient pulsar and spectroscopically classified the suggested counterpart (star A or B mentioned in their study) as a B1-B2III-Ve star. On the other hand, the variable MACHO source 207.16202.30 lies $> 14''$ away of X-ray source 5_16 (unlikely the correct counterpart; Coe et al. 2005a).

Chandra **source 6_1:** We identify source O_6_77228 as the optical counterpart of X-ray source 6_1 (in agreement with Coe et al. 2005a). This is source [2dF]No.5054 classified as a B1-5(II)e star (Evans et al. 2004). It also appears as a candidate Be star in the compilation of Mennickent et al. (2002; [MPG02]No.341). For more details see §A.3.

Chandra **source 6_20:** Source O_6_311169 (single match) is proposed here as the optical counterpart of X-ray source 6_20. It is the brightest counterpart identified in this study, while it has been identified as the emission-line object [MA93]No.739 (peculiar Hα emission-line star with FeII and [FeII] emission; $\sim 0.17''$ from the OGLE-II source, and $\sim 0.8''$ from the X-ray source). The latter source has been identified as a B[e] star by Massey & Duffy (2001). We only propose the above OGLE-II source as the counterpart of *Chandra* source 6_20, and we note that further analysis of this peculiar system is required so as to confirm its nature (see also A.1).

A.6. *Chandra* sources with bright optical counterparts ($M_{V_o} \leq -0.25$) only between the 1σ and 2σ search radii

Out of the 33 X-ray sources without any OGLE-II or MCPS match in the 1σ search radius, there are 7 *Chandra* sources with counterparts in the 2σ search radius. These sources are presented in Table 12. The description of this table is similar to that of Tables 2-6 (given in §3.1), with the only difference that there is only one table for all the sources found in the different *Chandra* fields (separated by double horizontal lines). In Table 13 we also present the optical and X-ray properties of these sources (see also §8.3).

A.7. *Chandra* sources with optical counterparts in the locus of OB stars and hard or possibly hard spectrum between the 1σ and 2σ search radii

Chandra **source 3_2:** This source is a pulsar (Edge et al. 2004). However, both of its optical matches in the MCPS catalog presented in Table 2 (no overlap with OGLE-II) are faint stars. Due to the high chance coincidence probability of faint sources, we do not propose any of them as counterpart of X-ray source 3_2. Instead, looking for counterparts between the 1σ and 2σ search radii, we find MCPS source Z_2806702 (in agreement with Edge et al. 2004). This is a bright star ($V = 16.78$, $B - V = -0.12$), which is located $4.27''$ away from the X-ray position. Although no spectroscopic data for these 3 sources are available, the early-type nature of MCPS source Z_2806702, make us believe this is the most likely counterpart. Recently, Haberl & Eger (2008; ATel#1529) suggested that *Chandra* source 3_2 is a background AGN and not a Be-XRB pulsar, with an optical counterpart one of the two faint stars with V=20.3 mag found in the 1σ search radius.

Chandra **source 4_13:** We have identified source O_5_90858 as the optical counterpart of 4_13. However, when we look for counterparts between the 1σ and 2σ search radii, we find 2 sources brighter than O_5_90858. These sources, O_5_90493 and O_5_90535, ($5.47''$ and $4.10''$ away from the X-ray source, respectively) are both of OB spectral type ($V = 15.57$, $B - V = -0.07$ and $V = 16.34$, $B - V = 0.23$, respectively). The possibly hard X-ray spectrum of 4_13 suggests that this is a new candidate Be-XRB. However, only optical spectroscopy could determine the exact type of these bright stars and the true counterpart of *Chandra* source 4_13.

Chandra **source 4_19:** The optical source O_5_261182 is found $2.27''$ away from *Chandra* source 4_19 (between the 1σ and 2σ search radius), and it is an OB spectral-type star ($V = 18.16$, $B - V = -0.08$). In combination with its possibly hard X-ray spectrum, we propose this is a new HMXB. Optical spectroscopy will definitely determine if this source is

also a new Be-XRB.

REFERENCES

Alcock, C., et al. 1997, ApJ, 486, 697

Antoniou, V., Hatzidimitriou, D., Zezas, A., & Reig, P. 2008, ApJ, submitted

Azzopardi, M., & Vigneau, J. 1982, A&AS, 50, 291

Bica, E. L. D., & Schmitt, H. R. 1995, ApJS, 101, 41

Binney, J., & Merrifield, M. 1998, Galactic astronomy / James Binney and Michael Merrifield. Princeton, NJ : Princeton University Press, 1998. (Princeton series in astrophysics)

Buckley, D. A. H., Coe, M. J., Stevens, J. B., van der Heyden, K., Angelini, L., White, N., & Giommi, P. 2001, MNRAS, 320, 281

Cardelli, J. A., Clayton, G. C., & Mathis, J. S. 1989, ApJ, 345, 245

Cioni, M.-R., et al. 2000, A&AS, 144, 235

Clark, G., Doxsey, R., Li, F., Jernigan, J. G., & van Paradijs, J. 1978, ApJ, 221, L37

Coe, M. J., Edge, W. R. T., Galache, J. L., & McBride, V. A. 2005a, MNRAS, 356, 502

Coe, M. J., Negueruela, I., & McBride, V. A. 2005b, MNRAS, 362, 952

Coe, M. J., & Orosz, J. A. 2000, MNRAS, 311, 169

Corbet, R., Marshall, F. E., Lochner, J. C., Ozaki, M., & Ueda, Y. 1998, IAU Circ., 6803, 1

Corbet, R., Markwardt, C. B., Marshall, F. E., Laycock, S., & Coe, M. 2002, IAU Circ., 7932, 2

Cowley, A. P., Schmidtke, P. C., McGrath, T. K., Ponder, A. L., Fertig, M. R., Hutchings, J. B., & Crampton, D. 1997, PASP, 109, 21

Crowl, H. H., Sarajedini, A., Piatti, A. E., Geisler, D., Bica, E., Clariá, J. J., & Santos, J. F. C., Jr. 2001, AJ, 122, 220

Dickey, J. M., & Lockman, F. J. 1990, ARA&A, 28, 215

Dobrzycki, A., Macri, L. M., Stanek, K. Z., & Groot, P. J. 2003a, AJ, 125, 1330

Dobrzycki, A., Stanek, K. Z., Macri, L. M., & Groot, P. J. 2003b, AJ, 126, 734

Dray, L. M. 2006, MNRAS, 370, 2079

Edge, W. R. T., & Coe, M. J. 2003, MNRAS, 338, 428

Edge, W. R. T., Coe, M. J., Galache, J. L., McBride, V. A., Corbet, R. H. D., Markwardt, C. B., & Laycock, S. 2004, MNRAS, 353, 1286

Evans, C. J., Howarth, I. D., Irwin, M. J., Burnley, A. W., & Harries, T. J. 2004, MNRAS, 353, 601

Fabrycky, D. 2005, MNRAS, 359, 117

Garmany, C. D., Conti, P. S., & Massey, P. 1987, AJ, 93, 1070

Garmire, G. P., Bautz, M. W., Ford, P. G., Nousek, J. A., & Ricker, G. R. 2003, Proc. SPIE, 4851, 28

Gehrels, N. 1986, ApJ, 303, 336

Gordon, K. D., Clayton, G. C., Misselt, K. A., Landolt, A. U., & Wolff, M. J. 2003, ApJ, 594, 279

Haberl, F., & Eger, P. 2008, The Astronomer's Telegram, 1529, 1

Haberl, F., Eger, P., & Pietsch, W. 2008, A&A, 489, 327

Haberl, F., Eger, P., Pietsch, W., Corbet, R. H. D., & Sasaki, M. 2008, A&A, 485, 177

Haberl, F., Filipović, M. D., Pietsch, W., & Kahabka, P. 2000, A&AS, 142, 41

Haberl, F., & Pietsch, W. 2004, A&A, 414, 667

Haberl, F., Pietsch, W., Schartel, N., Rodriguez, P., & Corbet, R. H. D. 2004, A&A, 420, L19

Haberl, F., & Sasaki, M. 2000, A&A, 359, 573

Harries, T. J., Hilditch, R. W., & Howarth, I. D. 2003, MNRAS, 339, 157

Harris, J., & Zaritsky, D. 2004, AJ, 127, 1531

Hilditch, R. W., Howarth, I. D., & Harries, T. J. 2005, MNRAS, 357, 304

Illarionov, A. F., & Sunyaev, R. A. 1975, A&A, 39, 185

Israel, G. L., Stella, L., Angelini, L., White, N. E., & Giommi, P. 1995, IAU Circ., 6277, 1

Ita, Y., et al. 2004, MNRAS, 353, 705

Janot-Pacheco, E., Motch, C., & Mouchet, M. 1987, A&A, 177, 91

Kahabka, P., & Pietsch, W. 1996, A&A, 312, 919

Kim, D.-W., et al. 2004, ApJS, 150, 19

Larsen, S. S., Clausen, J. V., & Storm, J. 2000, A&A, 364, 455

Laycock, S., Corbet, R. H. D., Coe, M. J., Marshall, F. E., Markwardt, C., & Lochner, J. 2005, ApJS, 161, 96

Laycock, S., Zezas, A., & Hong, J. 2008, arXiv:0809.1738

Lejeune, T., & Schaerer, D. 2001, A&A, 366, 538

Liu, Q. Z., van Paradijs, J., & van den Heuvel, E. P. J. 2005, A&A, 442, 1135

Liu, Q. Z., van Paradijs, J., & van den Heuvel, E. P. J. 2006, A&A, 455, 1165

Liu, Q. Z., van Paradijs, J., & van den Heuvel, E. P. J. 2007, A&A, 469, 807

Luck, R. E., Moffett, T. J., Barnes, T. G., III, & Gieren, W. P. 1998, AJ, 115, 605

Macomb, D. J., Fox, D. W., Lamb, R. C., & Prince, T. A. 2003, ApJ, 584, L79

Majid, W. A., Lamb, R. C., & Macomb, D. J. 2004, ApJ, 609, 133

Marshall, F. E., et al. 1998, IAU Circ., 6818, 1

Martayan, C., Frémat, Y., Hubert, A.-M., Floquet, M., Zorec, J., & Neiner, C. 2006, A&A, 452, 273

Martayan, C., Frémat, Y., Hubert, A.-M., Floquet, M., Zorec, J., & Neiner, C. 2007, A&A, 462, 683

Massey, P. 2002, ApJS, 141, 81

Massey, P., & Duffy, A. S. 2001, ApJ, 550, 713

Massey, P., Lang, C. C., Degioia-Eastwood, K., & Garmany, C. D. 1995, ApJ, 438, 188

Mathewson, D. S., Ford, V. L., Dopita, M. A., Tuohy, I. R., Mills, B. Y., & Turtle, A. J. 1984, ApJS, 55, 189

Matt, G., Fabian, A. C., Guainazzi, M., Iwasawa, K., Bassani, L., & Malaguti, G. 2000, MNRAS, 318, 173

McSwain, M. V., & Gies, D. R. 2005, ApJS, 161, 118

Mennickent, R. E., Pietrzyński, G., Gieren, W., & Szewczyk, O. 2002, A&A, 393, 887

Meyssonnier, N., & Azzopardi, M. 1993, A&AS, 102, 451

Monet, D. G., et al. 2003, AJ, 125, 984

Murphy, M. T., & Bessell, M. S. 2000, MNRAS, 311, 741

Oey, M. S., King, N. L., & Parker, J. W. 2004, AJ, 127, 1632

Paczynski, B. 2001, Acta Astronomica, 51, 81

Park, T., Kashyap, V. L., Siemiginowska, A., van Dyk, D. A., Zezas, A., Heinke, C., & Wargelin, B. J. 2006, ApJ, 652, 610

Raguzova, N. V., & Popov, S. B. 2005, Astronomical and Astrophysical Transactions, 24, 151

Ratnatunga, K. U., & Bahcall, J. N. 1985, ApJS, 59, 63

Reed, B. C. 2001, PASP, 113, 537

Russell, S. C., & Dopita, M. A. 1992, ApJ, 384, 508

Sasaki, M., Haberl, F., & Pietsch, W. 2000, A&AS, 147, 75

Sasaki, M., Pietsch, W., & Haberl, F. 2003, A&A, 403, 901

Schlegel, D. J., Finkbeiner, D. P., & Davis, M. 1998, ApJ, 500, 525

Schmidtke, P. C., & Cowley, A. P. 2005, AJ, 130, 2220

Schmidtke, P. C., & Cowley, A. P. 2006, AJ, 132, 919

Shtykovskiy, P., & Gilfanov, M. 2005, MNRAS, 362, 879

Silverman, J. D., et al. 2005, ApJ, 618, 123

Skrutskie, M. F., et al. 2006, AJ, 131, 1163

Soszynski, I., et al. 2002, Acta Astronomica, 52, 143

Stevens, J. B., Coe, M. J., & Buckley, D. A. H. 1999, MNRAS, 309, 421

Tucholke, H.-J., de Boer, K. S., & Seitter, W. C. 1996, A&AS, 119, 91

Udalski, A., Soszynski, I., Szymanski, M., Kubiak, M., Pietrzynski, G., Wozniak, P., & Zebrun, K. 1999, Acta Astronomica, 49, 437

Udalski, A., Soszynski, I., Szymanski, M., Kubiak, M., Pietrzynski, G., Wozniak, P., & Zebrun, K. 1998b, Acta Astronomica, 48, 563

Udalski, A., Szymanski, M., Kubiak, M., Pietrzynski, G., Wozniak, P., & Zebrun, K. 1998a, Acta Astronomica, 48, 147

van den Bergh, S. 2000, The galaxies of the Local Group, by Sidney Van den Bergh. Published by Cambridge, UK: Cambridge University Press, 2000 Cambridge Astrophysics Series Series, vol no: 35

van den Heuvel, E. P. J., Portegies Zwart, S. F., Bhattacharya, D., & Kaper, L. 2000, A&A, 364, 563

van Paradijs, J., & McClintock, J. E. 1995, X-ray Binaries, eds. W.H.G. Lewin, J. van Paradijs, and E.P.J. van den Heuvel (Cambridge: Cambridge Univ. Press), p. 58, 58

Webster, B. L., Martin, W. L., Feast, M. W., & Andrews, P. J. 1972, Nature, 240, 183

White, N. E., Nagase, F., & Parmar, A. N. 1995, X-ray Binaries, eds. W.H.G. Lewin, J. van Paradijs, and E.P.J. van den Heuvel (Cambridge: Cambridge Univ. Press), p. 1, 1

Wisniewski, J. P., & Bjorkman, K. S. 2006, ApJ, 652, 458

Wyrzykowski, L., et al. 2004, Acta Astronomica, 54, 1

Yokogawa, J., Imanishi, K., Tsujimoto, M., Koyama, K., & Nishiuchi, M. 2003, PASJ, 55, 161

Zacharias, N., Urban, S. E., Zacharias, M. I., Wycoff, G. L., Hall, D. M., Monet, D. G., & Rafferty, T. J. 2004, AJ, 127, 3043

Zaritsky, D., Harris, J., Thompson, I. B., & Grebel, E. K. 2004, AJ, 128, 1606

Zaritsky, D., Harris, J., Thompson, I. B., Grebel, E. K., & Massey, P. 2002, AJ, 123, 855

Zebrun, K., et al. 2001, Acta Astronomica, 51, 317

Zezas, A., Fabbiano, G., Rots, A. H., & Murray, S. S. 2002, ApJ, 577, 710

Zezas, A., McDowell, J. C., Hadzidimitriou, D., Kalogera, V., Fabbiano, G., & Taylor, P. 2003, The Local Group as an Astrophysical Laboratory, 111

Table 1. *Chandra* source data statistics

Chandra field	Right Ascension (J2000.0) (h m s)	Declination (J2000.0) (° ′ ″)	Detected sources	Sources with $D_{off-axis} < 10'$
[1]	[2]	[3]	[4]	[5]
3	00 56 46.14	-72 18 10.78	28 (11)	27 (10)
4	00 49 30.74	-73 16 52.34	38 (16)	36 (16)
5	00 53 11.45	-72 26 29.91	37 (11)	36 (11)
6	00 53 04.40	-72 42 18.22	28 (8)	28 (8)
7	00 49 25.09	-72 44 22.80	27 (11)	26 (11)

Table 2. Optical counterparts of X-ray sources in *Chandra* field 3

X-ray		Optical counterpart										Notes
Src	Rad. (″)	Src ID	R.A. (J2000.0)	Decl.	Offset (″)	V	δV	B-V	δ(B − V)	U-B	δ(U − B)	
[1]	[2]	[3]	[4]	[5]	[6]	[7]	[8]	[9]	[10]	[11]	[12]	[13]
3_1	1.58	**O_7_267132**	00 57 19.80	-72 25 34.0	0.13	19.76	0.30	99.99	99.99	···	···	u, c
		O_7_267163	00 57 19.84	-72 25 33.5	0.54	19.54	0.33	99.99	99.99	···	···	
		(Z_3066294)	00 57 19.87	-72 25 34.0	0.21	18.66	0.06	0.78	0.08	-0.63	0.09	
		O_7_269933	00 57 19.77	-72 25 35.4	1.39	21.51	0.55	99.99	99.99	···	···	
3_2	2.18	**Z_2804383**	00 55 27.52	-72 11 00.5	2.01	20.30	0.07	-0.38	0.14	-0.33	0.16	u, c
		Z_2804939	00 55 27.75	-72 10 58.7	0.28	20.30	0.08	1.17	0.20	-1.85	0.22	
3_3	1.50	**O_8_49531**	00 57 36.01	-72 19 33.8	0.14	16.01	0.02	-0.02	0.04	···	···	c
		Z_3103982	00 57 36.09	-72 19 33.6	0.53	15.99	0.03	0.01	0.17	-1.05	0.17	
3_4	1.50	**O_8_56601**	00 57 32.76	-72 13 01.9	0.54	18.19	0.02	0.37	0.04	···	···	n, c
		Z_3096372	00 57 32.79	-72 13 01.9	0.62	18.28	0.04	0.20	0.05	-0.60	0.06	
3_5*	1.50	···	···	···	···	···	···	···	···	···	···	···
3_7	1.50	**Z_3075967**	00 57 24.02	-72 23 56.4	1.30	14.71	0.03	-0.07	0.03	-1.04	0.04	n
3_9	1.50	**Z_3003005**	00 56 52.62	-72 12 03.7	0.67	21.21	0.10	-0.55	0.12	99.99	99.99	n
3_12	1.80	**Z_3051372**	00 57 13.57	-72 23 59.1	1.41	21.14	0.11	0.51	0.21	99.99	99.99	n
3_14*	1.68	···	···	···	···	···	···	···	···	···	···	···
3_15	1.73	**O_8_49051**	00 57 44.04	-72 22 15.6	1.69	20.89	0.12	0.47	0.27	···	···	n
		Z_3122823	00 57 44.06	-72 22 15.7	1.61	20.91	0.10	0.33	0.18	0.11	0.35	
3_17	1.50	**Z_3072898**	00 57 22.72	-72 17 57.8	1.05	21.85	0.24	0.04	0.43	-0.35	0.58	n
3_18	1.50	**Z_2893439**	00 56 05.56	-72 21 59.0	0.72	15.88	0.03	-0.04	0.03	-1.09	0.04	c
3_19	2.88	**Z_3049033**	00 57 12.56	-72 10 45.6	2.71	17.95	0.04	-0.07	0.04	-0.80	0.27	u
		Z_3050592	00 57 13.23	-72 10 45.7	0.60	16.99	0.03	0.61	0.04	-0.08	0.05	
3_22	2.50	**Z_2899335**	00 56 08.08	-72 11 32.9	1.44	20.31	0.08	0.12	0.12	0.21	0.24	n
3_26	1.50	**Z_2871193**	00 55 56.04	-72 17 32.3	0.41	20.45	0.20	-0.35	0.22	99.99	99.99	n

*Sources which have OGLE-II coverage (thus available on-line finding charts) but no counterpart(s) (either in OGLE-II or MCPS catalogs).

Note. — Sources 3_6, 3_8, 3_10, 3_11, 3_13, 3_16, 3_20, 3_21, 3_23 to 3_25, 3_27, and 3_28 do not have OGLE-II coverage (thus no finding charts), and any MCPS counterpart(s).

Table 3. Optical counterparts of X-ray sources in *Chandra* field 4

X-ray					Optical counterpart							Notes
Src	Rad. ($''$)	Src ID	R.A. (J2000.0)	Decl. (J2000.0)	Offset ($''$)	V	δV	B-V	δ(B − V)	U-B	δ(U − B)	
[1]	[2]	[3]	[4]	[5]	[6]	[7]	[8]	[9]	[10]	[11]	[12]	[13]
4_1	1.50	**O_5_180026**	00 50 44.71	-73 16 05.0	0.55	15.44	0.04	-0.04	0.05	···	···	c
		Z_2131651	00 50 44.75	-73 16 05.3	0.60	15.48	0.04	-0.11	0.05	-0.91	0.04	
4_2	1.50	**O_5_111490**	00 49 13.63	-73 11 37.4	0.47	16.52	0.02	0.10	0.04	···	···	c
		Z_1938257	00 49 13.68	-73 11 37.5	0.54	16.44	0.04	0.19	0.05	-0.92	0.04	
		O_5_115042	00 49 13.57	-73 11 39.1	1.31	21.53	0.48	99.99	99.99	···	···	
4_3	2.10	**O_5_271074**	00 50 57.12	-73 10 07.7	0.28	14.54	0.01	-0.06	0.01	···	···	c
		Z_2159045	00 50 57.16	-73 10 07.8	0.14	14.35	0.05	0.08	0.06	-0.88	0.04	
4_4	1.50	**O_4_159896**	00 48 18.67	-73 20 59.7	0.54	16.58	0.02	-0.10	0.03	···	···	n, c
		Z_1825706	00 48 18.71	-73 20 59.7	0.38	16.18	0.04	0.25	0.04	-0.77	0.04	
		O_4_159964	00 48 18.86	-73 20 59.5	0.53	19.70	0.38	0.42	0.67	···	···	
		O_4_160861	00 48 18.69	-73 21 00.6	0.80	99.99	99.99	99.99	99.99	···	···	
		O_4_161021	00 48 18.58	-73 20 59.3	1.08	20.11	0.40	99.99	99.99	···	···	
		O_4_161025	00 48 18.90	-73 20 58.8	1.22	19.50	0.27	1.38	0.41	···	···	
		O_4_162035	00 48 19.05	-73 20 59.9	1.13	20.35	0.39	-0.02	0.47	···	···	
4_5	1.50	**O_5_111500**	00 49 29.81	-73 10 58.0	0.61	16.30	0.01	0.09	0.02	···	···	c
		Z_1971979	00 49 29.87	-73 10 58.2	0.65	16.15	0.03	0.20	0.05	-0.88	0.05	
4_6	1.50	**O_5_96912**	00 49 48.26	-73 22 10.9	0.59	21.29	0.40	-0.89	0.41	···	···	u
		Z_2010981	00 49 48.28	-73 22 11.1	0.53	19.99	0.06	0.70	0.12	-0.11	0.31	
		O_5_98236	00 49 48.12	-73 22 11.7	0.41	21.18	0.44	99.99	99.99	···	···	
4_7	1.82	O_5_11870	00 48 53.48	-73 24 56.9	1.26	99.99	99.99	99.99	99.99	···	···	c
		O_5_13241	00 48 53.44	-73 24 57.5	0.65	20.00	0.20	99.99	99.99	···	···	
		(Z_1896638)	00 48 53.51	-73 24 57.3	0.96	18.66	0.09	1.56	0.22	99.99	99.99	
		O_5_13232	00 48 53.27	-73 24 59.8	1.78	19.71	0.08	0.10	0.10	···	···	
		O_5_13242	00 48 53.68	-73 24 57.9	1.33	20.47	0.19	99.99	99.99	···	···	
		O_5_13244	00 48 53.33	-73 24 56.7	1.39	20.23	0.29	99.99	99.99	···	···	
		O_5_13245	00 48 53.25	-73 24 57.8	0.60	21.67	0.53	99.99	99.99	···	···	
		O_5_14615	00 48 53.54	-73 24 58.7	0.95	21.32	0.30	99.99	99.99	···	···	
		O_5_16026	00 48 53.68	-73 24 57.0	1.70	20.32	0.41	99.99	99.99	···	···	
4_8	3.99	**O_4_171264**	00 48 14.13	-73 10 03.5	0.63	15.74	0.04	0.01	0.05	···	···	n, c
		Z_1816472	00 48 14.18	-73 10 03.9	0.30	15.30	0.05	0.26	0.06	-0.50	0.05	
		O_4_171332	00 48 14.09	-73 10 04.6	0.55	17.78	0.05	1.64	0.28	···	···	
		O_4_171856	00 48 13.26	-73 10 04.8	3.93	19.42	0.06	0.62	0.13	···	···	
		Z_1814706	00 48 13.31	-73 10 04.8	3.70	19.60	0.15	0.13	0.17	99.99	99.99	
		O_4_171863	00 48 14.47	-73 10 03.2	1.67	18.54	0.16	-0.03	0.19	···	···	
		O_4_172639	00 48 13.57	-73 10 03.9	2.53	19.62	0.14	0.20	0.25	···	···	
		O_4_173769	00 48 13.57	-73 10 01.7	3.49	20.86	0.13	0.53	0.30	···	···	
		O_4_174934	00 48 14.77	-73 10 04.4	2.71	99.99	99.99	99.99	99.99	···	···	

Table 3—Continued

X-ray Src	X-ray Rad. (″)	Optical counterpart Src ID	R.A. (J2000.0)	Decl. (J2000.0)	Offset (″)	V	δV	B-V	δ(B − V)	U-B	δ(U − B)	Notes
[1]	[2]	[3]	[4]	[5]	[6]	[7]	[8]	[9]	[10]	[11]	[12]	[13]
		O_4_174937	00 48 14.70	-73 10 01.0	3.93	99.99	99.99	99.99	99.99	···	···	
4_10	3.30	O_4_156816†	00 48 32.97	-73 23 56.6	2.96	19.04	0.03	0.71	0.09	···	···	n
		O_5_11978†	00 48 32.96	-73 23 56.6	2.95	19.01	0.04	0.75	0.07	···	···	
		Z_1854839	00 48 32.97	-73 23 56.8	3.11	19.05	0.06	0.86	0.10	0.20	0.18	
		O_4_156830†	00 48 32.62	-73 23 54.2	1.32	17.80	0.02	-0.10	0.04	···	···	
		O_5_11982†	00 48 32.61	-73 23 54.2	1.36	17.81	0.02	-0.07	0.03	···	···	
		Z_1854152	00 48 32.64	-73 23 54.2	1.27	17.67	0.09	0.07	0.10	-0.57	0.07	
		O_4_158666	00 48 33.23	-73 23 50.7	3.28	20.52	0.09	0.81	0.26	···	···	
		O_5_15242	00 48 32.94	-73 23 54.1	0.47	21.02	0.32	-0.30	0.44	···	···	
		O_5_15268	00 48 32.91	-73 23 52.4	1.26	20.60	0.10	0.45	0.22	···	···	
		Z_1854803	00 48 32.95	-73 23 52.6	1.13	20.68	0.16	0.43	0.24	99.99	99.99	
4_11	1.87	**O_4_164855**	00 48 03.69	-73 16 59.8	1.05	18.88	0.04	-0.10	0.05	···	···	n
		Z_1795179	00 48 03.81	-73 17 00.1	1.40	18.20	0.07	0.36	0.09	-0.85	0.10	
4_12*	1.76	···	···	···	···	···	···	···	···	···	···	···
4_13	3.39	**O_5_90858**	00 49 50.80	-73 25 01.1	1.96	18.41	0.05	0.10	0.09	···	···	n
		Z_2016443	00 49 50.90	-73 25 01.3	2.07	18.35	0.08	0.09	0.10	-0.47	0.09	
		O_5_91343	00 49 51.51	-73 24 58.3	2.48	19.26	0.04	0.00	0.05	···	···	
		Z_2017849	00 49 51.57	-73 24 58.8	2.59	18.98	0.09	0.33	0.11	-0.55	0.12	
		O_5_92158	00 49 51.00	-73 25 00.3	1.00	20.62	0.23	-0.19	0.28	···	···	
		O_5_92159	00 49 51.35	-73 25 00.2	1.82	20.21	0.11	0.06	0.14	···	···	
		O_5_93600	00 49 50.48	-73 25 01.2	2.87	21.64	0.47	99.99	99.99	···	···	
		O_5_93617	00 49 51.76	-73 24 59.7	3.36	20.57	0.16	0.08	0.20	···	···	
4_14	1.93	**O_5_90506**	00 49 42.02	-73 23 14.2	1.93	14.98	0.02	0.05	0.03	···	···	c
		O_5_94651	00 49 41.68	-73 23 13.0	1.49	21.16	0.64	0.16	0.92	···	···	
		O_5_94669	00 49 42.34	-73 23 11.2	1.87	21.74	0.38	99.99	99.99	···	···	
4_15	1.50	O_5_21583	00 49 10.74	-73 17 16.9	0.51	20.18	0.22	99.99	99.99	···	···	n, c
		O_5_22301	00 49 10.95	-73 17 16.9	1.20	19.28	0.18	0.58	0.18	···	···	
		Z_1932585	00 49 10.91	-73 17 17.1	1.00	18.81	0.07	1.00	0.09	0.06	0.17	
		O_5_23325	00 49 10.51	-73 17 16.9	0.92	20.33	0.40	99.99	99.99	···	···	
		(Z_1931568)	00 49 10.44	-73 17 16.4	1.47	19.94	0.09	0.73	0.11	99.99	99.99	
4_16	1.50	**O_5_27768**	00 49 05.48	-73 14 10.2	1.29	19.93	0.07	0.84	0.20	···	···	n
4_17	1.61	**O_5_180008**	00 50 47.99	-73 18 17.6	0.99	15.30	0.07	0.05	0.10	···	···	n, c
		Z_2138888	00 50 48.03	-73 18 17.9	0.67	15.07	0.03	0.12	0.05	-1.00	0.05	
		O_5_180929	00 50 48.27	-73 18 17.4	1.27	19.42	0.30	-0.42	0.38	···	···	
4_18	1.92	**O_5_92756**	00 49 49.51	-73 23 06.8	0.99	19.91	0.07	-0.02	0.10	···	···	n
		Z_2013579	00 49 49.52	-73 23 06.9	1.05	19.94	0.08	0.24	0.10	-0.29	0.19	
		O_5_94741	00 49 49.96	-73 23 04.9	1.72	21.09	0.23	0.38	0.34	···	···	
4_19	1.82	**O_5_262679**	00 50 55.26	-73 18 02.3	1.40	19.41	0.09	-0.26	0.10	···	···	n
		Z_2154899	00 50 55.29	-73 18 02.6	1.15	19.05	0.06	0.16	0.08	-0.24	0.11	

Table 3—Continued

X-ray Src	X-ray Rad. (″)	Src ID	Optical counterpart R.A. (J2000.0)	Decl. (J2000.0)	Offset (″)	V	δV	B-V	δ(B − V)	U-B	δ(U − B)	Notes
[1]	[2]	[3]	[4]	[5]	[6]	[7]	[8]	[9]	[10]	[11]	[12]	[13]
4_20	2.72	**O_5_259514**	00 50 59.04	-73 20 57.7	1.87	21.07	0.15	0.54	0.25	···	···	n
4_21	3.22	**O_5_256084**	00 51 01.70	-73 21 35.9	2.59	17.93	0.06	0.88	0.15	···	···	n, c
		(Z_2169351)	00 51 01.74	-73 21 36.3	2.63	17.18	0.11	2.03	0.13	-1.22	0.12	
		O_5_256315	00 51 01.93	-73 21 34.7	1.39	18.63	0.04	0.76	0.09	···	···	
		Z_2169776	00 51 01.93	-73 21 35.0	1.38	18.36	0.10	0.81	0.12	-0.81	0.12	
		O_5_256826	00 51 02.26	-73 21 36.6	1.75	18.33	0.04	-0.18	0.05	···	···	
		Z_2170562	00 51 02.28	-73 21 37.0	2.20	18.06	0.10	0.16	0.11	-0.62	0.06	
		O_5_259099	00 51 01.88	-73 21 37.5	3.09	20.13	0.10	0.12	0.15	···	···	
		O_5_259115	00 51 02.66	-73 21 36.1	2.16	21.16	0.31	0.76	0.58	···	···	
		O_5_259158	00 51 01.97	-73 21 32.7	2.47	20.88	0.17	-0.48	0.20	···	···	
		O_5_260535	00 51 01.61	-73 21 33.9	2.91	21.25	0.27	-0.13	0.36	···	···	
4_22	3.81	O_5_90840	00 49 55.97	-73 25 16.6	3.20	18.40	0.03	0.68	0.06	···	···	n
		Z_2027202	00 49 56.01	-73 25 17.0	2.87	18.21	0.04	0.96	0.24	99.99	99.99	
		O_5_91270	00 49 56.15	-73 25 19.0	2.32	18.26	0.03	-0.07	0.03	···	···	
		Z_2027575	00 49 56.20	-73 25 19.3	2.32	18.13	0.04	0.04	0.07	-0.41	0.08	
		O_5_92049	00 49 56.66	-73 25 21.3	3.29	19.49	0.05	-0.05	0.07	···	···	
		Z_2028724	00 49 56.74	-73 25 21.7	3.66	19.43	0.07	0.03	0.09	99.99	99.99	
		O_5_92063	00 49 56.97	-73 25 16.5	2.06	21.28	0.23	0.65	0.36	···	···	
		O_5_92077	00 49 56.77	-73 25 14.5	3.55	20.74	0.11	0.76	0.18	···	···	
		O_5_93443	00 49 55.90	-73 25 17.8	3.18	20.23	0.15	0.01	0.21	···	···	
4_23	1.50	**O_5_101577**	00 49 57.52	-73 16 55.1	1.46	99.99	99.99	99.99	99.99	···	···	u
		Z_2029266	00 49 57.00	-73 16 54.1	1.39	19.30	0.12	1.43	0.17	99.99	99.99	
4_24	1.50	**O_5_179505**	00 50 10.08	-73 19 30.8	0.83	20.96	0.40	0.13	0.47	···	···	n, c
4_25	2.33	**O_5_176711**	00 50 42.94	-73 21 40.0	2.13	19.49	0.11	-0.18	0.11	···	···	n
		(Z_2127712)	00 50 42.95	-73 21 40.5	2.29	18.86	0.06	0.27	0.07	-0.12	0.09	
		O_5_178210	00 50 42.72	-73 21 40.2	1.27	20.26	0.33	0.31	0.37	···	···	
4_26	1.58	**O_5_193908**	00 50 05.32	-73 11 45.7	0.61	21.54	0.32	99.99	99.99	···	···	n
4_27*	1.50	···	···	···	···	···	···	···	···	···	···	···
4_28	1.50	**O_5_25130**	00 48 47.13	-73 17 20.3	1.20	21.61	0.38	99.99	99.99	···	···	n
4_29	3.06	**O_5_266399**	00 51 09.80	-73 13 34.8	2.15	19.20	0.04	0.66	0.08	···	···	n
		O_5_268082	00 51 10.02	-73 13 34.2	1.11	20.28	0.26	1.01	0.39	···	···	
		(Z_2187387)	00 51 09.93	-73 13 34.3	1.51	18.99	0.12	1.18	0.24	0.25	0.38	
		O_5_267042	00 51 10.35	-73 13 35.4	1.27	20.37	0.30	0.14	0.41	···	···	
		O_5_268096	00 51 09.89	-73 13 32.1	2.66	20.84	0.26	0.51	0.43	···	···	
		O_5_269842	00 51 10.48	-73 13 34.3	0.89	20.11	0.22	0.19	0.26	···	···	
4_30	1.50	**O_5_25176**	00 48 54.33	-73 17 16.1	0.80	20.47	0.15	0.29	0.33	···	···	n
4_31	2.48	**O_5_33605**	00 48 44.36	-73 10 26.3	2.39	20.33	0.25	1.06	0.39	···	···	n
		O_5_34786	00 48 44.83	-73 10 27.4	0.24	21.22	0.29	1.20	0.59	···	···	

Table 3—Continued

X-ray Src	Rad. (″)	Src ID	R.A. (J2000.0)	Decl.	Optical counterpart Offset (″)	V	δV	B-V	δ(B − V)	U-B	δ(U − B)	Notes
[1]	[2]	[3]	[4]	[5]	[6]	[7]	[8]	[9]	[10]	[11]	[12]	[13]
		O_5_37833	00 48 45.24	-73 10 29.0	2.29	21.35	0.25	0.12	0.39	···	···	
4_32	1.50	**O_5_111737**	00 49 27.21	-73 12 12.8	1.34	18.62	0.04	0.76	0.07	···	···	n, c
		O_5_114647	00 49 27.07	-73 12 11.7	0.34	20.98	0.47	0.33	0.59	···	···	
4_33	1.50	**O_5_99201**	00 49 56.12	-73 20 37.2	1.39	20.73	0.10	0.03	0.16	···	···	n
4_34*	1.50	···	···	···	···	···	···	···	···	···	···	···
4_35	1.50	**O_5_101481**	00 49 42.72	-73 17 20.2	1.47	19.36	0.23	0.88	0.55	···	···	n
		O_5_101851	00 49 42.87	-73 17 21.2	0.35	20.98	0.49	99.99	99.99	···	···	
4_36[d]	1.51	O_5_187956	00 50 45.14	-73 15 40.3	1.33	20.53	0.40	99.99	99.99	···	···	n, c
		Z_2132222[o]	00 50 45.02	-73 15 40.7	1.29	18.27	0.04	0.91	0.06	-0.04	0.13	
4_37	1.73	O_4_166430	00 48 08.62	-73 15 48.6	1.26	21.05	0.18	-0.12	0.21	···	···	n
		Z_1805231	00 48 08.68	-73 15 49.0	1.68	19.71	0.12	-0.12	0.18	99.99	99.99	
		O_4_166445	00 48 08.41	-73 15 46.4	1.17	20.60	0.14	0.26	0.20	···	···	

[†]Sources detected in two neighboring OGLE-II fields.

[o]Just outside the error circle of the X-ray source there is another OGLE-II source (not listed in these tables), that it is most likely related to the detected MCPS source within the search radius.

[d]OGLE-II detected two sources instead of one star (suggested by the visual inspection of the finding chart).

*Sources which have OGLE-II coverage (thus available on-line finding charts) but no counterpart(s) (either in OGLE-II or MCPS catalogs).

Note. — Sources 4_9 and 4_38 do not have OGLE-II coverage (thus no finding charts), and any MCPS counterpart(s).

Table 4. Optical counterparts of X-ray sources in *Chandra* field 5

X-ray					Optical counterpart							Notes
Src	Rad. (″)	Src ID	R.A. (J2000.0)	Decl.	Offset (″)	V	δV	B-V	δ(B − V)	U-B	δ(U − B)	
[1]	[2]	[3]	[4]	[5]	[6]	[7]	[8]	[9]	[10]	[11]	[12]	[13]
5_1**	1.50	**Z_2311496**	00 52 05.69	-72 26 04.0	0.55	14.91	0.02	0.00	0.03	-0.97	0.04	c
5_2**	1.50	**Z_2498173**	00 53 23.90	-72 27 15.4	0.24	16.19	0.12	-0.09	0.12	-1.05	0.04	c
5_3	1.62	**O_6_85614**	00 51 53.11	-72 31 48.3	0.54	14.90	0.12	-0.27	0.13	···	···	c
		Z_2282823	00 51 53.18	-72 31 48.4	0.43	14.38	0.02	0.41	0.03	-1.13	0.11	
		O_6_85986	00 51 53.30	-72 31 49.1	0.69	99.99	99.99	99.99	99.99	···	···	
5_4	2.50	**O_7_70843**	00 54 46.37	-72 25 22.6	0.79	15.58	0.02	99.99	99.99	···	···	n, c
		Z_2707354	00 54 46.39	-72 25 22.7	0.83	15.36	0.05	0.14	0.06	-1.11	0.13	
		O_7_71473	00 54 46.06	-72 25 24.0	1.23	19.57	0.13	99.99	99.99	···	···	
		O_7_71474	00 54 45.79	-72 25 23.3	1.97	19.30	0.05	99.99	99.99	···	···	
		O_7_71481	00 54 46.08	-72 25 21.4	1.73	18.83	0.09	99.99	99.99	···	···	
		O_7_73194	00 54 46.02	-72 25 21.9	1.43	19.68	0.24	99.99	99.99	···	···	
5_6**	4.85	**Z_2748033**	00 55 03.63	-72 22 31.2	3.60	17.86	0.03	-0.03	0.05	-0.79	0.06	n
		Z_2749296	00 55 04.18	-72 22 25.9	4.61	20.82	0.11	0.79	0.21	99.99	99.99	
		Z_2749725	00 55 04.37	-72 22 30.3	0.16	20.03	0.05	2.01	0.20	99.99	99.99	
		Z_2750215	00 55 04.58	-72 22 34.5	4.22	20.34	0.12	-0.02	0.15	-0.52	0.15	
		Z_2751240	00 55 04.99	-72 22 27.6	3.83	19.94	0.06	0.58	0.11	99.99	99.99	
5_7	3.07	**O_7_70829**	00 54 56.17	-72 26 47.6	1.19	15.30	0.01	-0.04	0.02	···	···	c
		Z_2730786	00 54 56.26	-72 26 47.4	1.21	15.27	0.03	-0.05	0.04	-1.07	0.04	
		O_7_72789	00 54 56.10	-72 26 49.4	1.41	20.62	0.27	0.42	0.43	···	···	
		O_7_72806	00 54 56.67	-72 26 46.0	2.92	20.37	0.22	0.24	0.43	···	···	
		O_7_74196	00 54 55.76	-72 26 49.1	2.70	20.84	0.33	0.47	0.54	···	···	
5_8	1.97	**O_7_71334**	00 54 36.72	-72 26 38.1	1.61	19.16	0.05	0.78	0.06	···	···	n
		Z_2683599	00 54 36.80	-72 26 37.8	1.34	19.10	0.05	0.83	0.07	0.30	0.14	
5_9**	1.50	Z_2530728	00 53 37.65	-72 24 10.4	1.28	19.68	0.11	0.40	0.14	0.10	0.18	n, c
		Z_2531366	00 53 37.93	-72 24 08.1	1.33	18.19	0.06	0.59	0.07	-0.13	0.09	
5_10**	2.70	**Z_2702542**	00 54 44.44	-72 23 58.1	2.17	19.37	0.07	0.85	0.09	-0.47	0.16	n
		Z_2702553	00 54 44.45	-72 24 00.0	2.53	21.23	0.17	0.06	0.21	99.99	99.99	
		Z_2705059	00 54 45.46	-72 23 58.5	2.50	21.92	0.37	-0.22	0.41	99.99	99.99	
5_12**	1.50	**Z_2406014**	00 52 45.10	-72 28 43.4	0.35	14.92	0.08	0.00	0.09	-0.97	0.04	n, c
5_13**	3.92	Z_2561198	00 53 50.54	-72 18 19.4	2.54	19.95	0.06	-0.53	0.14	1.16	0.19	n
		Z_2563156	00 53 51.34	-72 18 17.4	1.84	19.65	0.14	-0.40	0.16	-0.06	0.14	
5_14	2.69	**O_7_72871**	00 54 51.25	-72 26 31.1	2.23	20.70	0.21	-0.58	0.23	···	···	n
		O_7_74351	00 54 50.61	-72 26 30.6	1.43	21.73	0.32	0.53	0.50	···	···	
5_15	2.61	**O_7_71429**	00 54 48.97	-72 25 44.6	0.50	19.00	0.10	0.18	0.12	···	···	c
		(Z_2713702)	00 54 49.04	-72 25 45.2	0.92	18.81	0.05	0.42	0.08	-0.98	0.09	
		O_7_72057	00 54 48.31	-72 25 45.1	2.53	19.22	0.04	-0.05	0.07	···	···	
		Z_2712098	00 54 48.36	-72 25 45.3	2.36	19.21	0.08	-0.01	0.13	-0.34	0.12	

Table 4—Continued

X-ray Src	Rad. (″)	Src ID	Optical counterpart R.A. (J2000.0)	Decl. (J2000.0)	Offset (″)	V	δV	B-V	δ(B − V)	U-B	δ(U − B)	Notes
[1]	[2]	[3]	[4]	[5]	[6]	[7]	[8]	[9]	[10]	[11]	[12]	[13]
		O_7_72059	00 54 48.74	-72 25 43.4	1.44	20.54	0.08	0.18	0.16	···	···	
		(Z_2713147)	00 54 48.81	-72 25 44.0	0.76	20.25	0.18	0.76	0.25	99.99	99.99	
		O_7_73093	00 54 48.79	-72 25 47.3	2.59	20.57	0.15	1.17	0.57	···	···	
		O_7_73100	00 54 48.88	-72 25 46.1	1.37	20.12	0.09	-0.13	0.12	···	···	
5_16**	1.50	**Z_2573354**	00 53 55.38	-72 26 45.3	0.83	14.72	0.03	-0.07	0.03	-1.02	0.04	c
5_18**	4.51	Z_2205777	00 51 18.29	-72 30 01.4	2.34	21.38	0.18	0.51	0.26	99.99	99.99	n
		Z_2207680	00 51 19.15	-72 30 01.0	2.74	18.90	0.05	0.31	0.06	-0.22	0.08	
		Z_2208320	00 51 19.45	-72 30 05.8	4.50	21.61	0.18	-0.03	0.24	99.99	99.99	
5_21	1.88	O_6_324429	00 53 52.41	-72 32 01.2	1.67	19.26	0.22	0.69	0.32	···	···	n
		(Z_2565806)	00 53 52.40	-72 32 01.1	1.58	18.51	0.06	1.63	0.23	-2.24	0.23	
		O_6_324585	00 53 52.20	-72 32 01.1	1.87	19.08	0.12	0.02	0.15	···	···	
		O_6_327160	00 53 52.44	-72 31 59.0	0.53	21.46	0.42	99.99	99.99	···	···	
5_22	2.34	**O_6_87363**	00 51 58.97	-72 30 57.6	0.88	19.63	0.06	-0.03	0.08	···	···	n, c
		Z_2296070	00 51 59.01	-72 30 57.5	0.75	19.64	0.08	0.07	0.09	-0.41	0.08	
5_23**	3.34	**Z_2288276**	00 51 55.61	-72 20 40.2	2.57	17.99	0.03	-0.06	0.04	-0.69	0.05	n
		Z_2289471	00 51 56.13	-72 20 35.8	2.51	19.35	0.05	0.48	0.10	0.30	0.20	
5_24**	1.50	**Z_2595629**	00 54 03.92	-72 26 32.8	0.78	14.95	0.03	0.01	0.04	-1.13	0.06	n, c
5_25**	3.02	**Z_2686280**	00 54 37.90	-72 22 11.4	1.81	18.48	0.04	0.98	0.07	0.08	0.11	n
		Z_2687267	00 54 38.30	-72 22 08.9	1.38	20.83	0.09	0.22	0.14	99.99	99.99	
5_26**	3.15	Z_2264995	00 51 45.19	-72 21 53.5	2.80	19.57	0.06	0.83	0.10	0.53	0.34	n, c
		Z_2266383	00 51 45.82	-72 21 50.2	1.88	19.22	0.09	-0.03	0.10	-0.39	0.08	
5_27**	1.50	**Z_2556246**	00 53 48.53	-72 28 01.9	1.48	19.65	0.06	0.98	0.11	0.74	0.40	n
5_28**	1.50	**Z_2359566**	00 52 25.73	-72 23 12.0	0.87	19.40	0.07	0.88	0.09	0.02	0.16	n, c
5_29**	1.50	**Z_2581383**	00 53 58.50	-72 26 14.4	0.78	17.81	0.04	-0.14	0.05	-0.82	0.06	n, c
5_30	2.64	**O_6_324153**†	00 54 28.58	-72 31 06.5	2.45	19.39	0.04	1.71	0.19	···	···	n, c
		O_7_66235†	00 54 28.59	-72 31 06.5	2.40	19.38	0.04	1.69	0.13	···	···	
		O_6_327594	00 54 29.65	-72 31 06.2	2.41	99.99	99.99	99.99	99.99	···	···	
		Z_2663497°	00 54 28.90	-72 31 08.5	2.62	19.96	0.12	0.03	0.14	-0.34	0.14	
5_31**	1.68	**Z_2562687**	00 53 51.14	-72 21 24.1	0.90	20.96	0.17	0.49	0.24	99.99	99.99	n, c
5_32**	2.30	**Z_2315739**	00 52 07.48	-72 21 25.3	2.22	15.20	0.03	-0.07	0.03	-0.62	0.04	n
5_33**	1.50	**Z_2578607**	00 53 57.43	-72 24 43.0	1.07	20.80	0.14	0.38	0.19	99.99	99.99	n
5_34	1.69	**O_6_327685**	00 54 04.67	-72 30 54.1	1.20	20.78	0.15	0.20	0.21	···	···	n
		Z_2598422°	00 54 04.96	-72 30 53.5	1.69	19.51	0.07	0.42	0.10	-0.35	0.12	
5_36**	3.19	Z_2510874	00 53 29.23	-72 18 31.6	2.48	21.31	0.19	-0.04	0.23	0.21	0.44	n
		Z_2511547	00 53 29.52	-72 18 35.6	1.89	19.70	0.10	0.15	0.11	-0.08	0.14	
5_37*	1.69	···	···	···	···	···	···	···	···	···	···	···

†Sources detected in two neighboring OGLE-II fields.

°Just outside the error circle of the X-ray source there is another OGLE-II source (not listed in these tables), that it is most likely related to the detected MCPS source within the search radius.

*Source with OGLE-II coverage (thus available on-line finding chart) but no counterpart(s) (either in OGLE-II or MCPS catalogs).

**Sources which do not have OGLE-II coverage (thus no available on-line finding charts) but they have MCPS counterparts within their search radius.

Note. — Sources 5_5, 5_11, 5_17, 5_19, 5_20, and 5_35 do not have OGLE-II coverage (thus no finding charts), and any MCPS counterpart(s).

Table 5. Optical counterparts of X-ray sources in *Chandra* field 6

X-ray Src	X-ray Rad. (″)	Src ID	Optical counterpart R.A. (J2000.0)	Decl. (J2000.0)	Offset (″)	V	δV	B-V	δ(B − V)	U-B	δ(U − B)	Notes
[1]	[2]	[3]	[4]	[5]	[6]	[7]	[8]	[9]	[10]	[11]	[12]	[13]
6_1	1.50	**O_6_77228**	00 52 08.95	-72 38 02.9	0.58	15.03	0.02	0.14	0.03	···	···	c
		Z_2319498	00 52 09.07	-72 38 03.1	0.64	15.23	0.03	-0.08	0.03	-0.81	0.04	
6_2	1.91	**O_7_47103**	00 54 55.87	-72 45 10.7	0.40	15.01	0.01	-0.02	0.01	···	···	c
		Z_2729974	00 54 55.91	-72 45 10.6	0.61	15.00	0.03	-0.03	0.04	-0.93	0.18	
6_3	1.50	**O_6_153267**	00 52 42.20	-72 47 21.0	1.38	18.15	0.07	-0.14	0.08	···	···	n
		Z_2399147	00 52 42.27	-72 47 20.9	1.30	17.81	0.06	0.04	0.08	-0.52	0.07	
		O_6_154606	00 52 42.24	-72 47 19.1	0.54	20.16	0.09	0.52	0.15	···	···	
		O_6_155950	00 52 42.40	-72 47 20.6	1.15	20.39	0.21	0.09	0.27	···	···	
6_4	1.86	**O_6_147662**	00 52 52.28	-72 48 29.8	0.27	14.42	0.05	-0.10	0.05	···	···	c
		Z_2423181	00 52 52.35	-72 48 29.8	0.56	14.36	0.03	-0.05	0.04	-0.97	0.04	
		O_6_152322	00 52 51.93	-72 48 28.5	1.84	99.99	99.99	99.99	99.99	···	···	
6_5	1.69	**O_6_79076**	00 52 03.31	-72 38 30.2	0.84	20.44	0.17	0.37	0.19	···	···	n
		Z_2305973	00 52 03.30	-72 38 30.4	0.64	19.88	0.06	0.39	0.12	99.99	99.99	
6_6	2.41	O_6_148861	00 52 45.77	-72 49 19.1	1.30	19.76	0.08	0.88	0.14	···	···	n, c
		Z_2407810	00 52 45.86	-72 49 19.0	1.41	19.76	0.07	1.19	0.16	99.99	99.99	
		O_6_149910	00 52 45.24	-72 49 18.2	2.00	19.55	0.05	-0.02	0.06	···	···	
		Z_2406433	00 52 45.28	-72 49 18.2	1.82	19.48	0.07	0.10	0.08	99.99	99.99	
6_7*	1.50	···	···	···	···	···	···	···	···	···	···	···
6_8	2.06	**O_6_306524**	00 54 21.68	-72 45 34.0	2.02	17.60	0.01	1.12	0.06	···	···	n
		Z_2644493	00 54 21.71	-72 45 34.0	1.95	17.37	0.06	1.26	0.07	0.74	0.11	
		O_6_307574	00 54 22.34	-72 45 32.0	1.58	19.14	0.05	0.03	0.07	···	···	
		Z_2646086	00 54 22.33	-72 45 31.9	1.57	18.99	0.06	0.20	0.14	-0.38	0.14	
		O_6_308458	00 54 22.06	-72 45 34.5	1.89	19.88	0.14	0.14	0.15	···	···	
		O_6_310253	00 54 22.00	-72 45 32.5	0.13	21.24	0.32	0.51	0.39	···	···	
		O_6_310266	00 54 22.08	-72 45 31.1	1.55	20.46	0.14	0.10	0.21	···	···	
6_9	1.50	**O_6_238962**	00 53 32.39	-72 43 17.3	1.15	19.93	0.14	-0.14	0.16	···	···	n
		O_6_240354	00 53 32.43	-72 43 15.6	1.37	99.99	99.99	99.99	99.99	···	···	
6_10	1.50	**O_6_157291**	00 52 59.08	-72 45 10.2	1.12	20.65	0.15	0.27	0.20	···	···	n
6_11	3.09	O_6_322008†	00 54 27.55	-72 37 20.6	2.13	21.07	0.19	0.12	0.24	···	···	n
		O_7_60612†	00 54 27.55	-72 37 20.7	2.19	21.12	0.33	0.05	0.41	···	···	
		O_6_322014†	00 54 26.64	-72 37 19.5	2.53	21.10	0.44	-0.11	0.44	···	···	
		O_7_59068†	00 54 26.68	-72 37 19.3	2.33	20.41	0.13	0.24	0.27	···	···	
		Z_2657832	00 54 26.75	-72 37 19.3	2.01	20.07	0.20	0.29	0.22	0.36	0.26	
		O_6_322031†	00 54 27.53	-72 37 18.2	1.77	21.43	0.31	0.47	0.46	···	···	
		O_7_60644†	00 54 27.49	-72 37 18.2	1.63	21.50	0.20	0.29	0.35	···	···	
		O_6_323805†	00 54 27.80	-72 37 18.2	2.86	21.07	0.16	0.29	0.22	···	···	
		O_7_60649†	00 54 27.84	-72 37 18.1	3.07	21.15	0.16	0.22	0.22	···	···	
		Z_2657679°	00 54 26.69	-72 37 17.3	2.92	17.07	0.03	0.36	0.05	0.03	0.05	
6_12	1.55	**O_6_235232**	00 53 39.01	-72 47 17.4	0.27	99.99	99.99	99.99	99.99	···	···	n

Table 5—Continued

X-ray Src	Rad. (″)	Src ID	R.A. (J2000.0)	Decl.	Optical counterpart Offset (″)	V	δV	B-V	δ(B − V)	U-B	δ(U − B)	Notes
[1]	[2]	[3]	[4]	[5]	[6]	[7]	[8]	[9]	[10]	[11]	[12]	[13]
6_13	2.60	O_6_151822	00 52 31.58	-72 49 15.4	1.03	21.24	0.21	0.48	0.35	···	···	n
		Z_2373703	00 52 31.66	-72 49 15.4	1.31	21.61	0.24	1.24	0.55	99.99	99.99	
		O_6_152785	00 52 31.33	-72 49 18.1	2.01	20.74	0.17	0.12	0.26	···	···	
6_14	1.66	O_6_168813	00 52 44.92	-72 36 36.3	1.48	21.17	0.26	99.99	99.99	···	···	n
		O_6_169942	00 52 44.90	-72 36 38.5	0.78	20.79	0.28	0.68	0.38	···	···	
		O_6_169953	00 52 44.50	-72 36 37.7	1.57	20.47	0.34	99.99	99.99	···	···	
		O_6_169962	00 52 45.04	-72 36 37.1	1.07	20.36	0.12	0.22	0.14	···	···	
6_15	1.50	**O_6_74072**	00 52 11.10	-72 43 57.2	0.63	21.05	0.14	0.43	0.32	···	···	n
		Z_2324388	00 52 11.15	-72 43 57.3	0.79	21.35	0.23	0.99	0.49	99.99	99.99	
6_16	2.05	**O_6_228490**	00 53 15.78	-72 48 49.1	1.30	19.68	0.07	0.67	0.12	···	···	n
		Z_2478947	00 53 15.86	-72 48 49.1	1.10	19.59	0.06	0.72	0.10	0.01	0.26	
		O_6_231394	00 53 16.33	-72 48 49.5	1.62	21.09	0.21	0.44	0.33	···	···	
6_17	1.50	**O_6_248830**	00 53 33.42	-72 37 22.9	1.49	21.03	0.12	0.11	0.19	···	···	n
6_18[†c]	1.50	**O_6_74071**	00 52 10.10	-72 43 57.2	0.39	20.27	0.08	0.38	0.13	···	···	n
		Z_2322033	00 52 10.15	-72 43 57.3	0.29	20.41	0.14	0.78	0.25	-0.93	0.34	
6_19	3.87	**O_6_321630**	00 54 11.42	-72 35 12.0	1.14	21.02	0.20	99.99	99.99	···	···	n
		O_6_323167	00 54 11.05	-72 35 11.6	0.96	21.41	0.24	0.26	0.32	···	···	
		Z_2615243	00 54 11.06	-72 35 12.0	0.65	21.37	0.17	0.46	0.31	-0.37	0.47	
6_20	1.50	**O_6_311169**	00 54 09.53	-72 41 42.9	0.62	13.71	0.14	0.39	0.19	···	···	n, c
		Z_2611188[‡]	00 54 09.57	-72 41 42.9	0.64	13.82	0.05	-0.05	0.13	-0.67	0.12	
6_21	1.50	**O_6_242351**	00 53 25.24	-72 39 41.5	1.47	19.14	0.05	0.75	0.06	···	···	n, c
		O_6_245027	00 53 24.89	-72 39 42.3	0.96	20.97	0.19	0.37	0.26	···	···	
6_22	3.46	**O_7_48946**	00 54 49.96	-72 45 02.3	1.11	20.08	0.08	-0.09	0.13	···	···	n
		O_7_50553	00 54 49.86	-72 45 03.4	1.84	20.28	0.07	0.09	0.16	···	···	
		(Z_2715848)	00 54 49.95	-72 45 02.6	1.16	19.50	0.06	0.05	0.07	-0.07	0.08	
		O_7_48950	00 54 50.25	-72 45 02.5	0.21	21.47	0.32	1.00	0.81	···	···	
		O_7_50544	00 54 50.55	-72 45 04.4	2.51	21.35	0.11	0.33	0.31	···	···	
		(Z_2717021)	00 54 50.44	-72 45 05.3	3.06	21.50	0.20	0.98	0.46	99.99	99.99	
		O_7_50568	00 54 49.59	-72 45 02.1	2.77	21.26	0.16	0.40	0.30	···	···	
		O_7_50583	00 54 49.72	-72 45 00.7	2.76	21.67	0.28	-0.36	0.35	···	···	
		(Z_2715501)	00 54 49.80	-72 45 00.9	2.36	20.77	0.14	0.28	0.26	99.99	99.99	
		O_7_50584	00 54 50.52	-72 45 00.9	2.04	21.55	0.29	0.01	0.35	···	···	
6_23	1.50	**O_6_158108**	00 52 40.00	-72 42 44.4	0.56	17.10	0.05	1.42	0.15	···	···	n, c
		Z_2393742	00 52 40.01	-72 42 44.5	0.49	16.92	0.05	1.21	0.07	1.92	0.16	
		O_6_159120	00 52 39.85	-72 42 46.1	1.29	18.95	0.05	-0.08	0.06	···	···	
6_24*	1.74	···	···	···	···	···	···	···	···	···	···	···
6_25	2.66	O_6_247697	00 53 08.98	-72 34 51.5	1.73	20.06	0.09	0.72	0.14	···	···	n
		O_6_250104	00 53 08.63	-72 34 53.9	2.42	20.95	0.23	0.36	0.28	···	···	
		O_6_250120	00 53 08.91	-72 34 53.4	2.38	21.31	0.27	-0.01	0.30	···	···	

Table 5—Continued

X-ray Src	X-ray Rad. (″)	Optical counterpart Src ID	R.A. (J2000.0)	Decl. (J2000.0)	Offset (″)	V	δV	B-V	δ(B − V)	U-B	δ(U − B)	Notes
[1]	[2]	[3]	[4]	[5]	[6]	[7]	[8]	[9]	[10]	[11]	[12]	[13]
		O_6_250136	00 53 08.23	-72 34 51.1	1.68	19.93	0.08	-0.08	0.09	···	···	
		Z_2461085	00 53 08.32	-72 34 51.3	1.28	20.04	0.13	-0.13	0.14	0.06	0.29	
		O_6_250146	00 53 08.66	-72 34 50.0	1.52	99.99	99.99	99.99	99.99	···	···	
6_26*	1.50	···	···	···	···	···	···	···	···	···	···	···
6_27*	1.91	···	···	···	···	···	···	···	···	···	···	···
6_28*	2.79	···	···	···	···	···	···	···	···	···	···	···

†Sources detected in two neighboring OGLE-II fields.

‡The I band photometry in the MCPS catalog was replaced with that from the OGLE-II (see Zaritsky et al. (2002) for more details).

°Just outside the error circle of the X-ray source there is another OGLE-II source (not listed in these tables), that it is most likely related to the detected MCPS source within the search radius.

fcThe finding chart of *Chandra* source 6_18 includes also source 6_15 as these sources are too near to each other.

*Sources which have OGLE-II coverage (thus available on-line finding charts) but no counterpart(s) (either in OGLE-II or MCPS catalogs).

Table 6. Optical counterparts of X-ray sources in *Chandra* field 7

X-ray			Optical counterpart									Notes
Src	Rad. (″)	Src ID	R.A. (J2000.0)	Decl.	Offset (″)	V	δV	B-V	δ(B − V)	U-B	δ(U − B)	
[1]	[2]	[3]	[4]	[5]	[6]	[7]	[8]	[9]	[10]	[11]	[12]	[13]
7_1	1.50	**O_5_65517**	00 49 03.34	-72 50 52.1	0.45	16.94	0.06	0.09	0.10	···	···	c
		Z_1916984	00 49 03.41	-72 50 52.3	0.35	16.78	0.04	0.08	0.06	-0.84	0.05	
		O_5_65743	00 49 03.30	-72 50 53.7	1.20	18.86	0.23	0.15	0.38	···	···	
		(Z_1916967)	00 49 03.40	-72 50 53.9	1.35	18.08	0.06	0.07	0.12	-0.32	0.13	
		O_5_66768	00 49 03.24	-72 50 53.2	0.86	18.89	0.28	-0.08	0.37	···	···	
7_2**	1.50	**Z_1976595**	00 49 32.05	-72 39 25.2	0.40	20.50	0.09	0.33	0.13	99.99	99.99	n
7_3	1.60	O_5_147467	00 50 00.38	-72 49 28.9	0.76	20.75	0.29	99.99	99.99	···	···	n, c
		O_5_149072	00 50 00.17	-72 49 28.8	0.19	20.78	0.42	99.99	99.99	···	···	
		O_5_149088	00 50 00.50	-72 49 28.0	1.56	22.12	0.53	99.99	99.99	···	···	
		O_5_146630	00 50 00.30	-72 49 28.1	0.88	20.60	0.35	99.99	99.99	···	···	
		(Z_2036310)	00 50 00.34	-72 49 28.4	0.78	19.53	0.07	1.30	0.11	0.01	0.35	
		O_5_147479	00 50 00.20	-72 49 27.6	1.28	21.77	0.42	99.99	99.99	···	···	
7_4	3.08	**O_5_140754**	00 49 44.22	-72 52 08.4	2.10	17.52	0.07	1.58	0.17	···	···	u, c
		Z_2002622	00 49 44.34	-72 52 08.6	1.83	17.28	0.07	1.52	0.08	99.99	99.99	
		O_5_141207	00 49 44.43	-72 52 09.7	0.76	17.85	0.05	0.23	0.16	···	···	
		Z_2003040	00 49 44.52	-72 52 10.0	0.79	17.60	0.08	0.01	0.09	-0.48	0.07	
		O_5_141868	00 49 44.41	-72 52 10.7	0.36	19.82	0.12	1.09	0.44	···	···	
		O_5_142924	00 49 44.25	-72 52 09.9	0.72	20.83	0.41	-0.64	0.53	···	···	
		O_5_144727	00 49 44.95	-72 52 11.8	2.93	21.32	0.26	0.50	0.40	···	···	
		O_5_144764	00 49 44.74	-72 52 08.3	2.67	21.20	0.44	1.23	0.65	···	···	
7_5	3.32	**O_4_144169**	00 47 36.44	-72 45 41.0	3.32	21.73	0.22	-0.54	0.32	···	···	n
		(Z_1739792)	00 47 36.51	-72 45 40.8	2.73	21.18	0.16	0.41	0.25	99.99	99.99	
		O_4_144189	00 47 36.13	-72 45 37.7	0.93	22.00	0.26	99.99	99.99	···	···	
		Z_1739697	00 47 36.46	-72 45 36.8	2.33	21.41	0.23	0.83	0.33	99.99	99.99	
7_6**	1.50	Z_1944671	00 49 16.78	-72 39 43.4	1.48	21.64	0.21	0.01	0.32	99.99	99.99	n, c
		Z_1945182	00 49 17.04	-72 39 45.5	1.45	17.70	0.04	-0.18	0.04	-0.61	0.05	
7_7	1.81	**O_4_195564**†	00 48 30.01	-72 49 00.3	0.90	21.75	0.15	99.99	99.99	···	···	n
		O_5_68900†	00 48 29.99	-72 49 00.3	0.81	21.86	0.27	99.99	99.99	···	···	
7_9	2.16	O_5_235644	00 50 49.19	-72 41 52.5	2.12	99.99	99.99	99.99	99.99	···	···	c
		O_5_316703	00 50 49.60	-72 41 53.8	0.77	13.49	0.03	1.61	0.04	···	···	
		Z_2142356	00 50 49.61	-72 41 53.6	0.59	13.51	0.07	1.41	0.12	1.22	0.12	
		O_5_317836	00 50 49.99	-72 41 51.8	1.98	19.49	0.57	1.85	0.70	···	···	
		O_5_318825	00 50 50.09	-72 41 52.9	1.97	19.90	0.45	99.99	99.99	···	···	
7_10	1.50	**O_5_157856**	00 49 55.41	-72 42 22.9	0.73	20.79	0.17	0.50	0.26	···	···	n
		Z_2025973	00 49 55.45	-72 42 22.5	1.12	21.32	0.20	0.39	0.24	-1.00	0.37	
7_11*	1.50	···	···	···	···	···	···	···	···	···	···	···
7_12	1.94	**O_4_199309**	00 48 20.06	-72 40 11.8	0.91	19.50	0.04	0.77	0.10	···	···	n
7_13	1.50	**O_5_158486**	00 49 34.46	-72 41 06.8	0.37	21.19	0.16	0.16	0.21	···	···	n
7_15*	1.50	···	···	···	···	···	···	···	···	···	···	···

Table 6—Continued

X-ray Src	X-ray Rad. (″)	Src ID	Optical counterpart R.A. (J2000.0)	Decl. (J2000.0)	Offset (″)	V	δV	B-V	δ(B − V)	U-B	δ(U − B)	Notes
[1]	[2]	[3]	[4]	[5]	[6]	[7]	[8]	[9]	[10]	[11]	[12]	[13]
7_16	1.50	**O_4_195333**†	00 48 32.77	-72 46 52.8	0.90	21.40	0.21	99.99	99.99	···	···	u
		O_5_72601†	00 48 32.83	-72 46 52.9	0.98	21.37	0.34	0.47	0.38	···	···	
		O_4_195340†	00 48 33.02	-72 46 51.9	0.93	21.35	0.26	99.99	99.99	···	···	
		O_5_71331†	00 48 32.98	-72 46 51.7	0.78	21.48	0.24	99.99	99.99	···	···	
		Z_1853924°	00 48 32.53	-72 46 51.5	1.32	20.33	0.13	0.72	0.16	99.99	99.99	
7_17	5.29	**O_5_140807**	00 49 45.01	-72 54 00.9	4.47	18.36	0.06	0.94	0.11	···	···	u
		(Z_2004363)°	00 49 45.15	-72 54 00.7	5.08	17.19	0.06	1.75	0.17	0.41	0.19	
		O_5_141493	00 49 44.80	-72 54 00.3	3.63	19.91	0.08	0.68	0.17	···	···	
		O_5_140992	00 49 43.85	-72 54 02.2	1.28	18.38	0.03	0.04	0.03	···	···	
		Z_2001696	00 49 43.90	-72 54 02.3	1.31	18.36	0.04	0.13	0.05	-0.49	0.07	
		O_5_142293	00 49 44.43	-72 54 00.0	2.20	21.13	0.15	0.48	0.34	···	···	
		O_5_142299	00 49 44.54	-72 53 58.4	3.61	19.56	0.04	-0.01	0.07	···	···	
		Z_2003145	00 49 44.57	-72 53 58.6	3.54	19.48	0.23	0.08	0.23	-0.36	0.10	
		O_5_143631	00 49 44.31	-72 54 05.4	4.51	20.48	0.13	0.23	0.21	···	···	
		Z_2002614	00 49 44.33	-72 54 05.4	4.51	20.65	0.10	0.54	0.21	-0.76	0.28	
		O_5_143643	00 49 43.48	-72 54 04.9	4.43	21.39	0.22	0.53	0.48	···	···	
		O_5_143656	00 49 42.93	-72 54 03.0	5.07	20.86	0.15	0.13	0.21	···	···	
		Z_1999724	00 49 42.97	-72 54 03.0	4.89	21.22	0.22	1.03	0.47	-1.54	0.63	
		O_5_143702	00 49 44.22	-72 53 58.4	2.87	21.18	0.18	0.42	0.21	···	···	
		O_5_145404	00 49 44.94	-72 53 59.1	4.62	21.29	0.45	99.99	99.99	···	···	
7_18**	1.90	**Z_2068590**	00 50 15.46	-72 39 17.8	1.35	21.76	0.25	0.15	0.36	99.99	99.99	n
7_19	1.50	**O_5_146766**	00 49 41.66	-72 48 42.9	1.36	17.16	0.55	0.27	0.60	···	···	n, c
		O_5_147711	00 49 41.74	-72 48 43.7	1.36	19.77	0.44	-0.85	0.59	···	···	
		O_5_149497	00 49 41.49	-72 48 44.2	0.46	20.92	0.39	0.17	0.58	···	···	
		O_5_149522	00 49 41.53	-72 48 42.6	1.29	20.52	0.32	-0.17	0.53	···	···	
		O_5_150426	00 49 41.36	-72 48 44.8	1.03	21.53	0.63	-0.64	0.68	···	···	
7_20	1.94	**O_5_237353**	00 50 34.65	-72 40 38.3	1.62	20.30	0.07	99.99	99.99	···	···	n
		Z_2109958	00 50 34.67	-72 40 38.4	1.53	20.29	0.16	0.21	0.18	99.99	99.99	
		O_5_239470	00 50 34.96	-72 40 38.5	0.35	21.80	0.31	99.99	99.99	···	···	
7_21	1.57	**O_5_148716**	00 49 27.53	-72 50 01.6	0.47	21.22	0.23	0.33	0.30	···	···	n
		Z_1967182	00 49 27.61	-72 50 01.6	0.22	21.54	0.17	-0.01	0.21	99.99	99.99	
7_22*	1.50	···	···	···	···	···	···	···	···	···	···	···
7_23	1.50	**O_5_70749**	00 48 42.34	-72 46 56.9	0.21	19.43	0.04	-0.06	0.07	···	···	n
		Z_1874185	00 48 42.40	-72 46 57.0	0.21	19.46	0.04	0.07	0.07	-1.00	0.10	
7_24	1.91	O_4_194141	00 48 08.11	-72 47 10.7	0.73	20.56	0.14	0.53	0.28	···	···	n
		O_4_195236	00 48 08.29	-72 47 09.3	1.42	20.25	0.08	0.27	0.13	···	···	
7_25	3.01	O_5_64642	00 49 12.95	-72 52 10.5	1.75	20.91	0.19	0.60	0.26	···	···	n
		Z_1937045	00 49 13.08	-72 52 10.5	1.22	20.82	0.12	1.17	0.46	99.99	99.99	

Table 6—Continued

X-ray Src	X-ray Rad. (″)	Src ID	R.A. (J2000.0)	Decl. (J2000.0)	Optical counterpart Offset (″)	V	δV	B-V	δ(B − V)	U-B	δ(U − B)	Notes
[1]	[2]	[3]	[4]	[5]	[6]	[7]	[8]	[9]	[10]	[11]	[12]	[13]
		O_5_64650	00 49 13.30	-72 52 10.3	0.71	21.68	0.26	0.07	0.36	···	···	
		O_5_141206	00 49 13.72	-72 52 10.3	1.86	19.35	0.05	0.69	0.10	···	···	
		Z_1938468	00 49 13.79	-72 52 10.6	2.08	18.86	0.07	0.65	0.09	0.44	0.16	
		O_5_142914	00 49 13.68	-72 52 11.5	1.62	19.99	0.09	0.26	0.13	···	···	
7_26*	1.90	···	···	···	···	···	···	···	···	···	···	···
7_27	3.02	**O_5_221350**	00 50 18.35	-72 51 10.4	2.10	20.17	0.07	0.72	0.19	···	···	n
		O_5_224747	00 50 18.71	-72 51 08.6	1.87	20.98	0.12	0.28	0.21	···	···	
		O_5_224753	00 50 18.95	-72 51 08.3	2.17	21.26	0.23	0.10	0.34	···	···	
		(Z_2076011)	00 50 18.92	-72 51 08.8	1.70	20.83	0.14	-0.28	0.17	99.99	99.99	

†Sources detected in two neighboring OGLE-II fields.

°Just outside the error circle of the X-ray source there is another OGLE-II source (not listed in these tables), that it is most likely related to the detected MCPS source within the search radius.

*Sources with OGLE-II coverage (thus available on-line finding chart) but no counterpart(s) (either in OGLE-II or MCPS catalogs).

**Sources without OGLE-II coverage (thus no available on-line finding charts) but MCPS counterparts within their search radius.

Note. — Sources 7_8 and 7_14 do not have OGLE-II coverage (thus no finding charts), and any MCPS counterpart(s).

Table 7. Total number of counterparts

Chandra field ID	Overlap by OGLE-II survey	Catalog used	X-ray sources with total number of counterparts 0	1	2	> 2
[1]	[2]	[3]	[4]	[5]	[6]	[7]
3	partial	O	2	3	0	1
		Z	14	11	2	0
		combined	14	10	2	1
4	full	O	3	14	8	11
		Z	14	16	3	3
		combined	3	12	11	10
5	partial	O	1	3	3	4
		Z	7	19	6	4
		combined	6	13	9	8
6	full	O	5	9	8	6
		Z	11	13	3	1
		combined	5	9	8	6
7	partial	O	4	6	4	8
		Z	9	10	5	1
		combined	5	8	3	10

Table 8. Additional optical info

X-ray source ID	Type*	Ref.	C/part of associated X-ray source	Ref.	Other sources within 1.5″	Ref.
[1]	[2]	[3]	[4]	[5]	[6]	[7]
3_1	AGN variable	[DSM03] [ZSW01]	OGLE00571981-7225337	[SPH03]	[USNO-A2.0]0150-00625436	[SPH03]
3_2	Be-XBP or bkg AGN?	[ECG04] [HE08]	Z_2806702	[ECG04],[CEG05]	...	...
3_3	Be-XBP Be? Be candidate	[MFL03] [SPH03] [MPG02]	[MA93]1020 [MA93]1020≡O_8_49531 O_8_49531≡ ≡[MACHO]207.16432.1575	[MFL03],[HP04] [SPH03] [CEG05] [CEG05]	[M02]40790	[M02]
3_4	...	...	...	...	[USNO-B1.0]0177-0042040 J005732.7-721302 J005732.7-721301 S01020206684 [2MASS]J00573272-7213022	[MLC03] [DENIS05] [DENIS05] [GSC2.2] [SCS06]
3_7	HMXB? blue star B2 (II)	[SG05] [M02] [EHI04]	[2dF]1224≡Z_3075967	[SG05]	S0102022296901 [M02]40184 [USNO-B1.0]0176-0040752 [UCACA2]01162515 [2MASS]J00572397-7223566 J005723.8-722356	[GSC2.2] [M02] [MLC03] [ZA04] [SCS06] [DENIS05]
3_18	HMXB?, P Be? Be-XBP	[SPH03] [HP04] [CEG05]	[MA93]904 Z_2893439≡[MA93]904≡ ≡[MACHO]207.16374.21 [MACHO]207.16374.21≡ ≡[MA93]904	[HP04] [CEG05] [CEG05] [SC06] [SC06]	[2MASS]J00560554-7221595	[SCS06]
4_1	HMXB, Be star blue star HMXB,Be/X Be-XBP B0.5V-B1V eclips.binary#550	[SHP00] [M02] [HFP00] [YIT03] [CNM05] [WUK04]	star1 O_5_180026≡ ≡[MACHO]212.16019.30 [MA93]387	[CSM97] [CEG05] [CEG05] [SC05]	[M02]17504 [MACS#013]0050-732	[M02] [TBS96]
4_2	Be-XBP variable star Be candidate	[CEG05] [ITM04] [MPG02]	O_5_111490≡ ≡[MACHO]212.15906.2446	[CEG05] [CEG05]	[USNO-B1.0]0168-0025357 [M02]12955 J004913.6-731137 S0102311264259 [2MASS]J00491360-7311378	[MLC03] [M02] [DENIS05] [GSC2.2] [SCS06]
4_3	Be? Be/X? blue star	[HP04] [HS00] [M02]	[MA93]414	[HP04],[HS00]	[M02]18200 OB 114, O 53 [MACS#023]0050-731 S0102311270531 [UCAC2]01000912 J005057.11-731008.0 J005057.1-731007	[M02] [OKP04] [TBS96] [GSC2.2] [ZA04] [CI00] [DENIS05]

Table 8—Continued

X-ray source ID	Type*	Ref.	C/part of associated X-ray source	Ref.	Other sources within 1.5″	Ref.
[1]	[2]	[3]	[4]	[5]	[6]	[7]
4_4	...	...	...	...	S0102330258235	[GSC2.2]
					[USNO-B1.0]0166-0028183	[MLC03]
					[M02]10496	[M02]
					[2MASS]J00481877-7320598	[SCS06]
					J004818.7-732100	[DENIS05]
4_5	Be?	[HP04]	[MA93]300	[HP04],[HS00]	[M02]13712	[M02]
	Be/X?	[HS00]			S0102311265986	[GSC2.2]
	variable star	[ITM04]			[USNO-B1.0]0168-0025726	[MLC03]
	Be-XRB	[HEP08]			J004929.8-731058	[DENIS03]
					[2MASS]J00492984-7310583	[SCS06]
4_7	...	...	...	...	[2MASS]J00485340-7324573	[SCS06]
					[USNO-B1.0]0165-0028919	[MLC03]
					J004853.5-732457	[DENIS05]
4_8	Be-XBP	[HEP08]	...	...	[M02]10291	[M02]
	Be candidate	[MPG02]			J004814.1-731003	[DENIS05]
					S0102311267622	[GSC2.2]
					[UCAC2]01000224	[ZA04]
					[2MASS]J00481410-7310045	[SCS06]
					[USNO-B1.0]0168-0024147	[MLC03]
4_14	Be-XBP	[EC03]	O_5_90506 ?	[EC03]	...	...
			[MA93]315	[HS00]		
			O_5_90506≡	[CEG05]		
			≡[MACHO]212.15960.12	[CEG05]		
4_15	...	...	...	...	[2MASS]J00491077-7317171	[SCS06]
					J004910.7-731717	[DENIS05]
4_17	Be candidate	[MPG02]	...	...	OB 110	[OKP04]
					J005047.9-731817	[DENIS05]
					[2MASS]J00504799-7318180	[SCS06]
					S0102330234535	[GSC2.2]
					J005048.05-731818.1	[CI00]
4_21	SNR	[SHP00]	...	...	[USNO-B1.0]0166-0031693	[MLC03]
4_24	...	...	...	...	[USNO-B1.0]0166-0030591	[MLC03]
					S0102330259641	[GSC2.2]
4_32	...	...	...	...	[USNO-B1.0]0167-0029373	[MLC03]
					[USNO-B1.0]0167-0029382	[MLC03]
					J004926.7-731211	[DENIS05]
					S0102311263515	[GSC2.2]
4_36	...	...	...	...	J005044.9-731540	[DENIS05]
5_1	SMC-X3	[CDL78]	[MA93]531	[HS00]	[2dF]0839≡Z_2311496	[EHI04]
	Be-XRB	[HS00],[HP04]	Z_2311496	[CEG05]	[USNO-B1.0]0175-0027384	[MLC03]
	P	[ECG04]			[M02]22302	[M02]
	B0-5 (II)e	[EHI04]			OB 143	[OKP04]
	blue star	[M02]			J005205.6-722604	[DENIS05]

Table 8—Continued

X-ray source ID	Type*	Ref.	C/part of associated X-ray source	Ref.	Other sources within 1.5″	Ref.
[1]	[2]	[3]	[4]	[5]	[6]	[7]
					J005205.63-722604.0	[CI00]
					J005205.7-722603	[DENIS05]
					[MACS#001]0052-724	[TBS96]
					S0102022289632	[GSC2.2]
					[2MASS]00520563-7226042	[SCS06]
5_2	Be/X?	[HS00]	[MA93]667	[HS00]	[USNO-B1.0]0175-0030153	[MLC03]
	Be?	[HP04]	[MA93]667≡	[ECG04]	[M02]26743	[M02]
	Be-XBP or	[ECG04]	≡[MACHO]207.16202.50	[ECG04]	S0102022287762	[GSC2.2]
	source not located		Z_2498173	[CEG05]	[2MASS]00532381-7227152	[SCS06]
	in the SMC ?				J005323.95-722715.5	[CI00]
	($N_H < 0.01 \times 10^{22} cm^{-2}$)				[MACS#010]0053-724	[TBS96]
5_3	Be-XRB	[HS00],[HP04]	[MA93]506	[HS00]	[2dF]0828≡O_6_85614	[EHI04]
	P	[ISA95]	star 1≡[MA93]506	[SCB99]	[M02]21514	[M02]
	B0-5	[EHI04]	or star 2 ?		OB 135, O 64	[OKP04]
	Be candidate	[MPG02]	O_6_85614≡[MA93]506≡	[SC06]	[MACS#016]0051-725	[TBS96]
	B2	[AV82]	≡[MACHO]208.16087.9	[SC06]	[USNO-B1.0]0174-0029686	[MLC03]
					J005153.1-723148≡	[DENIS05]
					≡J005153.20-723148.5	[SCS06]
					S0102311350027	[GSC2.2]
					[2MASS]00515317-7231487	[SCS06]
					[UCAC2]01078761	[ZA04]
5_4	...	...	...	...	[MB00]134	[MB00]
					[MA93]798	[MA93]
					[M02]31155	[M02]
					OB 191, O 93	[OKP04]
					[USNO-B1.0]0175-0032932	[MLC03]
					J005446.3-722522	[DENIS05]
					J005446.3-722521	[DENIS05]
					J005446.31-722522.7	[CI00]
					S0102022292484	[GSC2.2]
					[2MASS]00544633-7225228	[SCS06]
					[UCAC2]01162180	[ZA04]
5_7	Be-XRB	[HS00]	O_7_70829≡[MA93]810	[SPH03]	[M02]31710	[M02]
	Be candidate	[MPG02]	[MACHO]207.16259.23≡	[SC05]	J005456.1-722647	[DENIS05]
	P	[MLS98]	≡O_7_70829≡[MA93]810	[SC05]	J005456.2-722647	[DENIS05]
	variable	[ZSW01]	[MA93]810	[HS00]	[USNO-B1.0]0175-0033267	[MLC03]
					J005456.18-722647.6	[CI00]
					S0102022341688	[GSC2.2]
					[2MASS]00545618-7226478	[SCS06]
					[UCAC2]01162201	[ZA04]
5_9	...	...	...	...	J005337.9-722408	[DENIS05]
					J005337.9-722408	[DENIS05]
					S0102022297258	[GSC2.2]

Table 8—Continued

X-ray source ID	Type*	Ref.	C/part of associated X-ray source	Ref.	Other sources within 1.5″	Ref.
[1]	[2]	[3]	[4]	[5]	[6]	[7]
					[2MASS]00533785-7224088	[SCS06]
5_12	blue star	[M02]	···	···	[M02]24501	[M02]
					OB 155	[OKP04]
					J005245.1-722843	[DENIS05]
					J005245.1-722843	[DENIS05]
					[2MASS]00524508-7228437	[SCS06]
					[UCACA2]01161880	[ZA04]
5_15	Quasar	[DMS03]	O_7_71429	[DMS03]	[USNO-B1.0]0175-0033000	[MLC03]
	Be candidate	[MPG02]			S0102022342014	[GSC2.2]
5_16	Be-XRB, P	[BCS01]	star A	[BCS01]	OB 179, O 84	[OKP04]
	B1-B2 III-Ve	[BCS01]	star B	[BCS01]	[M02]28479	[M02]
	blue star	[M02]	[MACHO]207.16202.30 ?	[CEG05]	[USNO-B1.0]0175-0031247	[MLC03]
			Z_2573354	[CEG05]	J005355.2-722645	[DENIS05]
					J005355.3-722645	[DENIS05]
					J005355.26-722645.0	[CI00]
					S0102022289128	[GSC2.2]
					[2MASS]00535518-7226448	[SCS06]
					[UCACA2]01162023	[ZA04]
5_22	···	···	···	···	[USNO-B1.0]0174-0029946	[MLC03]
5_24	Be-XBP	[HEP08]	···	···	[M02]28942	[M02]
	blue star	[M02]			[USNO-B1.0]0175-0031564	[MLC03]
					OB 179, O 84	[OKP04]
					J005403.8-722632	[DENIS05]
					J005403.9-722632	[DENIS05]
					J005403.88-722632.8	[CI00]
					S0102022290686	[GSC2.2]
					[2MASS]00540389-7226329	[SCS06]
					[UCACA2]01162049	[ZA04]
5_26	···	···	···	···	[USNO-B1.0]0176-0028501	[MLC03]
					[USNO-B1.0]0176-0028511	[MLC03]
5_28	···	···	···	···	[USNO-B1.0]0176-0029993	[MLC03]
5_29	···	···	···	···	[M02]28644	[M02]
					[USNO-B1.0]0175-0031361	[MLC03]
					S0102022289800	[GSC2.2]
5_30	high proper motion star	[SZU02]	···	···	···	···
5_31	···	···	···	···	[USNO-B1.0]0176-0032854	[MLC03]
6_1	transient P	[CMM02],[ECG04]	[MACS#004]0052-726	[ECG04]	[2dF]5054≡O_6_77228	[EHI04]
	Be-XBP	[SC05]	[MACHO]208.16085.24≡	[CEG05]	S0102311339902	[GSC2.2]
	Be candidate	[MPG02],[SC05]	≡O_6_77228	[CEG05]	[M02]22496	[M02]
	B1-5 (II)e	[EHI04]			[USNO-B1.0]0173-0035041	[MLC03]
	blue star	[M02]			[UCACA2]01078809	[ZA04]
					J005208.9-723803	[DENIS05]
					J005209.0-723802	[DENIS05]

Table 8—Continued

X-ray source ID	Type*	Ref.	C/part of associated X-ray source	Ref.	Other sources within 1.5″	Ref.
[1]	[2]	[3]	[4]	[5]	[6]	[7]
					J005209.05-723803.2	[CI00]
					[2MASS]00520896-7238032	[SCS06]
6_2	Be-XBP	[HPS04]	[MACHO]207.16254.16≡	[SC05]	OB 194	[OKP04]
	P	[ECG04]	≡[MA93]809	[SC05]	[USNO-B1.0]0172-0041290	[MLC03]
	O9V	[HPS04]	[M02]31699≡O_7_47103	[HPS04]	J005455.9-724510	[DENIS05]
	blue star	[M02]	[MA93]809	[HS00]	J005455.9-724511	[DENIS05]
			[MACHO]207.16254.16≡	[F05]	J005455.92-724510.7	[CI00]
			≡O_7_47103	[F05]	S0102311327234	[GSC2.2]
					[2MASS]00545586-7245108	[SCS06]
6_4	Be-XRB	[HS00]	[MA93]618≡AV138	[HS00]	[MACS#013]0053-728	[TBS96]
	blue star	[M02]			[M02]24914	[M02]
	Be candidate	[MPG02]			OB 162, O 72	[OKP04]
	B extr	[GCM87]			[USNO-B1.0]0171-0032820	[MLC03]
					J005252.2-724830	[DENIS05]
					J005252.2-724829	[DENIS05]
					J005252.09-724828.7	[CI00]
					S0102311317724	[GSC2.2]
					[2MASS]00525230-7248301	[SCS06]
6_6	···	···	···	···	[USNO-B1.0]0171-0032607	[MLC03]
6_20	B[e]	[MD01]	···	···	[MA93]739≡AV154	[MA93]
	candidate binary	[PAC01]			OB 182	[OKP04]
					[M02]29267	[M02]
					[USNO-B1.0]0173-0039498	[MLC03]
					J005409.5-724143	[DENIS05]
					J005409.4-724143	[DENIS05]
					J005409.61-724143.0	[CI00]
					S0102311333762	[GSC2.2]
					[2MASS]00540955-7241431	[SCS06]
					[UCAC2]01079173	[ZA04]
6_21	···	···	···	···	[USNO-B1.0]0173-0037830	[MLC03]
6_23	···	···	···	···	[USNO-B1.0]0172-0036877	[MLC03]
					J005239.9-724244	[DENIS05]
					J005239.9-724244	[DENIS05]
					J005239.70-724243.7	[CI00]
					S0102311364037	[GSC2.2]
					[2MASS]00523999-7242447	[SCS06]
7_1	P	[CML98]	star1(≡O_5_65517)	[SCB99](≡[CO00])	[M02]12482	[M02]
	Be-XRB	[SCB99]	star2(≡O_5_60831)	[SCB99](≡[CO00])	[USNO-B1.0]0171-0026413	[MLC03]
	Be candidate	[MPG02]			J004903.3-725052	[DENIS05]
					S0102311308679	[GSC2.2]
					[2MASS]00490331-7250527	[SCS06]
7_3	···	···	···	···	[USNO-B1.0]0171-0028042	[MLC03]
7_4	···	···	···	···	[USNO-B1.0]0171-0027633	[MLC03]

Table 8—Continued

X-ray source ID	Type*	Ref.	C/part of associated X-ray source	Ref.	Other sources within 1.5″	Ref.
[1]	[2]	[3]	[4]	[5]	[6]	[7]
					J004944.35-725209.0	[CI00]
					S0102311307192	[GSC2.2]
7_6	···	···	···	···	[USNO-B1.0]0173-0028925	[MLC03]
					J004916.9-723945	[DENIS05]
7_9	foreground star	[SHP00]	SkKM62	[SHP00]	[M02]17794	[M02]
					[USNO-B1.0]0173-0032145	[MLC03]
					J005049.6-724153	[DENIS05]
					J005049.68-724154.0	[CI00]
					S0102311364618	[GSC2.2]
					[2MASS]00504958-7241541	[SCS06]
					[MACS#012]0050-726	[TBS96]
7_19	star cluster	[BS95]	···	···	SMC-N32	[BS95]
	emission PN	[MB00]	···	···	[MB00]61	[MB00]
					[USNO-B1.0]0171-0027566	[MLC03]

*Be? Hα emission-line object as possible counterpart, no optical spectrum is available in the literature in this case, HMXB?: HMXB candidate, P: pulsar, Be/X?: very promising candidate for Be-XRBs, Be-XBP: Be-XRB pulsar

References. — Azzopardi & Vigneau (1982) [AV82], Bica et al. (1995) [BS95], Buckley et al. (2001) [BCS01], Cioni et al. (2000) [CI00], Clark et al. (1978) [CDL78], Coe et al. (2005a) [CEG05], Coe et al. (2005b) [CNM05], Coe & Orosz (2000) [CO00], Corbet et al. (1998) [CML98], Corbet et al. (2002) [CMM02], Cowley et al. (1997) [CSM97], DENIS Consortium (2003) [DENIS03], DENIS Consortium (2005) [DENIS05], Dobrzycki et al. (2003a) [DMS03], Dobrzycki et al. (2003b) [DSM03], Edge & Coe (2003) [EC03], Edge et al. (2004) [ECG04], Evans et al. (2004) [EHI04], Fabrycky, D. (2005) [F05], Garmany, Conti & Massey (1987) [GCM87], Haberl et al. (2000) [HFP00], Haberl & Pietsch (2004) [HP04], Haberl et al. (2004) [HPS04], Haberl & Sasaki (2000) [HS00], Haberl & Eger (2008) [HE08], Haberl et al. (2008) [HEP08], Israel et al. (1995) [ISA95], Ita et al. (2004) [ITM04], Macomb et al. (2003) [MFL03], Marshall et al. (1998) [MLS98], Massey 2002 [M02], Massey & Duffy (2001) [MD01], Mennickent et al. (2002) [MPG02], Meyssonnier & Azzopardi (1993) [MA93], Monet et al. (2003) [MLC03], Murphy & Bessell (2000) [MB00], Oey et al. (2004) [OKP04], Paczynski, B. (2001) [PAC01], Sasaki et al. (2000) [SHP00], Sasaki et al. (2003) [SPH03], Schmidtke & Cowley (2005,2006) [SC05,SC06], Shtykovskiy & Gilfanov (2005) [SG05], Soszynski et al. (2002) [SZU02], Stevens, Coe & Buckley (1999) [SCB99], STScI 2001 [GSC2.2], Tucholke, de Boer & Seitter (1996) [TBS96], Wyrzykowski et al. (2004) [WUK04], Yokogawa et al. (2003) [YIT03], Zacharias et al. (2004) [ZA04], Zebrun et al. (2001) [ZSW01]

Table 9. Chance associations between the *Chandra* sources and the OGLE-II stars

Magnitude range	Color range	Chance coincidence probability single matches r=1.5″	single matches r=2.5″	multiple matches r=1.5″	multiple matches r=2.5″
[1]	[2]	[3]	[4]	[5]	[6]
$M_{V_o} \leq -4.5$	all	0.01 ± 0.16	0.02 ± 0.14	0.01 ± 0.16	0.02 ± 0.12
	$(B-V)_o \leq -0.31^{\dagger}$	...	...	...	...
	$(B-V)_o > -0.31$	0.01 ± 0.15	0.02 ± 0.14	0.01 ± 0.15	0.02 ± 0.12
$-4.5 < M_{V_o} \leq -0.25$	all	0.47 ± 0.35	0.82 ± 0.17	0.24 ± 0.23	0.65 ± 0.24
	$(B-V)_o \leq -0.11$	0.19 ± 0.30	0.70 ± 0.28	0.19 ± 0.32	0.52 ± 0.33
	$(B-V)_o > -0.11$	0.31 ± 0.34	$0.81(> 0.61)$	0.24 ± 0.28	0.67 ± 0.31
$M_{V_o} > -0.25$	all	0.73 ± 0.17	0.35 ± 0.09	0.78 ± 0.20	$0.94(> 0.87)$

Note. — These are normalized chance coincidence probabilities (OGLE-II matches per *Chandra* source), thus not additive.

†In the range $M_{V_o} \leq -4.5$ and $(B-V)_o \leq -0.31$ there are not stars, thus the chance coincidence probability is not estimated there.

Table 10. Chance associations between the *Chandra* sources and the MCPS stars

Magnitude range	Color range	Chance coincidence probability single matches r=1.5″	single matches r=2.5″	multiple matches r=1.5″	multiple matches r=2.5″
[1]	[2]	[3]	[4]	[5]	[6]
$M_{V_o} \leq -4.5$	all	0.01 ± 0.15	0.05 ± 0.16	0.01 ± 0.15	0.04 ± 0.13
	$(B-V)_o \leq -0.31^{\dagger}$	...	...	...	...
	$(B-V)_o > -0.31$	0.01 ± 0.15	0.05 ± 0.15	0.01 ± 0.15	0.04 ± 0.13
$-4.5 < M_{V_o} \leq -0.25$	all	$0.72(> 0.41)$	$0.89(> 0.78)$	0.25 ± 0.17	0.57 ± 0.17
	$(B-V)_o \leq -0.11$	0.14 ± 0.26	0.56 ± 0.35	0.11 ± 0.19	0.39 ± 0.30
	$(B-V)_o > -0.11$	0.67 ± 0.32	$0.89(> 0.76)$	0.33 ± 0.24	0.59 ± 0.19
$M_{V_o} > -0.25$	all	$0.92(> 0.80)$	0.70 ± 0.09	$1.00(> 0.66)$	$1.00(> 0.85)$

Note. — These are normalized chance coincidence probabilities (MCPS matches per *Chandra* source), thus not additive.

†In the range $M_{V_o} \leq -4.5$ and $(B-V)_o \leq -0.31$ there are not stars, thus the chance coincidence probability is not estimated there.

Table 11. Summary of optical and X-ray properties for bright sources

X-ray		Optical properties							X-ray properties			ξ	[MA93]	Classification[‡]	
src. ID	src. ID	V	δV	BV	$\delta(BV)$	UB	$\delta(UB)$	Off.	spectrum*	pulsations	$F_x^{obs\dagger}$			this work	previous
[1]	[2]	[3]	[4]	[5]	[6]	[7]	[8]	[9]	[10]	[11]	[12]	[13]	[14]	[15]	[16]
3_1	O_7_267132	19.76	0.30	99.99	99.99	···	···	0.13	soft (S)	no(1)	$28.89^{+1.52}_{-1.62}$	$14.89^{+0.31}_{-0.31}$	···	unclass.	AGN
	O_7_267163	19.54	0.33	99.99	99.99	···	···	0.54				$14.67^{+0.33}_{-0.34}$			(type I)?
3_2	Z_2804383	20.30	0.07	-0.38	0.14	-0.33	0.16	2.01	hard (S)	SXP34.1(2)	$23.53^{+1.51}_{-1.38}$	$15.21^{+0.10}_{-0.09}$	···	Be-XBP	Be-XBP
	Z_2804939	20.30	0.08	1.17	0.20	-1.85	0.22	0.28				$15.21^{+0.11}_{-0.10}$			or
	Z_2806702•	16.78	0.03	-0.12	0.04	-0.77	0.06	4.27				$11.69^{+0.08}_{-0.07}$			AGN?
3_3	O_8_49531	16.01	0.02	-0.02	0.04	-1.05	0.17	0.14	hard (S)	SXP565(3)	$10.96^{+1.00}_{-1.01}$	$10.09^{+0.10}_{-0.10}$	1020 (0.4″)	Be-XBP	Be-XBP
3_4	O_8_56601	18.19	0.02	0.37	0.04	-0.60	0.06	0.54	soft (S)	···	$8.68^{+0.80}_{-0.96}$	$12.01^{+0.10}_{-0.12}$	···	unclass.	···
3_7	Z_3075967	14.71	0.03	-0.07	0.03	-1.04	0.04	1.30	hard? (HR)	no(4)	$3.10^{+0.56}_{-0.54}$	$7.42^{+0.20}_{-0.19}$	···	HMXB	HMXB?
3_18	Z_2893439	15.88	0.03	-0.04	0.03	-1.09	0.04	0.72	···	SXP140(5)	$1.22^{+0.54}_{-0.45}$	$7.57^{+0.48}_{-0.40}$	904 (2.2″)	Be-XBP	Be-XBP
3_19	Z_3049033	17.95	0.04	-0.07	0.04	-0.80	0.27	2.71	hard? (HR)	···	$1.02^{+0.32}_{-0.32}$	$9.45^{+0.34}_{-0.35}$	···	new HMXB	···
	Z_3050592	16.99	0.03	0.61	0.04	-0.08	0.05	0.60				$8.49^{+0.34}_{-0.35}$			
4_1	O_5_180026	15.44	0.04	-0.04	0.05	-0.91	0.04	0.55	hard (S)	SXP323(6)	$28.53^{+1.38}_{-1.51}$	$10.56^{+0.07}_{-0.07}$	387 (1.0″)	Be-XBP	Be-XBP
4_2	O_5_111490	16.52	0.02	0.10	0.04	-0.92	0.04	0.47	hard (S)	SXP913(7)	$15.13^{+1.10}_{-0.99}$	$10.95^{+0.08}_{-0.07}$	···	Be-XBP	Be-XBP
4_3	O_5_271074	14.54	0.01	-0.06	0.01	-0.88	0.04	0.28	hard (S)	SXP98.8?(16)	$21.67^{+1.48}_{-1.29}$	$9.36^{+0.08}_{-0.07}$	414 (0.6″)	new Be-XBP?	Be-XRB?
4_4	O_4_159896	16.58	0.02	-0.10	0.03	-0.77	0.04	0.54	hard (S)	no(4)	$9.17^{+0.84}_{-0.79}$	$10.47^{+0.10}_{-0.10}$	···	new HMXB	unclass.△
4_5	O_5_111500	16.30	0.01	0.09	0.02	-0.88	0.05	0.61	hard? (HR)	SXP892(16)	$15.88^{+1.53}_{-1.59}$	$10.79^{+0.11}_{-0.11}$	300: (0.3″)	Be-XBP	Be-XRB
4_8	O_4_171264	15.74	0.04	0.01	0.05	-0.50	0.05	0.63	hard? (HR)	SXP25.5(17)	$6.60^{+0.78}_{-0.70}$	$9.27^{+0.13}_{-0.12}$	···	Be-XBP	Be-XBP
	O_4_171332	17.78	0.05	1.64	0.28	···	···	0.55				$11.31^{+0.14}_{-0.13}$			
	O_4_171863	18.54	0.16	-0.03	0.19	···	···	1.67				$12.07^{+0.20}_{-0.20}$			
4_10	O_4_156830	17.80	0.02	-0.10	0.04	-0.57	0.07	1.32	soft (HR)	no(4)	$2.75^{+0.47}_{-0.46}$	$10.38^{+0.18}_{-0.18}$	···	unclass.	unclass.△
4_11	O_4_164855	18.88	0.04	-0.10	0.05	-0.85	0.10	1.05	hard? (HR)	no(4)	$1.12^{+0.28}_{-0.29}$	$10.48^{+0.28}_{-0.28}$	···	unclass.	unclass.△
	O_4_163513□ ≡ 1792709	15.21	0.01	1.55	0.05	1.09	0.07	4.17				$6.81^{+0.27}_{-0.28}$			
4_13	O_5_90858	18.41	0.05	0.10	0.09	-0.47	0.09	1.96	hard? (HR)	···	$2.24^{+0.45}_{-0.46}$	$10.77^{+0.22}_{-0.23}$	···	new HMXB	···
	O_5_90493• ≡Z_2014121	15.57	0.01	-0.07	0.02	-0.68	0.07	5.47				$7.93^{+0.22}_{-0.22}$			
	O_5_90535• ≡Z_2016144	16.34	0.02	0.23	0.02	0.02	0.06	4.10				$8.70^{+0.22}_{-0.22}$			
4_14	O_5_90506	14.98	0.02	0.05	0.03	···	···	1.93	hard? (HR)	SXP756(8)	$2.54^{+0.69}_{-0.59}$	$7.48^{+0.29}_{-0.25}$	315 (1.4″)	Be-XBP	Be-XBP
4_17	O_5_180008	15.30	0.07	0.05	0.10	-1.00	0.05	0.99	hard? (HR)	···	$0.89^{+0.33}_{-0.20}$	$6.66^{+0.40}_{-0.26}$	396 (3.9″)	new Be-XRB	···

Table 11. Summary of optical and X-ray properties of bright sources

X-ray src. ID	src. ID	Optical properties V	δV	BV	$\delta(BV)$	UB	$\delta(UB)$	Off.	X-ray properties spectrum*	pulsations	F_x^{obs} †	ξ	[MA93]	Classification‡ this work	previous
[1]	[2]	[3]	[4]	[5]	[6]	[7]	[8]	[9]	[10]	[11]	[12]	[13]	[14]	[15]	[16]
4_19	O_5_262679	19.41	0.09	-0.26	0.10	-0.24	0.11	1.40	hard? (HR)	···	$1.02^{+0.30}_{-0.32}$	$10.70^{+0.33}_{-0.35}$	···	new HMXB	···
	O_5_261182• ≡Z_2153646	18.16	0.03	-0.08	0.04	-0.61	0.05	2.27				$9.45^{+0.32}_{-0.34}$			
4_21	O_5_256084	17.93	0.06	0.88	0.15	···	···	2.59	···	···	$4.72^{+0.67}_{-0.64}$	$11.10^{+0.16}_{-0.16}$	···	unclass.	SNR⊗
	O_5_256315	18.63	0.04	0.76	0.09	-0.81	0.12	1.39				$11.80^{+0.16}_{-0.15}$			
	O_5_256826	18.33	0.04	-0.18	0.05	-0.62	0.06	1.75				$11.50^{+0.16}_{-0.15}$			
4_22	O_5_90840	18.40	0.03	0.68	0.06	99.99	99.99	3.20	···	···	$1.01^{+0.40}_{-0.29}$	$9.90^{+0.42}_{-0.31}$	···	new HMXB?	···
	O_5_91270	18.26	0.03	-0.07	0.03	-0.41	0.08	2.32				$9.76^{+0.42}_{-0.31}$			
4_32	O_5_111737	18.62	0.04	0.76	0.07	···	···	1.34	···	···	$0.48^{+0.20}_{-0.19}$	$9.31^{+0.46}_{-0.42}$	···	unclass.	···
4_36	Z_2132222	18.27	0.04	0.91	0.06	-0.04	0.13	1.29	···	no(16)	$0.51^{+0.23}_{-0.19}$	$9.03^{+0.50}_{-0.41}$	···	unclass.	···
5_1	Z_2311496	14.91	0.02	0.00	0.03	-0.97	0.04	0.55	hard (S)	SXP7.78(2)	$219.90^{+4.50}_{-5.34}$	$12.24^{+0.03}_{-0.03}$	531 (1.8″)	Be-XBP	Be-XBP
5_2	Z_2498173	16.19	0.12	-0.09	0.12	-1.05	0.04	0.24	hard (S)	SXP138(2)	$20.34^{+1.64}_{-1.70}$	$10.94^{+0.15}_{-0.15}$	667:(0.9″)	Be-XBP	Be-XBP
5_3	O_6_85614	14.90	0.12	-0.27	0.13	-1.13	0.11	0.54	hard (S)	SXP8.80(9)	$12.61^{+1.23}_{-1.26}$	$9.13^{+0.16}_{-0.16}$	506:(0.5″)	Be-XBP	Be-XBP
5_4	O_7_70843	15.58	0.02	0.14	0.06	-1.11	0.13	0.79	hard (HR)	···	$9.61^{+1.11}_{-1.14}$	$9.51^{+0.13}_{-0.13}$	798 (2.4″)	new Be-XRB⊕	···
5_6	Z_2748033	17.86	0.03	-0.03	0.05	-0.79	0.06	3.60	soft (HR)	···	$8.55^{+1.06}_{-1.04}$	$11.67^{+0.14}_{-0.14}$	···	unclass.	···
5_7	O_7_70829	15.30	0.01	-0.04	0.02	-1.07	0.04	1.19	hard? (HR)	SXP59.0(10)	$4.75^{+0.68}_{-0.79}$	$8.47^{+0.16}_{-0.18}$	810 (1.9″)	Be-XBP	Be-XBP
5_9	Z_2531366	18.19	0.06	0.59	0.07	-0.13	0.09	1.33	soft? (HR)	SXP7.83?(16)	$2.27^{+0.62}_{-0.54}$	$10.56^{+0.30}_{-0.26}$	···	unclass.	···
5_12	Z_2406014	14.92	0.08	0.00	0.09	-0.97	0.04	0.35	hard? (HR)	···	$1.37^{+0.39}_{-0.37}$	$6.74^{+0.32}_{-0.31}$	···	new Be-XRB⊕	···
5_15	O_7_71429	19.00	0.10	0.18	0.12	0.00	0.00	0.50	soft? (HR)	no(11) SXP358?(16)	$2.36^{+0.88}_{-0.72}$	$11.41^{+0.42}_{-0.35}$	···	unclass.	Quasar
5_16	Z_2573354	14.72	0.03	-0.07	0.03	-1.02	0.04	0.83	hard? (HR)	SXP46.6(12)	$0.78^{+0.31}_{-0.27}$	$5.93^{+0.43}_{-0.37}$	···	Be-XBP	Be-XBP
5_18	Z_2207680	18.90	0.05	0.31	0.06	-0.22	0.08	2.74	···	···	$0.98^{+0.34}_{-0.34}$	$10.36^{+0.38}_{-0.37}$	···	unclass.	···
5_23	Z_2288276	17.99	0.03	-0.06	0.04	-0.69	0.05	2.57	···	···	$1.25^{+0.48}_{-0.38}$	$9.71^{+0.42}_{-0.33}$	···	new HMXB?	···
5_24	Z_2595629	14.95	0.03	0.01	0.04	-1.13	0.06	0.78	···	SXP342(18)	$0.72^{+0.36}_{-0.24}$	$6.07^{+0.54}_{-0.37}$	···	Be-XBP	Be-XBP
5_25	Z_2686280	18.48	0.04	0.98	0.07	0.08	0.11	1.81	···	···	$0.99^{+0.35}_{-0.40}$	$9.95^{+0.39}_{-0.44}$	···	unclass.	···
5_29	Z_2581383	17.81	0.04	-0.14	0.05	-0.82	0.06	0.78	hard? (HR)	···	$0.61^{+0.32}_{-0.23}$	$8.75^{+0.57}_{-0.41}$	···	new HMXB	···
5_32	Z_2315739	15.20	0.03	-0.07	0.03	-0.62	0.04	2.22	soft? (HR)	···	$0.49^{+0.30}_{-0.24}$	$5.91^{+0.66}_{-0.52}$	···	unclass.	···
5_35	Z_2438540□	18.84	0.05	0.00	0.06	-0.48	0.08	2.58	···	···	$0.27^{+0.20}_{-0.15}$	$8.91^{+0.78}_{-0.59}$	···	unclass.	unclass.
6_1	O_6_77228	15.03	0.02	0.14	0.03	-0.81	0.04	0.58	hard (S)	SXP82.4(13)	$493.88^{+6.39}_{-7.32}$	$13.24^{+0.02}_{-0.03}$	···	Be-XBP	Be-XBP
6_2	O_7_47103	15.01	0.01	-0.02	0.01	-0.93	0.18	0.40	hard (S)	SXP504(2)	$47.52^{+2.06}_{-2.22}$	$10.68^{+0.05}_{-0.05}$	809 (1.7″)	Be-XBP	Be-XBP

Table 11. Summary of optical and X-ray properties for bright sources

X-ray		Optical properties							X-ray properties			ξ	[MA93]	Classification‡	
src. ID	src. ID	V	δV	BV	$\delta(BV)$	UB	$\delta(UB)$	Off.	spectrum*	pulsations	F_x^{obs} †			this work	previous
[1]	[2]	[3]	[4]	[5]	[6]	[7]	[8]	[9]	[10]	[11]	[12]	[13]	[14]	[15]	[16]
6_3	O_6_153267	18.15	0.07	-0.14	0.08	-0.52	0.07	1.38	soft? (HR)	···	$4.23^{+0.58}_{-0.65}$	$11.19^{+0.16}_{-0.18}$	···	unclass.	···
6_4	O_6_147662	14.42	0.05	-0.10	0.05	-0.97	0.04	0.27	hard? (HR)	···	$2.85^{+0.53}_{-0.53}$	$7.03^{+0.21}_{-0.21}$	618 (1.1″)	Be-XRB	Be-XRB
6_8	O_6_306524	17.60	0.01	1.12	0.06	0.74	0.11	2.02	soft? (HR)	···	$1.60^{+0.40}_{-0.42}$	$9.59^{+0.27}_{-0.28}$	···	unclass.	···
6_11	Z_2657679	17.07	0.03	0.36	0.05	0.03	0.05	2.92	hard? (HR)	···	$1.33^{+0.41}_{-0.35}$	$8.86^{+0.33}_{-0.29}$	···	new HMXB	···
	≡O_6_320020	17.10	0.02	0.26	0.03										
	≡O_7_57270	17.14	0.02	0.25	0.04										
6_20	O_6_311169	13.71	0.14	0.39	0.19	-0.67	0.12	0.62	···	···	$0.75^{+0.26}_{-0.29}$	$4.87^{+0.40}_{-0.44}$	739 (0.8″)	unclass.	B[e]
6_23	O_6_158108	17.10	0.05	1.42	0.15	1.92	0.16	0.56	···	···	$0.48^{+0.21}_{-0.19}$	$7.77^{+0.49}_{-0.44}$	···	unclass.	···
7_1	O_5_65517	16.94	0.06	0.09	0.10	-0.84	0.05	0.45	hard (S)	SXP74.7[14]	$15.04^{+1.37}_{-0.99}$	$11.36^{+0.12}_{-0.09}$	···	Be-XBP	Be-XBP
7_4	O_5_140754	17.52	0.07	1.58	0.17	99.99	99.99	2.10	···	···	$3.61^{+0.69}_{-0.55}$	$10.39^{+0.22}_{-0.18}$	···	unclass.	···
	O_5_141207	17.85	0.05	0.23	0.16	-0.48	0.07	0.76				$10.72^{+0.21}_{-0.17}$			
7_6	Z_1945182	17.70	0.04	-0.18	0.04	-0.61	0.05	1.45	hard? (HR)	···	$2.32^{+0.49}_{-0.45}$	$10.09^{+0.23}_{-0.22}$	···	new HMXB	···
7_9	O_5_316703	13.49	0.03	1.61	0.04	1.22	0.12	0.77	hard? (HR)	no[15]	$2.43^{+0.46}_{-0.52}$	$5.93^{+0.21}_{-0.24}$	···	fg star	fg star
7_17	O_5_140807	18.36	0.06	0.94	0.11	···	···	4.47	soft? (HR)	···	$1.07^{+0.36}_{-0.32}$	$9.91^{+0.37}_{-0.33}$	···	unclass.	···
	O_5_140992	18.38	0.03	0.04	0.03	-0.49	0.07	1.28				$9.93^{+0.36}_{-0.33}$			
7_19	O_5_146766	17.16	0.55	0.27	0.60	···	···	1.36	···	···	$0.73^{+0.25}_{-0.28}$	$8.30^{+0.66}_{-0.69}$	316 (2.9″)	new Be-XRB	···

Note. — BV and UB denote the B-V and U-B colors, respectively. The offset of the optical counterpart from the X-ray source position is given in arcseconds. SXP stands for SMC X-ray Pulsars followed by the pulse period in seconds to three significant figures (http://www.astro.soton.ac.uk/∼mjc/). A "?" denotes candidate X-ray pulsars from the work of Laycock, Zezas & Hong (2008).

†Absorbed flux in the $2.0 - 10.0$ keV energy band calculated from net counts, in units of 10^{-14} erg cm^{-2} s^{-1} (Zezas et al. 2008).

‡new HMXB?: candidate new HMXB (early-type counterpart but no information about the X-ray spectrum and or pulsations); Be-XBP: Be-XRB pulsar; fg star: foreground star; unclass.: sources with a soft X-ray spectrum or unavailable spectral information or without an early-type counterpart - cannot be classified without further information (e.g. optical spectroscopy, X-ray timing or spectral analysis). The references for the previously classified sources are given in Column [3] of Table 8.

*A "?" following the hard or soft X-ray spectrum indicates a possibly hard or soft spectrum, respectively (due to the small number of X-ray counts).

△unclassified: sources of uncertain nature (Shtykovskiy & Gilfanov 2005).

□These sources are discussed in §8.3. For *Chandra* source 4_11 more details can be found in §A.4, and for source 5_35 in §A.6.

•Sources with hard (or possibly hard) X-ray spectra and early-type counterparts (O or B) between the 1σ and 2σ search radii. For more details see §A.7 in the Appendix.

⊗More details are given in §A.2.

⊕Confirmed classification by optical follow-up spectroscopy of selected targets from our *Chandra* survey (Antoniou et al. 2008).

References. — (1) Dobrzycki et al. (2003b), (2) Edge et al. (2004), (3) Macomb et al. (2003), (4) Shtykovskiy & Gilfanov (2005), (5) Sasaki et al. (2003), (6) Yokogawa et al. (2003), (7) Coe et al. (2005a), (8) Edge & Coe (2003), (9) Israel et al. (1995), (10) Marshall et al. (1998), (11) Dobrzycki et al. (2003a), (12) Buckley et al. (2001), (13) Corbet et al. (2002), (14) Corbet et al. (1998), (15) Sasaki et al. (2000), (16) Laycock et al. (2008), (17) Haberl et al. (2008b), (18) Haberl et al. (2008a).

Table 12. Bright optical counterparts ($M_{V_o} \leq -0.25$) of X-ray sources within the 2σ search radius (no match(es) found in the 1σ search radius)

X-ray					Optical counterpart						
Src	Rad.* ($''$)	Src ID	R.A. (J2000.0)	Decl.	Offset ($''$)	V	δV	B-V	δ(B − V)	U-B	δ(U − B)
[1]	[2]	[3]	[4]	[5]	[6]	[7]	[8]	[9]	[10]	[11]	[12]
3_10	3.00	Z_2838059†	00 55 41.83	-72 18 10.9	1.93	14.18	0.04	1.46	0.26	1.28	0.26
3_24	3.00	Z_2989515†	00 56 46.83	-72 22 50.9	2.23	18.55	0.09	0.62	0.10	0.09	0.08
3_25	3.00	Z_2924823†	00 56 18.97	-72 15 09.8	2.08	17.90	0.03	1.16	0.04	0.91	0.12
3_27	3.00	Z_2894870†	00 56 06.19	-72 20 47.0	2.13	16.57	0.03	1.70	0.05	1.83	0.12
5_35	3.00	Z_2438540	00 52 58.84	-72 26 05.3	2.58	18.84	0.05	0.00	0.06	-0.48	0.08
5_37‡	3.38	O_6_324148	00 53 58.77	-72 31 14.3	2.25	16.94	0.04	1.09	0.08	···	···
		Z_2582218	00 53 58.82	-72 31 14.3	2.07	16.90	0.03	1.11	0.04	0.74	0.07
6_27‡	3.81	O_6_227467	00 53 33.75	-72 48 17.9	2.77	18.30	0.03	1.02	0.04	···	···
		Z_2521669	00 53 33.81	-72 48 17.9	2.63	18.23	0.05	1.10	0.09	1.29	0.23

*This is the 2σ search radius given in arcseconds.

†Single counterpart within the 2σ search radius.

‡For this source there is a finding chart.

Table 13. Summary of optical and X-ray properties of sources presented in Table 12

X-ray	Optical properties			X-ray properties			ξ	Classification
Src ID	M_{V_o}	$(B-V)_o$	Offset ($''$)	spectrum	pulsations	$F_x^{obs\dagger}$		this work & previous
[1]	[2]	[3]	[4]	[5]	[6]	[7]	[8]	[9]
3_10	-5.01	1.37	1.93	hard? (HR)	···	$1.50^{+0.39}_{-0.37}$	$6.10^{+0.28}_{-0.28}$	unclassified
3_24	-0.64	0.53	2.23	···	···	$0.39^{+0.26}_{-0.16}$	$9.00^{+0.73}_{-0.45}$	unclassified
3_25	-1.29	1.07	2.08	···	···	$0.44^{+0.24}_{-0.18}$	$8.48^{+0.60}_{-0.46}$	unclassified
3_27	-2.62	1.61	2.13	···	···	$0.37^{+0.25}_{-0.17}$	$6.97^{+0.72}_{-0.51}$	unclassified
5_35	-0.35	-0.09	2.58	···	···	$0.27^{+0.20}_{-0.15}$	$8.91^{+0.78}_{-0.59}$	unclassified
5_37‡	-2.25	1.00	2.25	···	···	$0.34^{+0.25}_{-0.17}$	$7.23^{+0.80}_{-0.56}$	unclassified
	-2.29	1.02	2.07	···				
6_27‡	-0.89	0.93	2.77	···	···	$0.30^{+0.22}_{-0.16}$	$8.48^{+0.77}_{-0.58}$	unclassified
	-0.96	1.01	2.63	···				

†Absorbed flux in the $2.0-10.0$ keV energy band calculated from net counts, in units of 10^{-14} erg cm^{-2} s^{-1} (Zezas et al. 2007, in preparation).

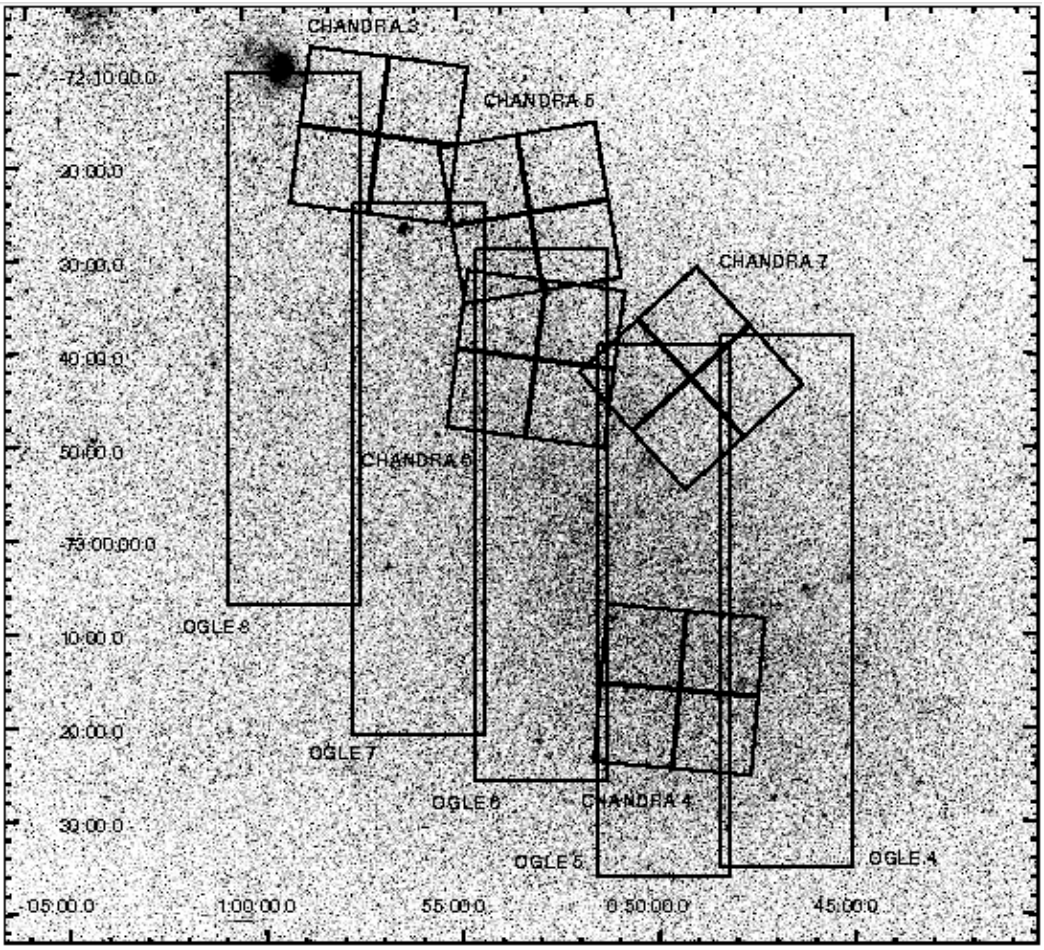

Fig. 1.— A DSS optical image of the center of the SMC (outline of the 5 observed *Chandra* fields ($16' \times 16'$) and the 5 overlapping OGLE-II fields).

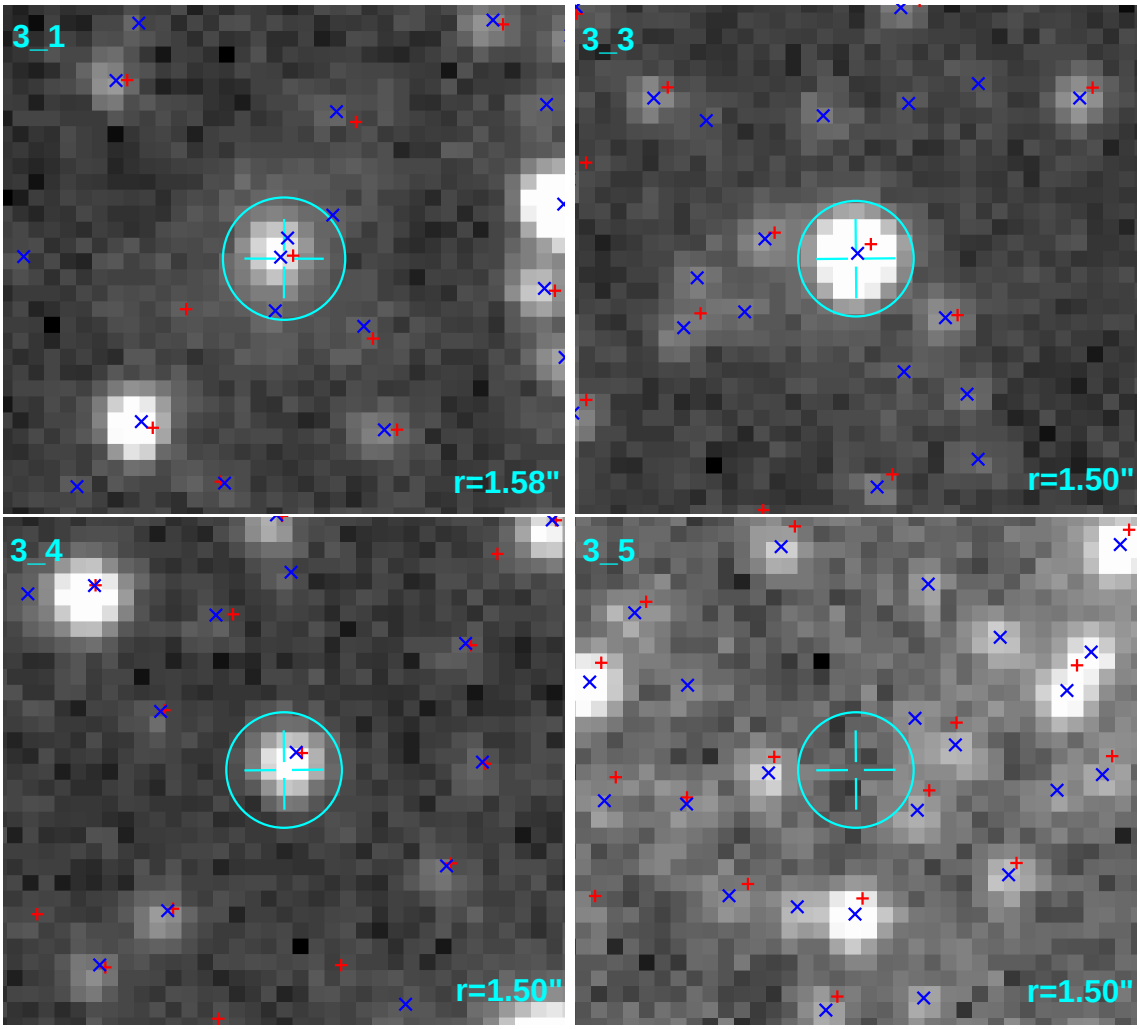

Fig. 2.— OGLE-II *I*-band images for Chandra sources in field 3. North is up and East to the right. × symbols are used for OGLE-II sources and + for MCPS sources. *This is an electronic Figure.*

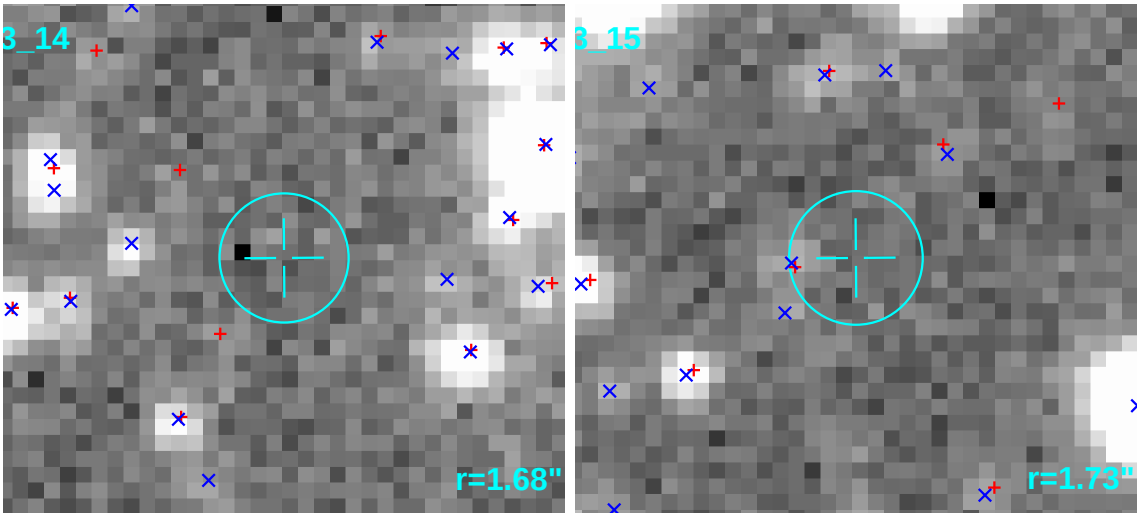
3_14
r=1.68"
3_15
r=1.73"

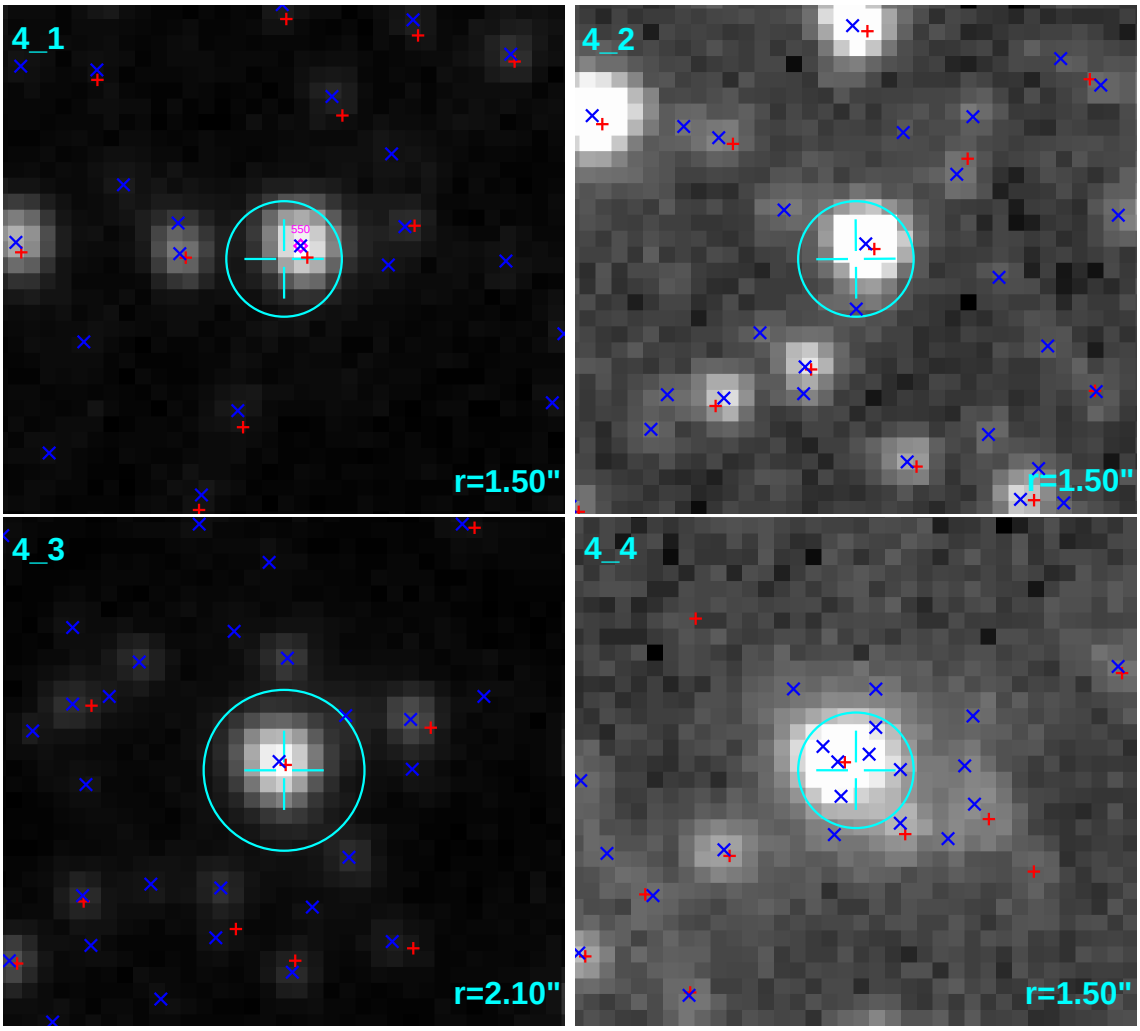

Fig. 3.— OGLE-II *I*-band images for Chandra sources in field 4. North is up and East to the right. × symbols are used for OGLE-II sources and + for MCPS sources. *This is an electronic Figure.*

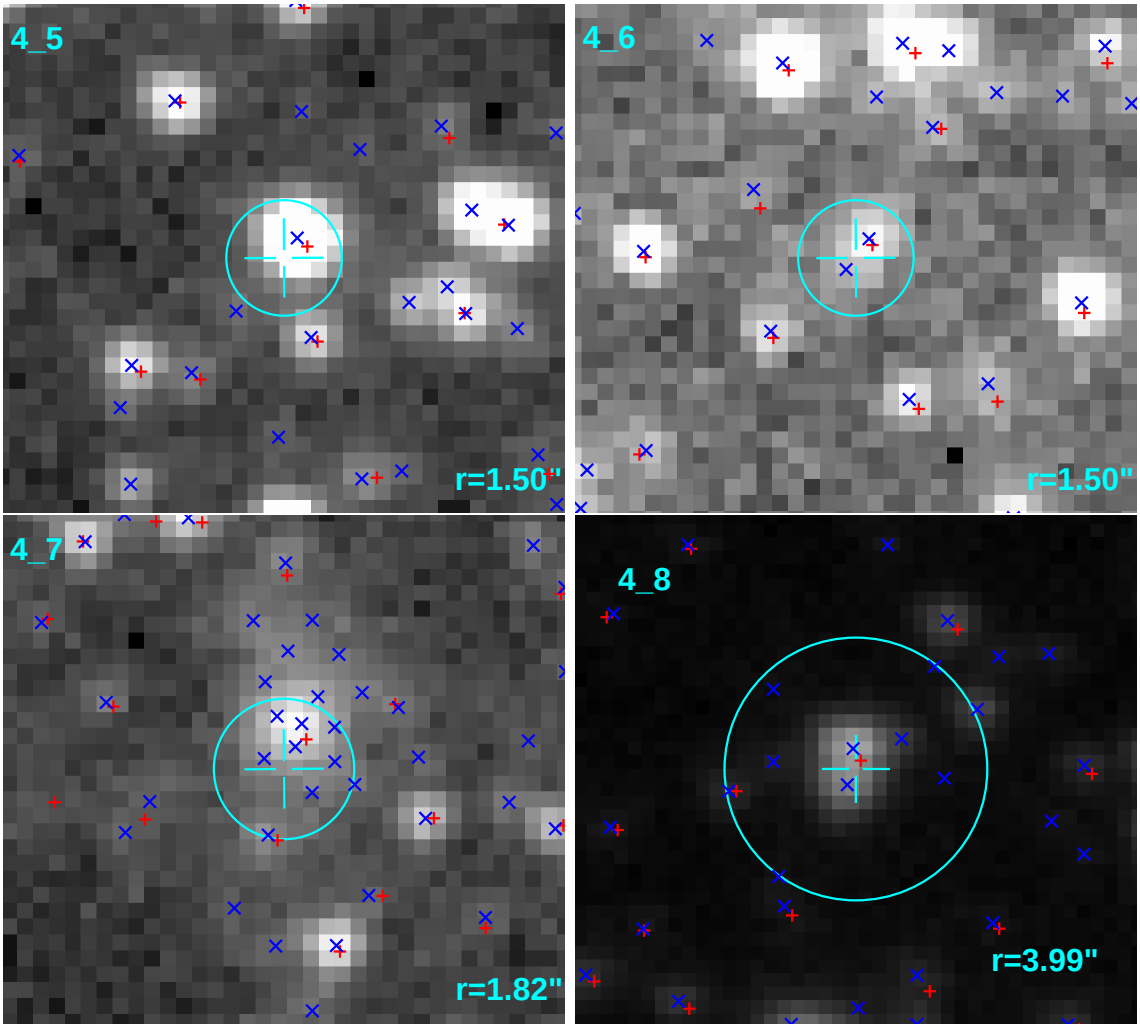
4_5
r=1.50"
4_6
r=1.50"
4_7
r=1.82"
4_8
r=3.99"

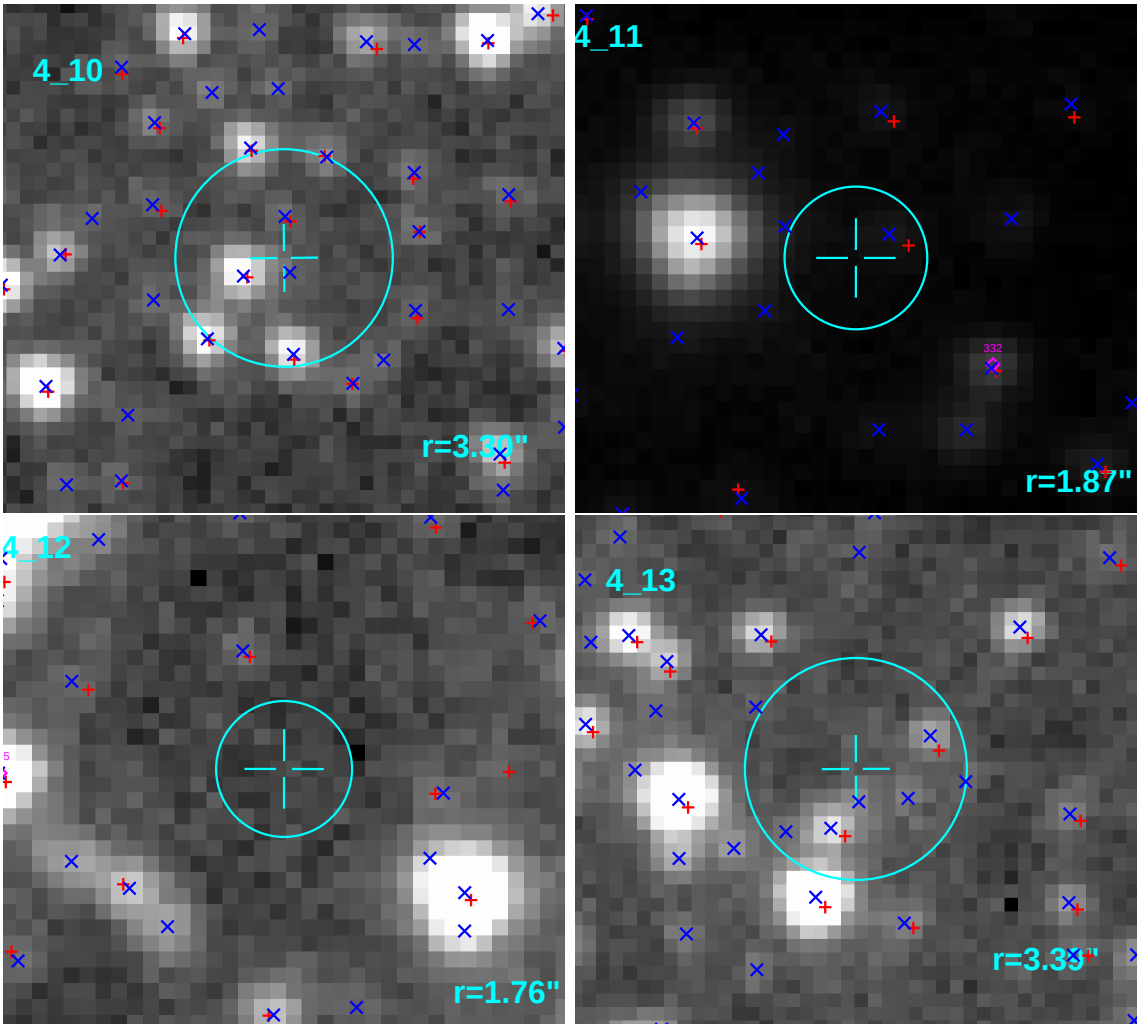
4_10
r=3.39"
4_11
r=1.87"
4_12
r=1.76"
4_13
r=3.39"

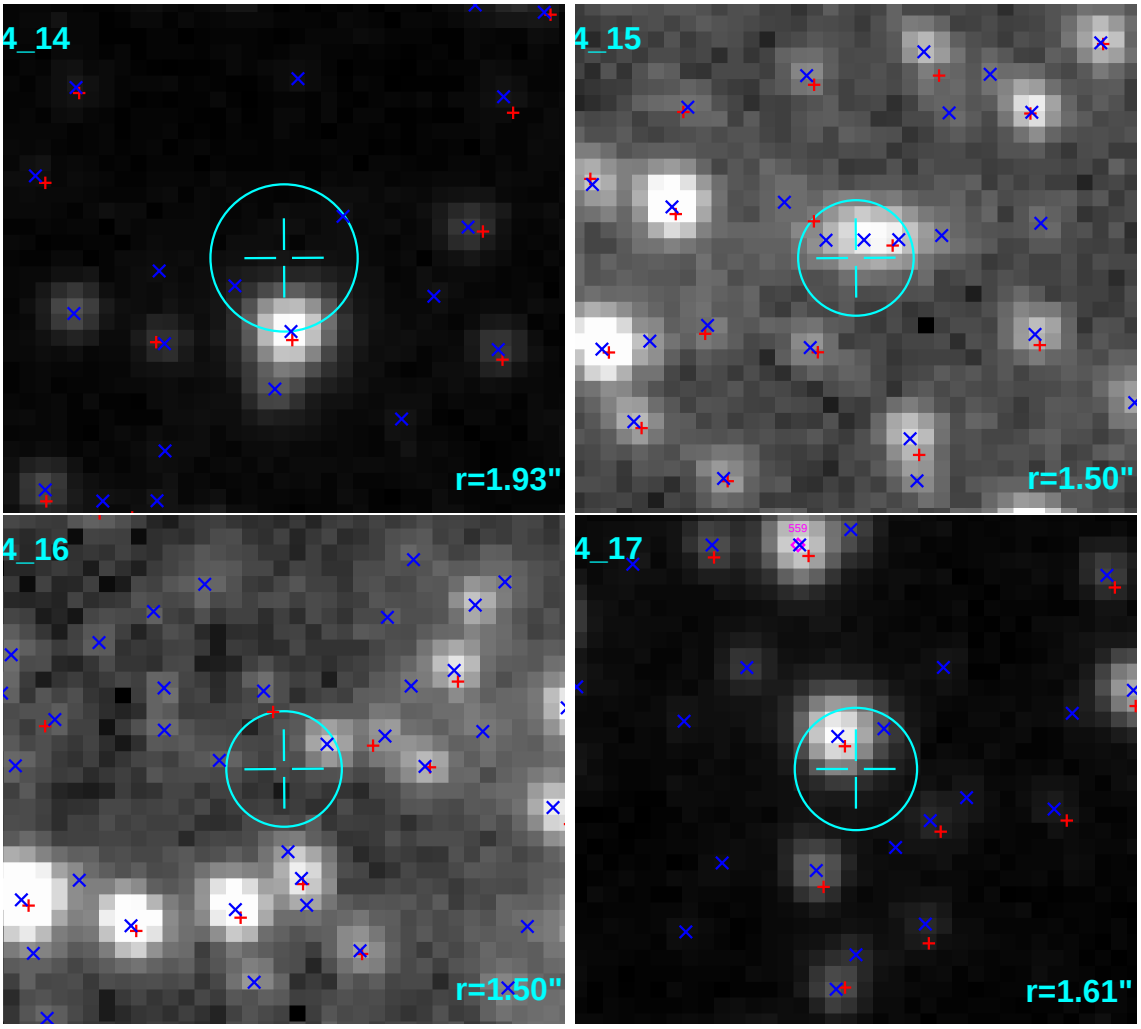
4_14
r=1.93"
4_15
r=1.50"
4_16
r=1.50"
4_17
r=1.61"

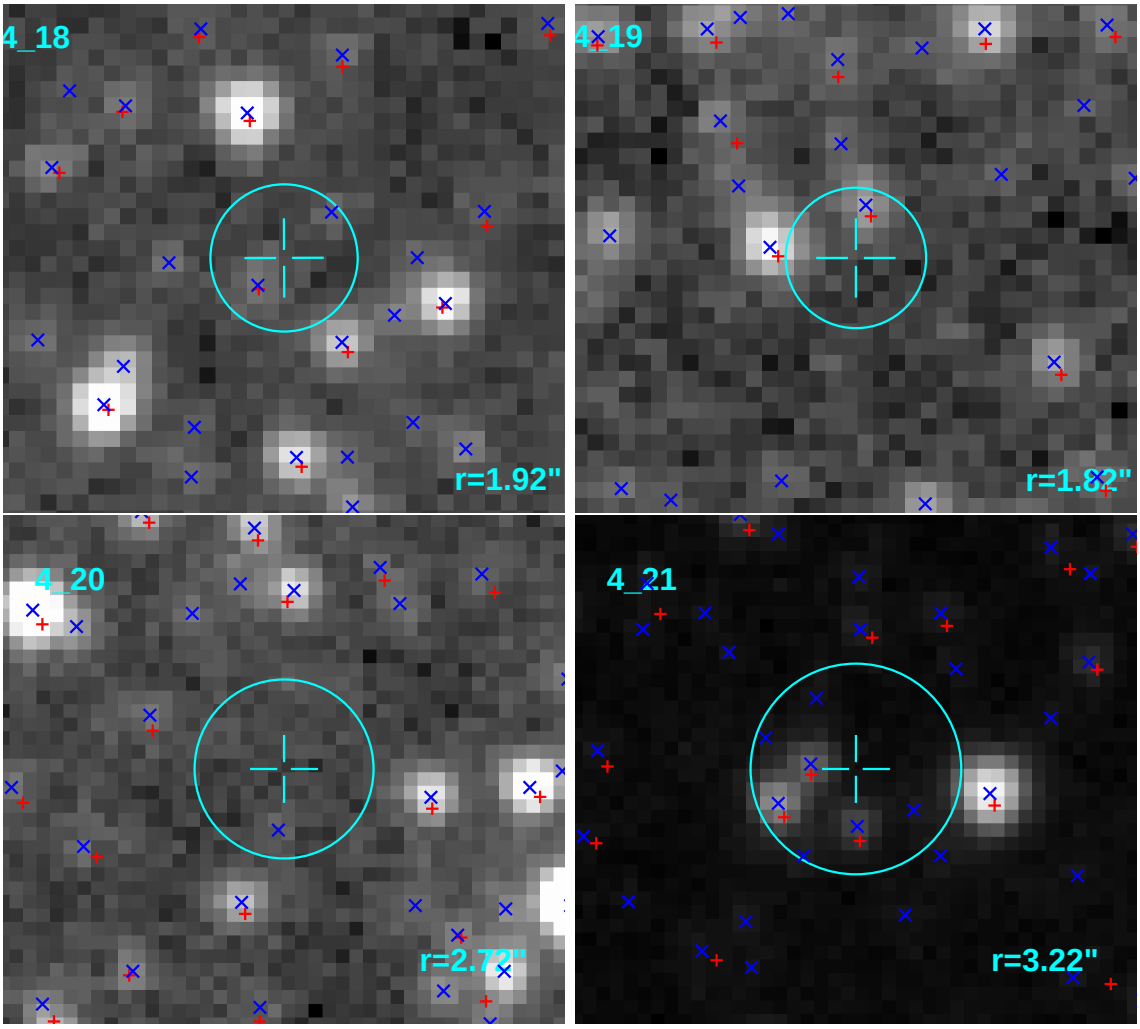
4_18
r=1.92"
4_19
r=1.82"
4_20
r=2.72"
4_21
r=3.22"

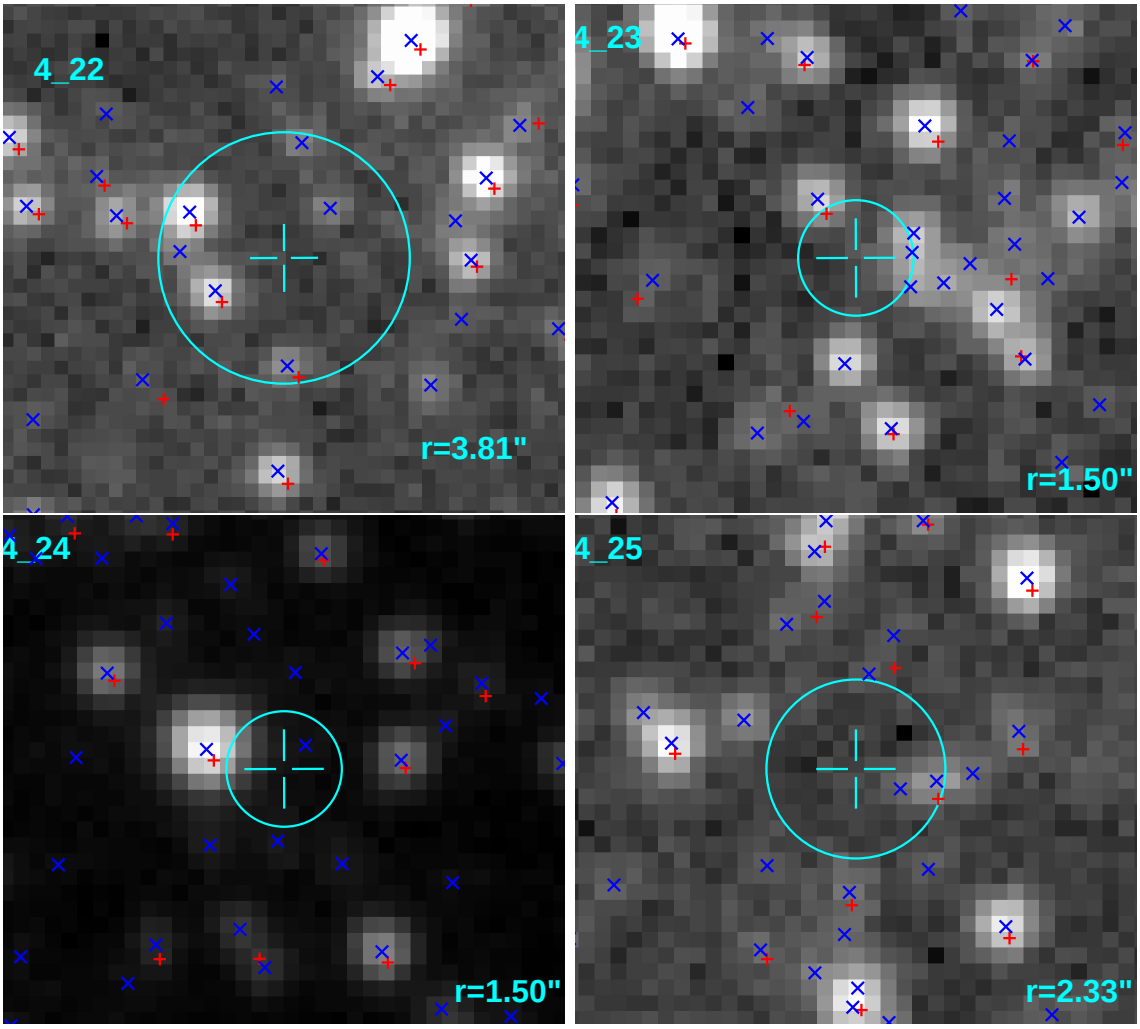
4_22
r=3.81"
4_23
r=1.50"
4_24
r=1.50"
4_25
r=2.33"

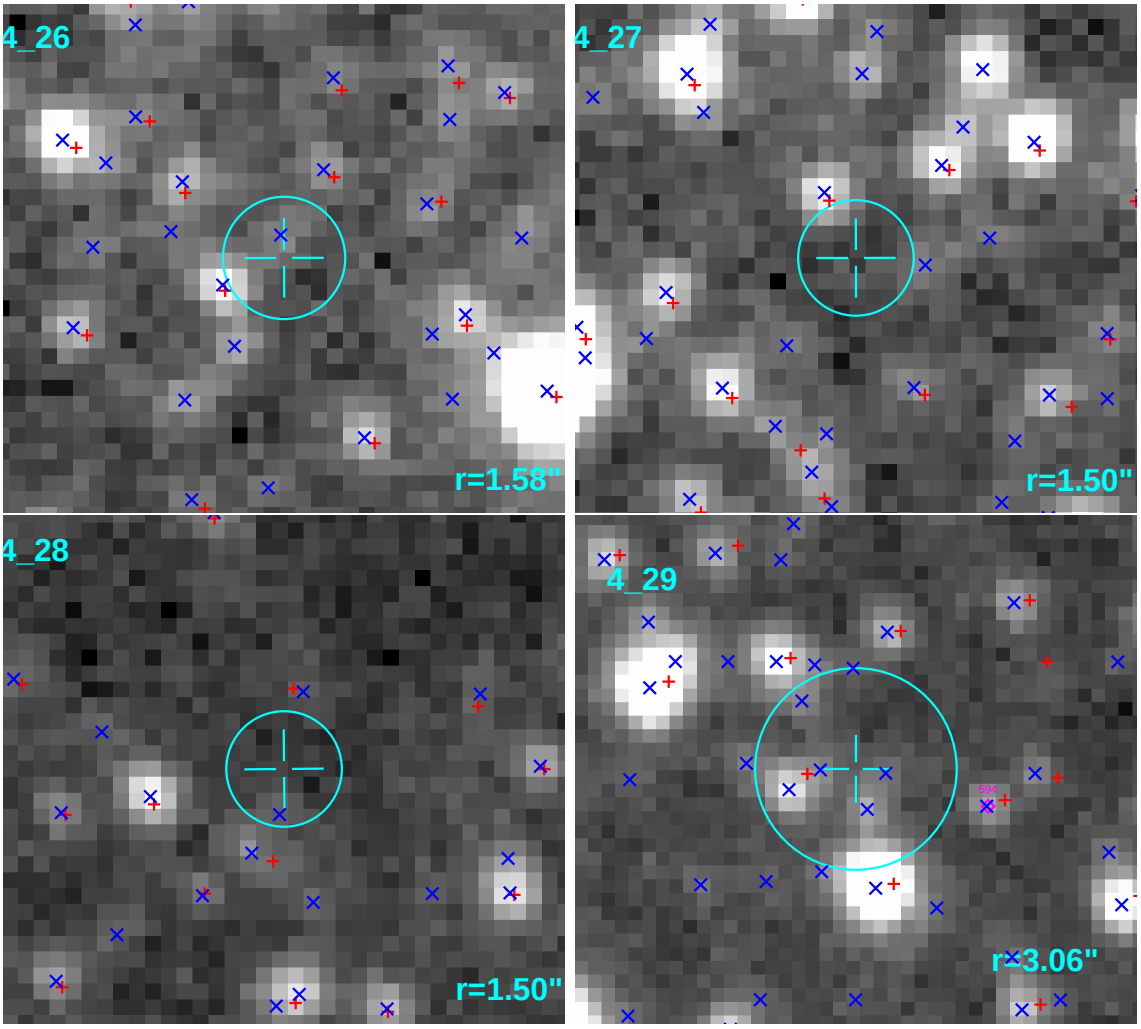
4_26
r=1.58"
4_27
r=1.50"
4_28
r=1.50"
4_29
r=3.06"

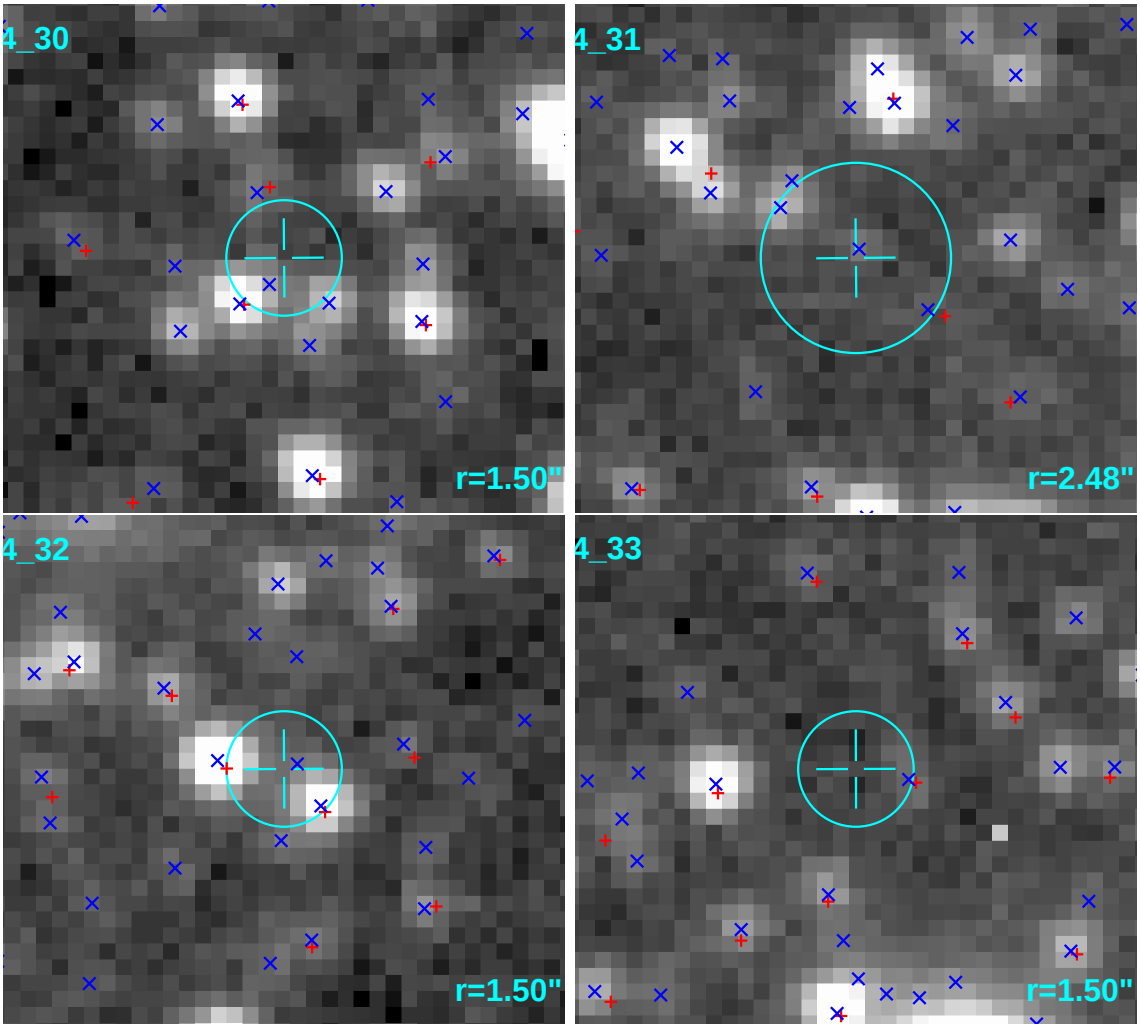
4_30
r=1.50"
4_31
r=2.48"
4_32
r=1.50"
4_33
r=1.50"

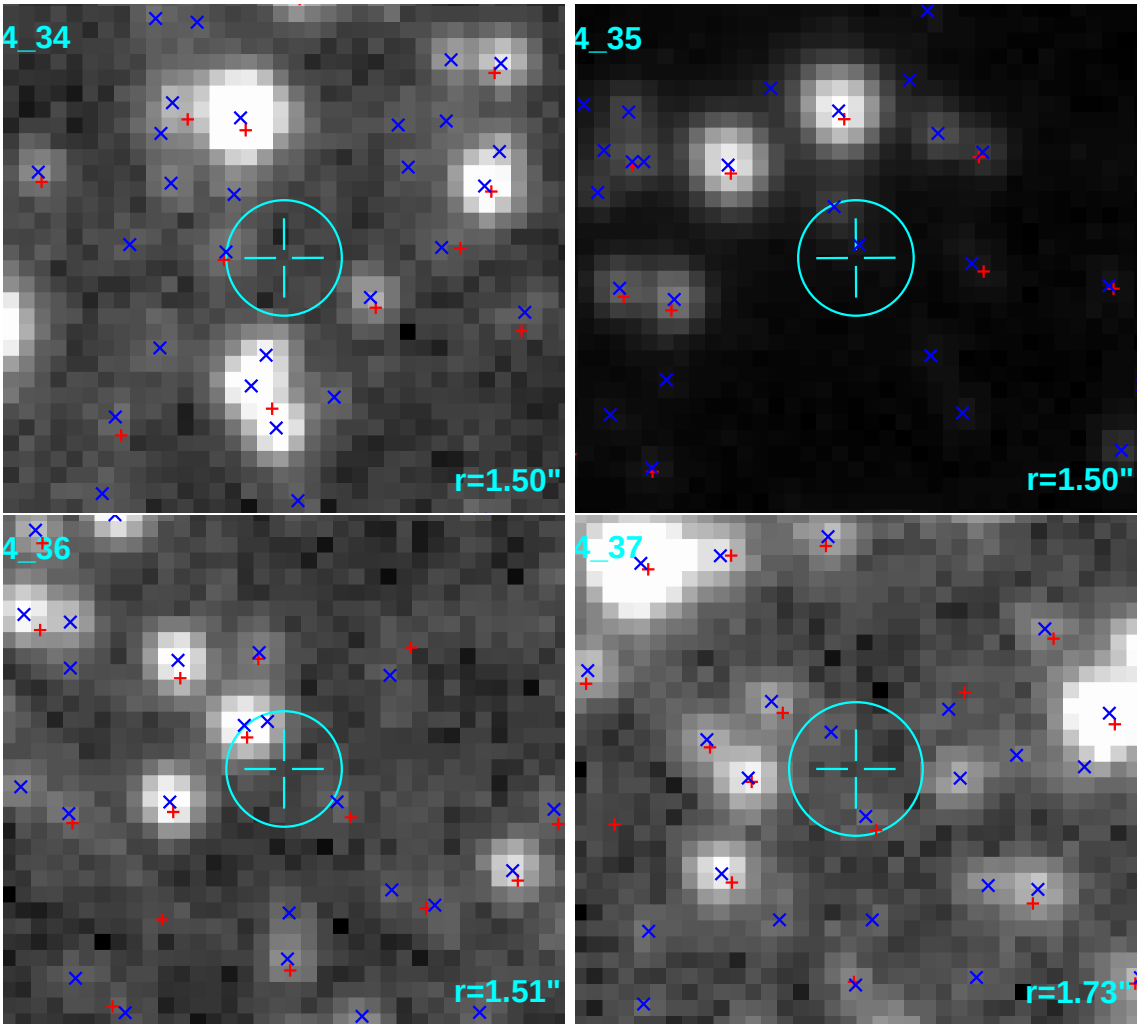
4_34
r=1.50"
4_35
r=1.50"
4_36
r=1.51"
4_37
r=1.73"

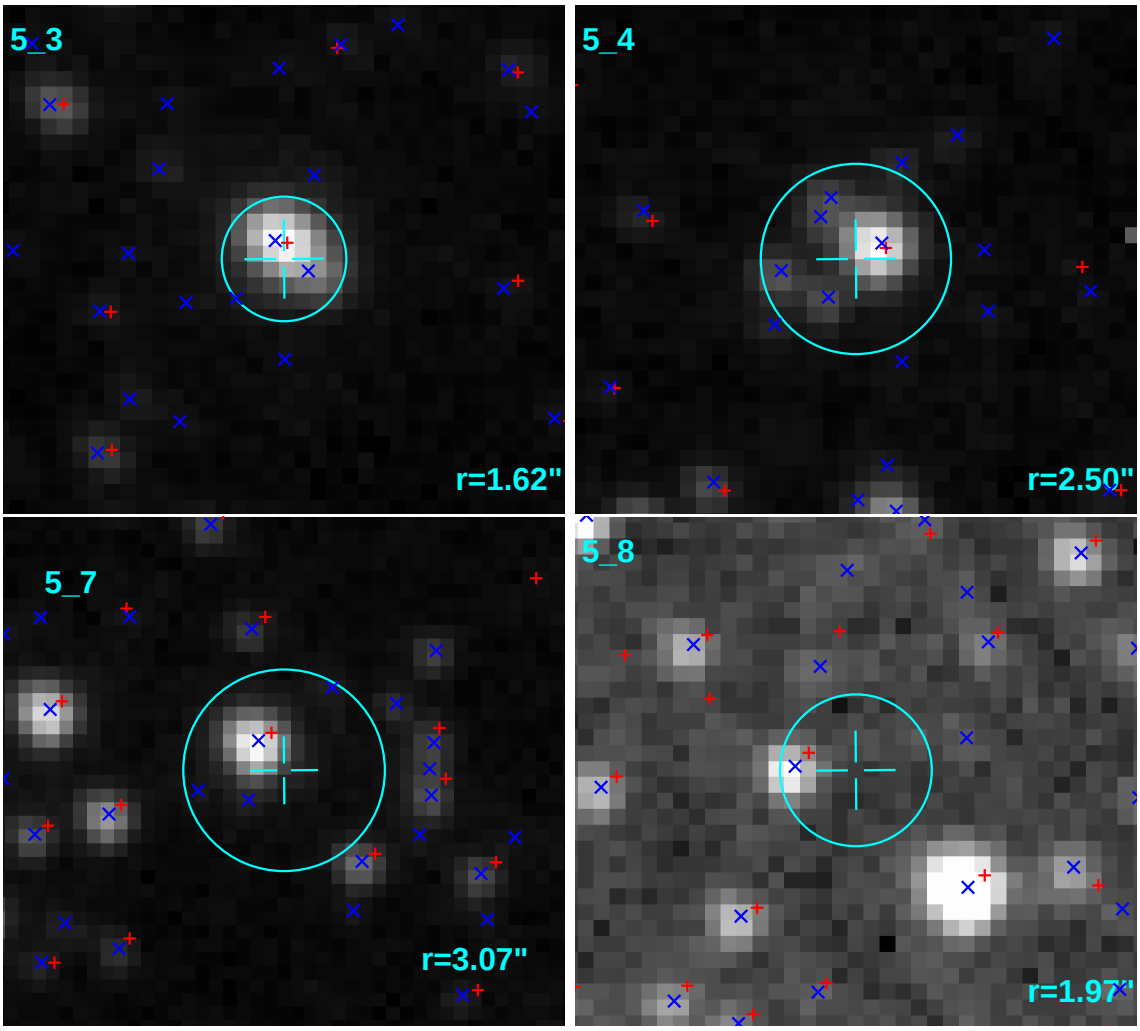

Fig. 4.— OGLE-II *I*-band images for Chandra sources in field 5. North is up and East to the right. × symbols are used for OGLE-II sources and + for MCPS sources. *This is an electronic Figure.*

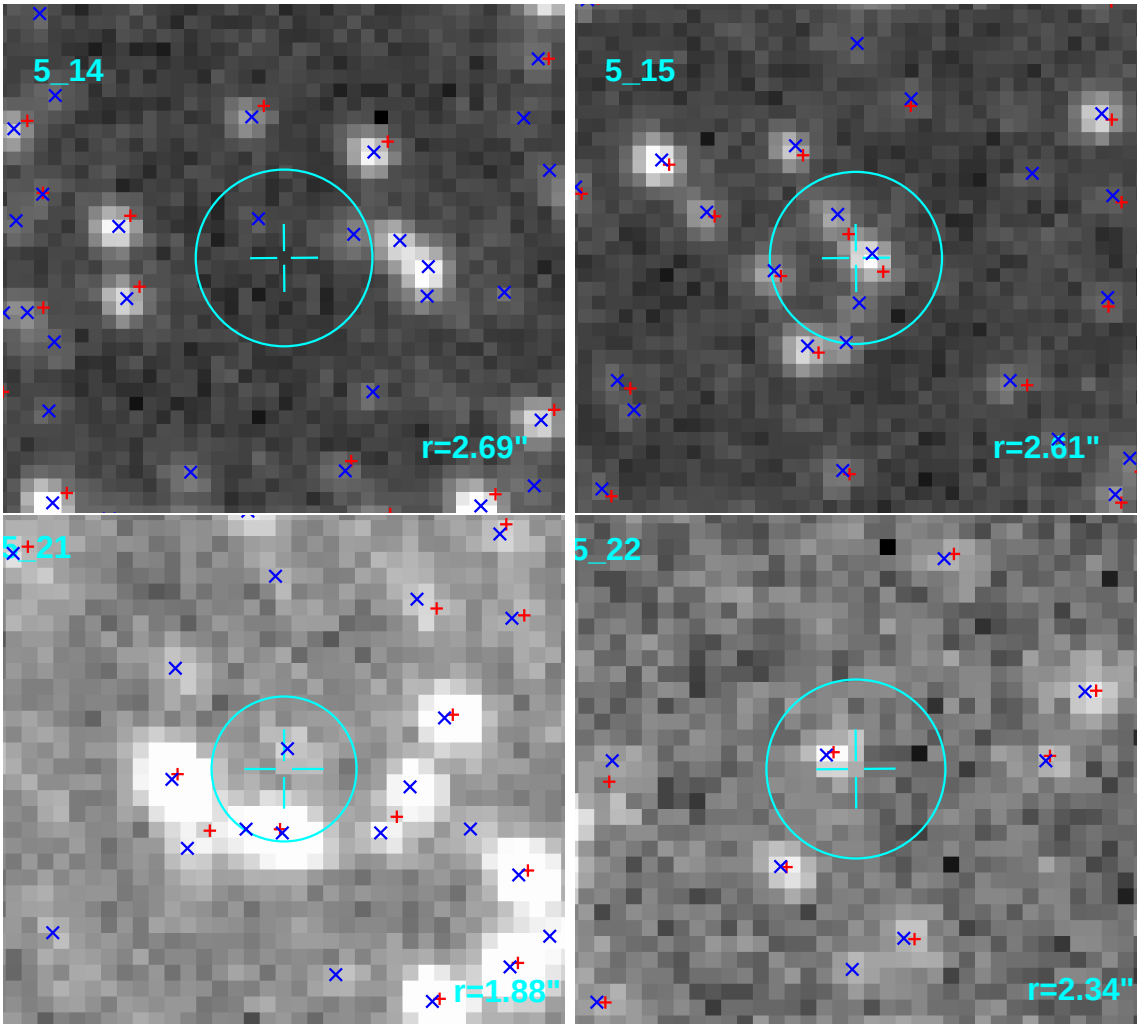
5_14
r=2.69"
5_15
r=2.61"
5_21
r=1.88"
5_22
r=2.34"

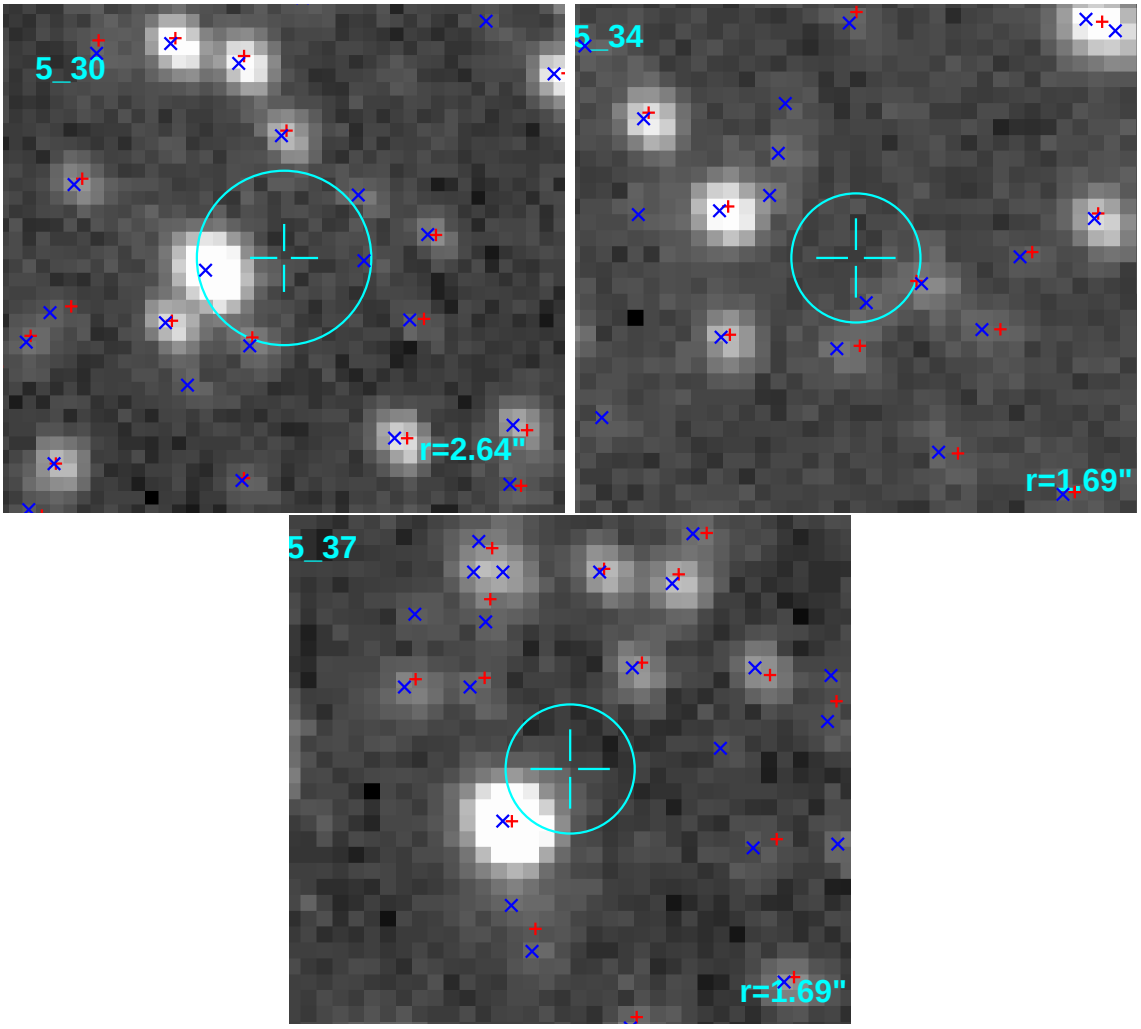
5_30
r=2.64"
5_34
r=1.69"
5_37
r=1.69"

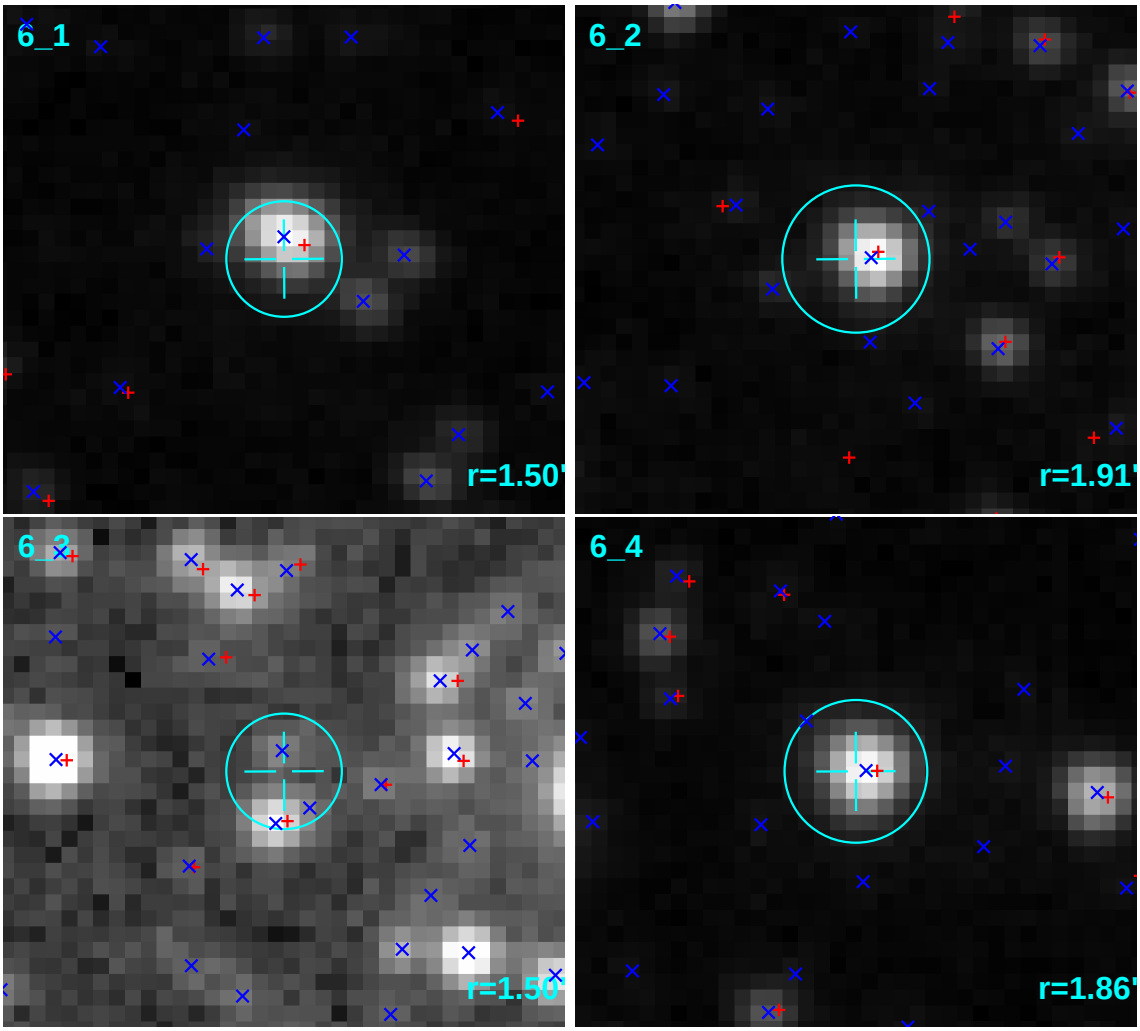

Fig. 5.— OGLE-II *I*-band images for Chandra sources in field 6. North is up and East to the right. × symbols are used for OGLE-II sources and + for MCPS sources. *This is an electronic Figure.*

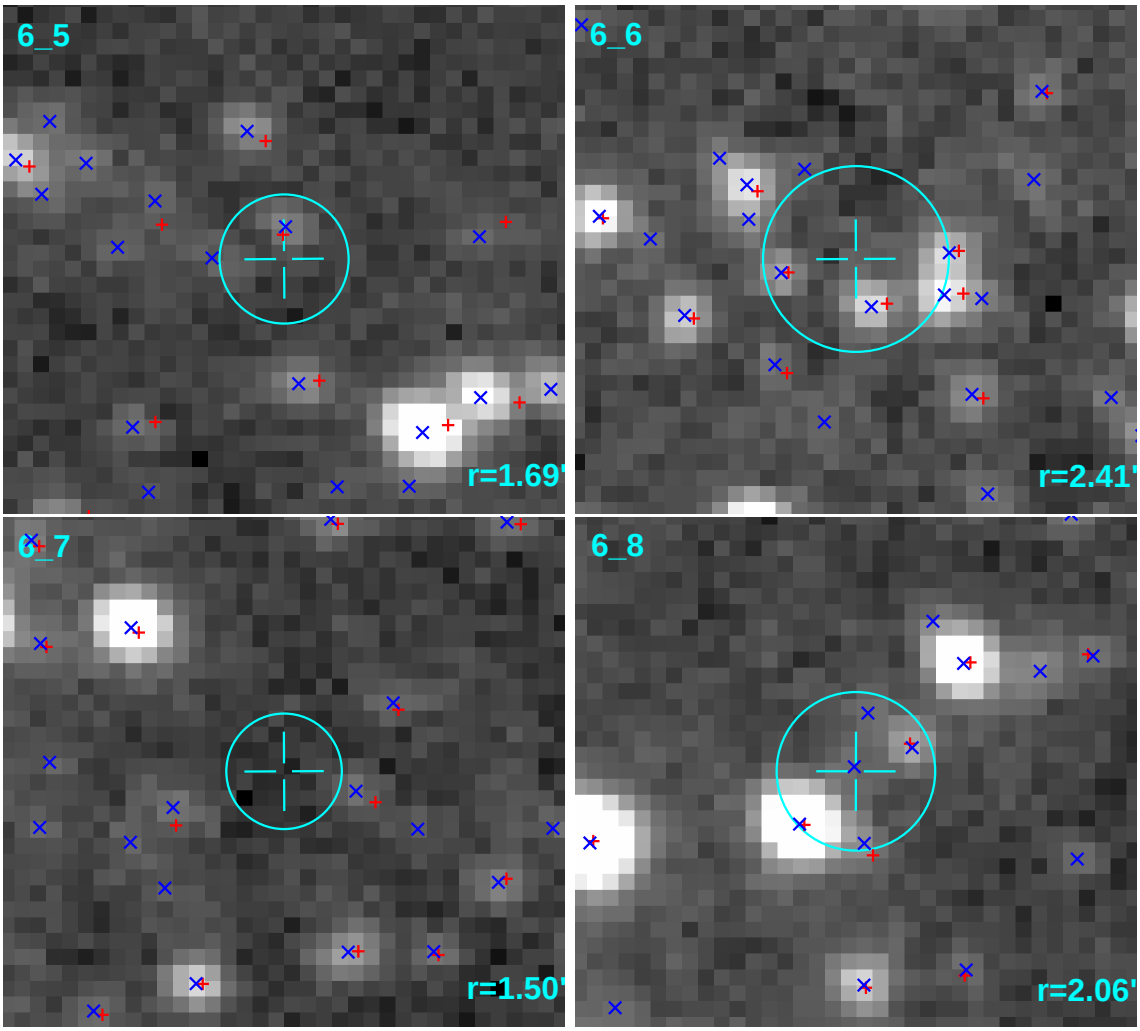
6_5
r=1.69'
6_6
r=2.41'
6_7
r=1.50'
6_8
r=2.06'

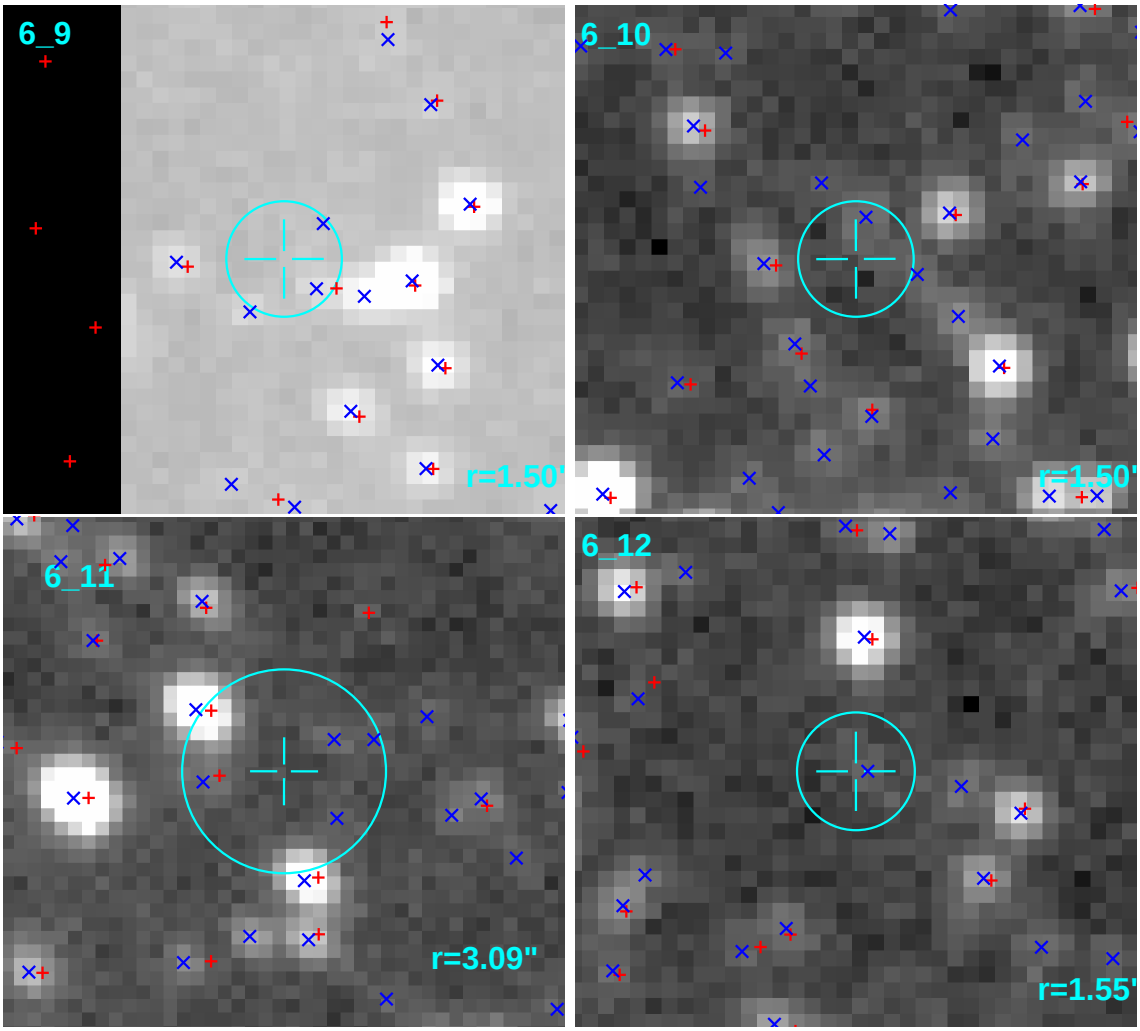
6_9
r=1.50"
6_10
r=1.50"
6_11
r=3.09"
6_12
r=1.55"

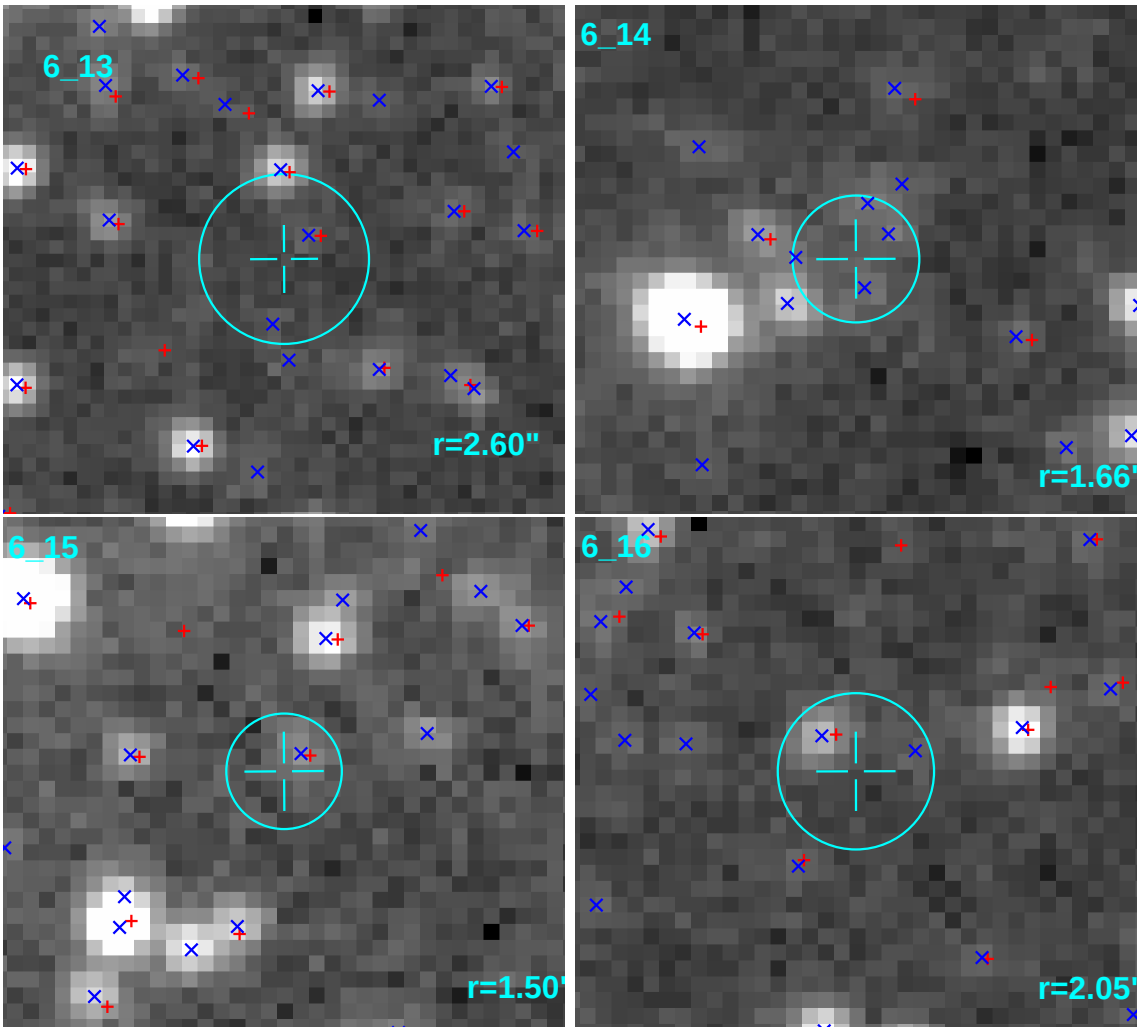
6_13
r=2.60"
6_14
r=1.66"
6_15
r=1.50"
6_16
r=2.05"

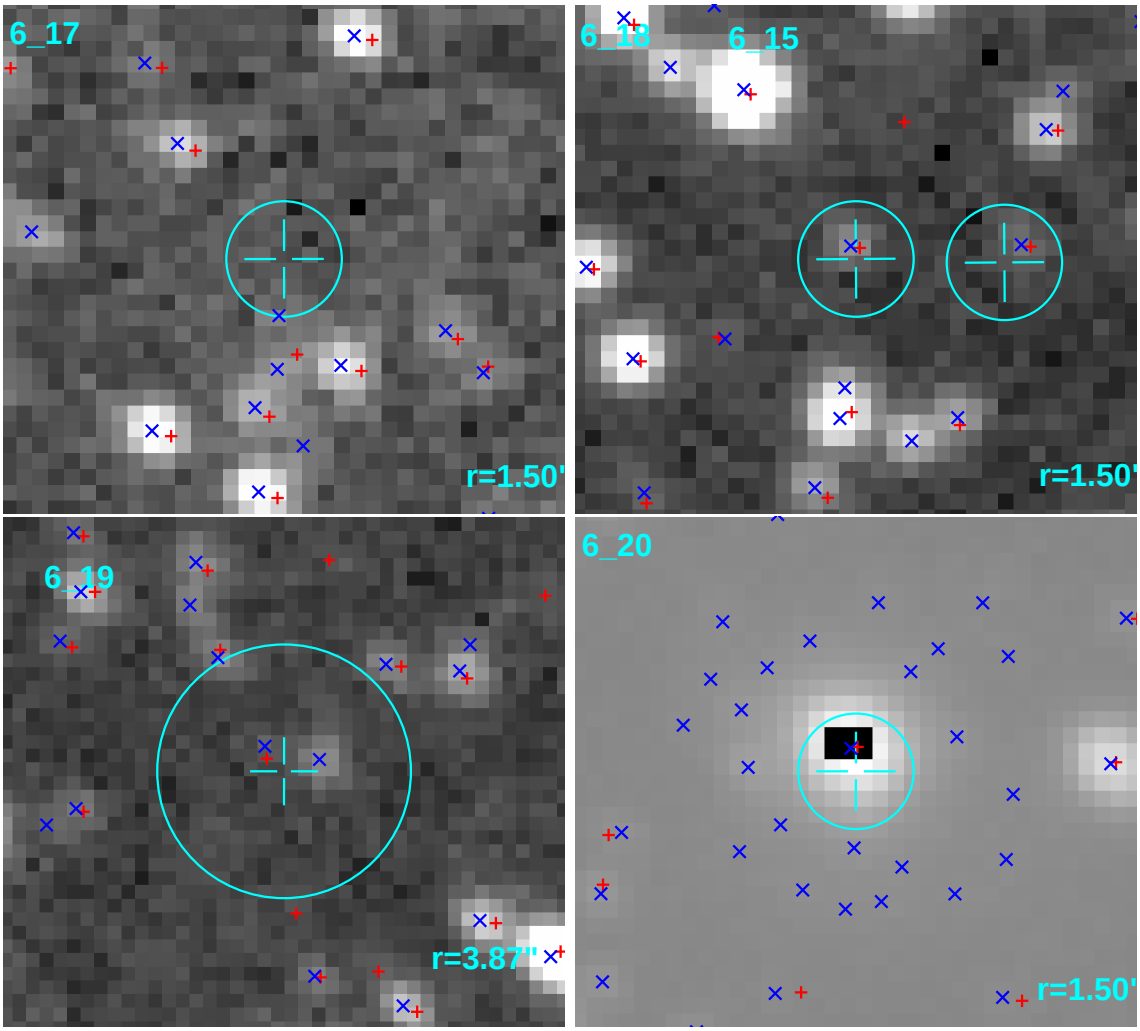
6_17
r=1.50'
6_18
6_15
r=1.50'
6_19
r=3.87"
6_20
r=1.50'

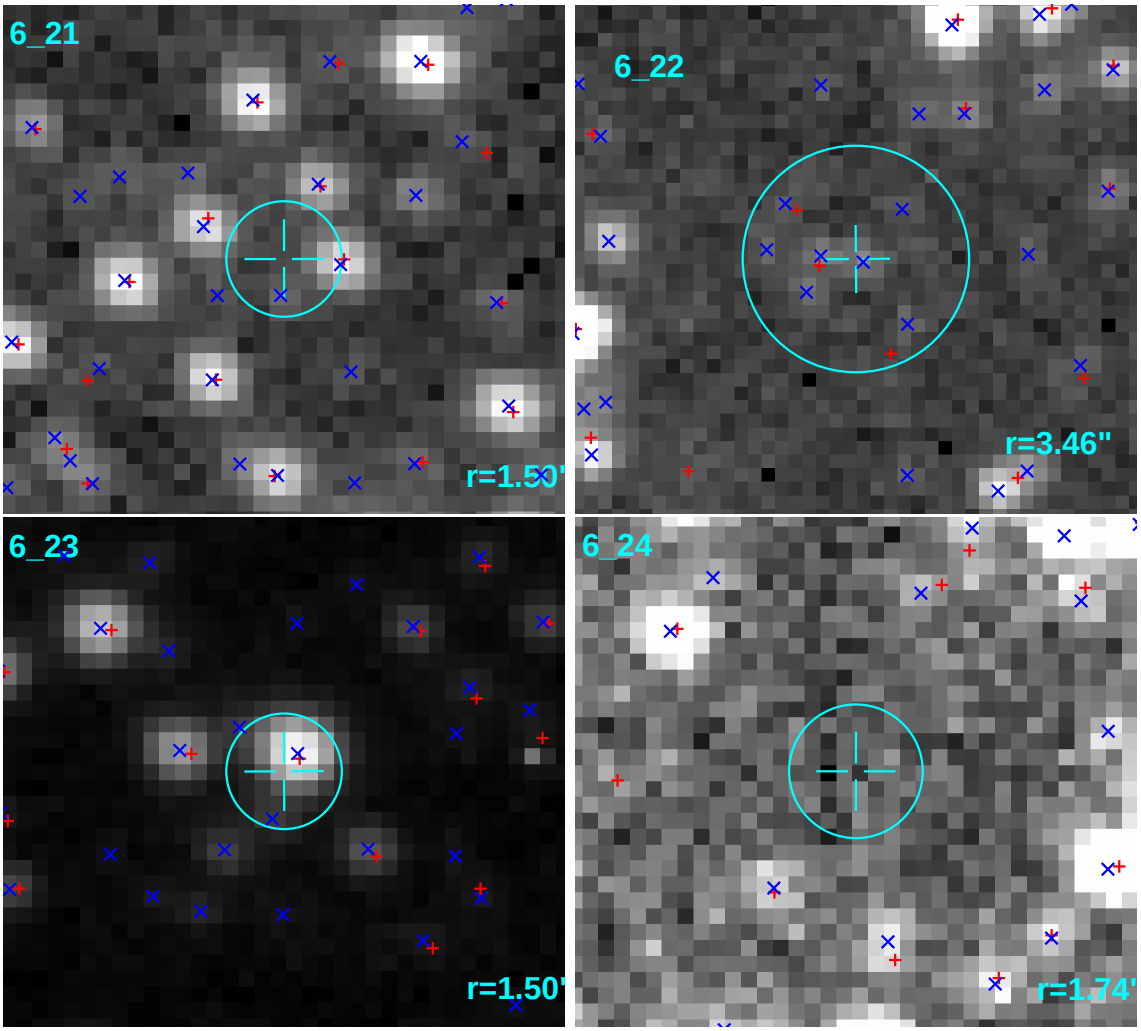
6_21
r=1.50"
6_22
r=3.46"
6_23
r=1.50"
6_24
r=1.74"

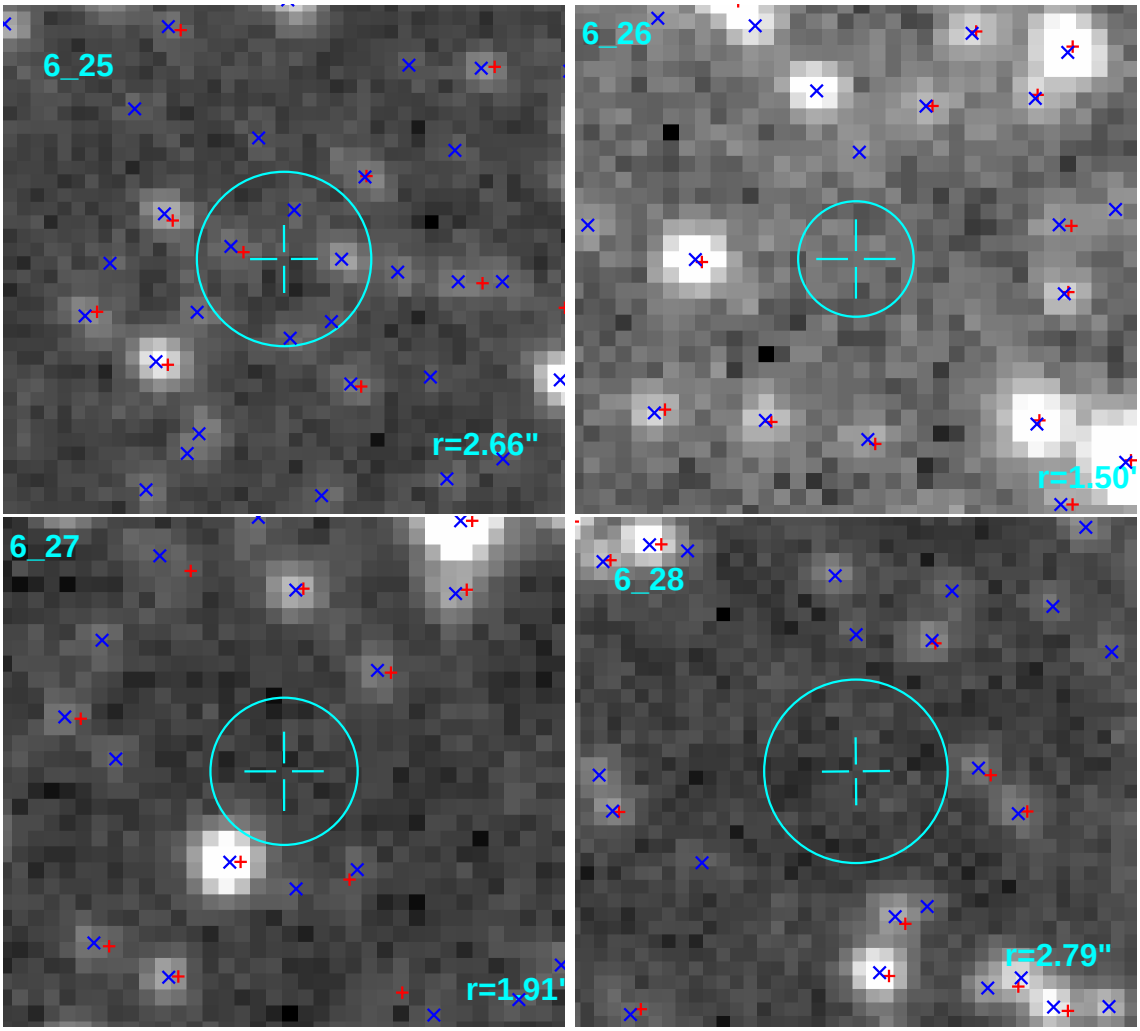
6_25
r=2.66"
6_26
r=1.50"
6_27
r=1.91"
6_28
r=2.79"

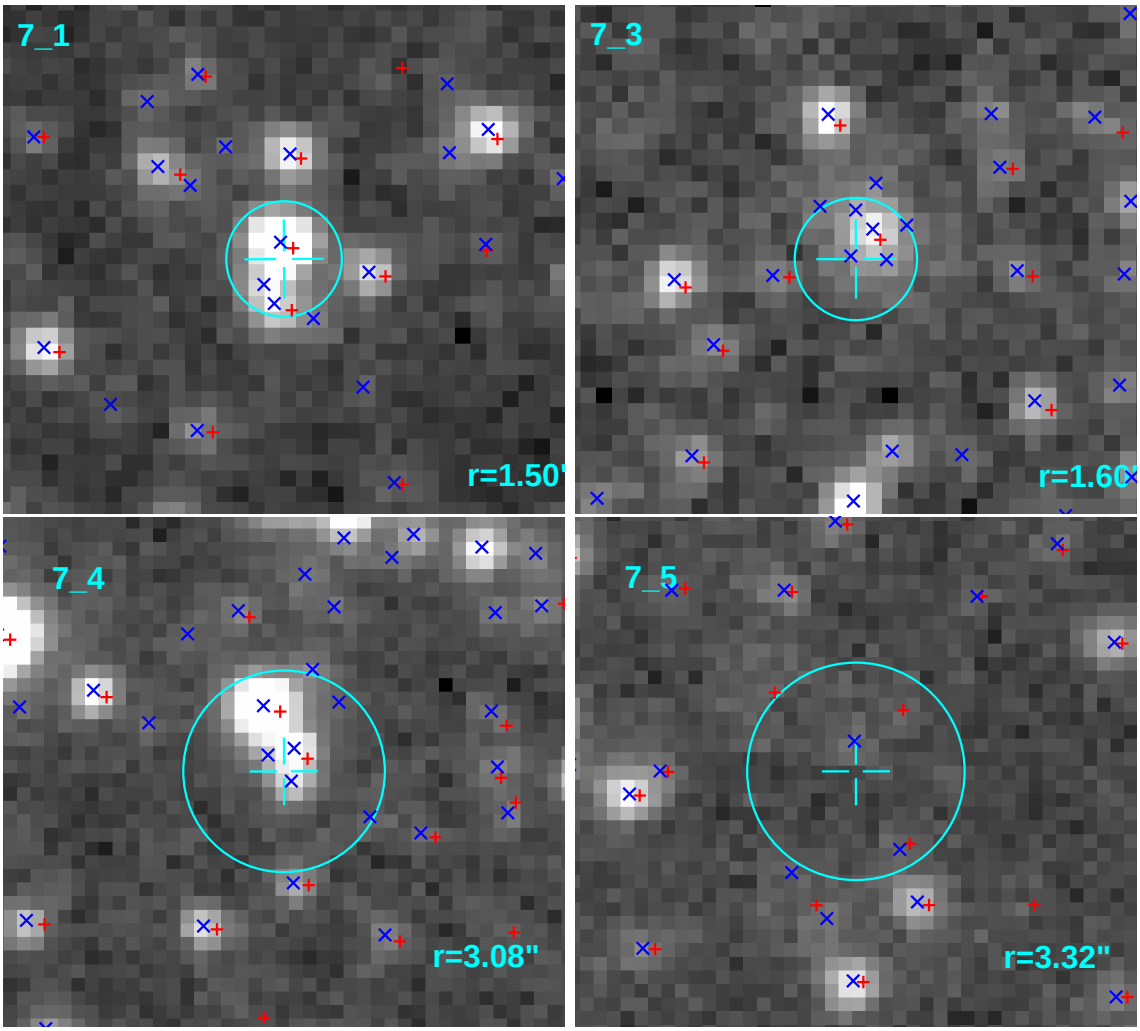

Fig. 6.— OGLE-II *I*-band images for Chandra sources in field 7. North is up and East to the right. × symbols are used for OGLE-II sources and + for MCPS sources. *This is an electronic Figure.*

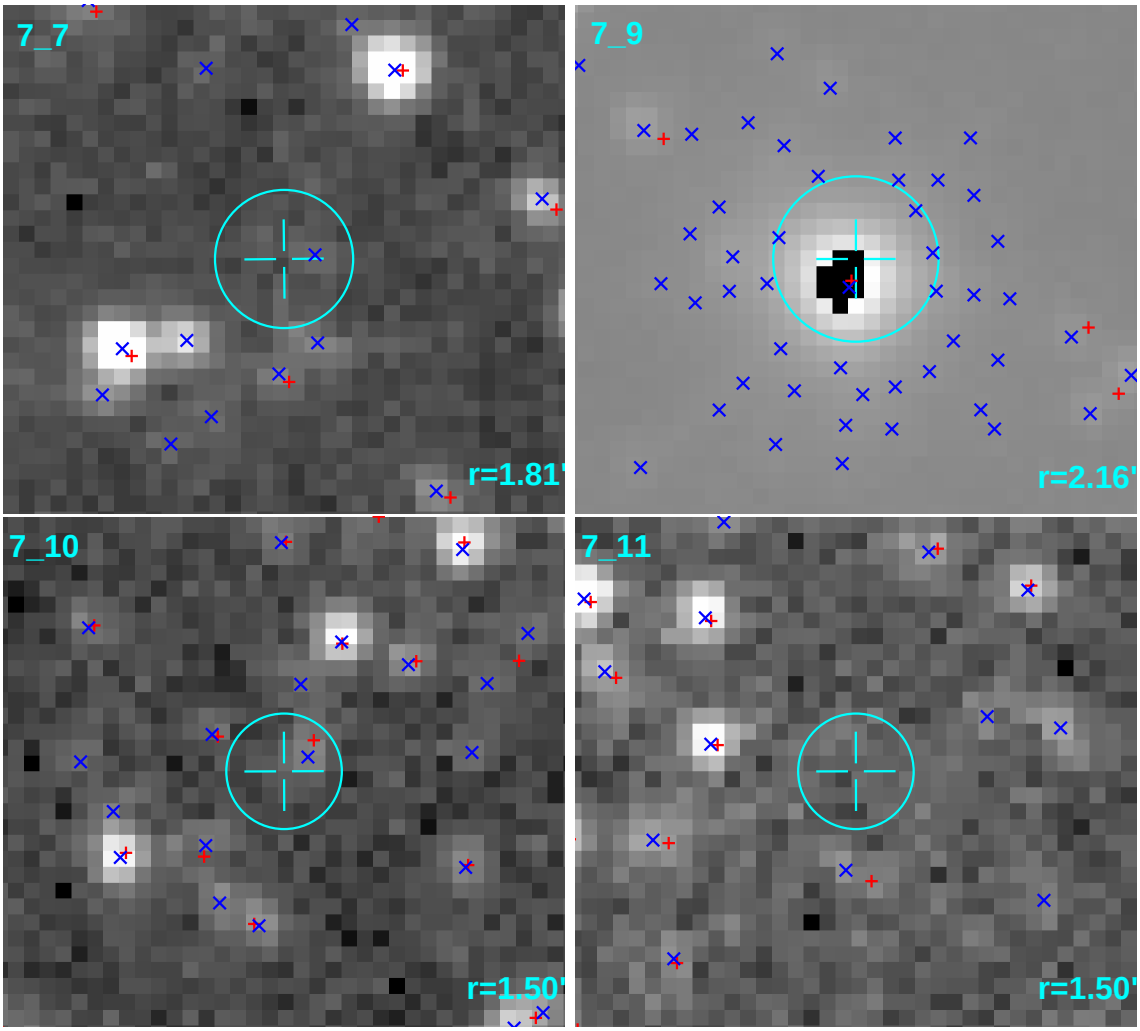
7_7
r=1.81'
7_9
r=2.16'
7_10
r=1.50'
7_11
r=1.50'

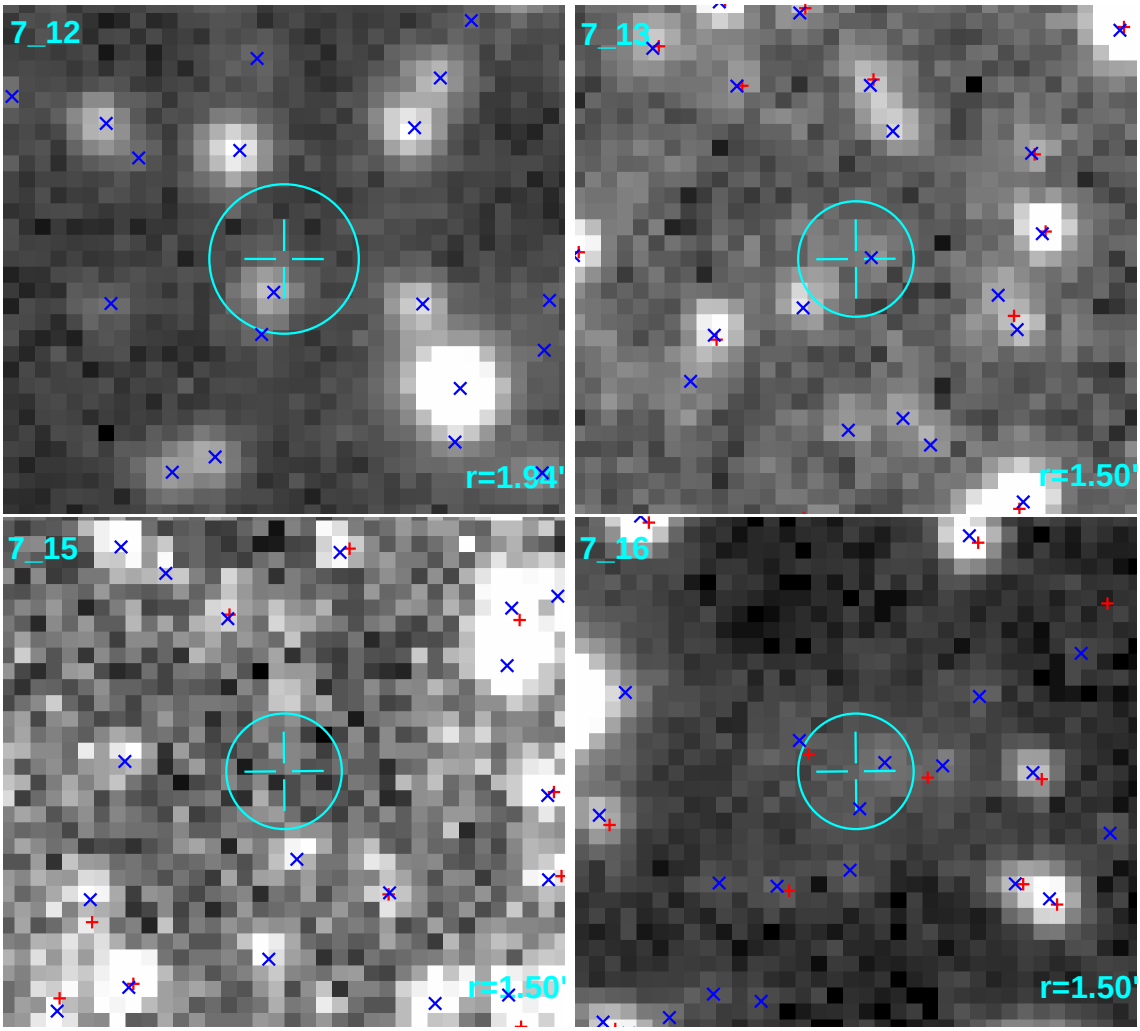
7_12
r=1.94'
7_13
r=1.50'
7_15
r=1.50'
7_16
r=1.50'

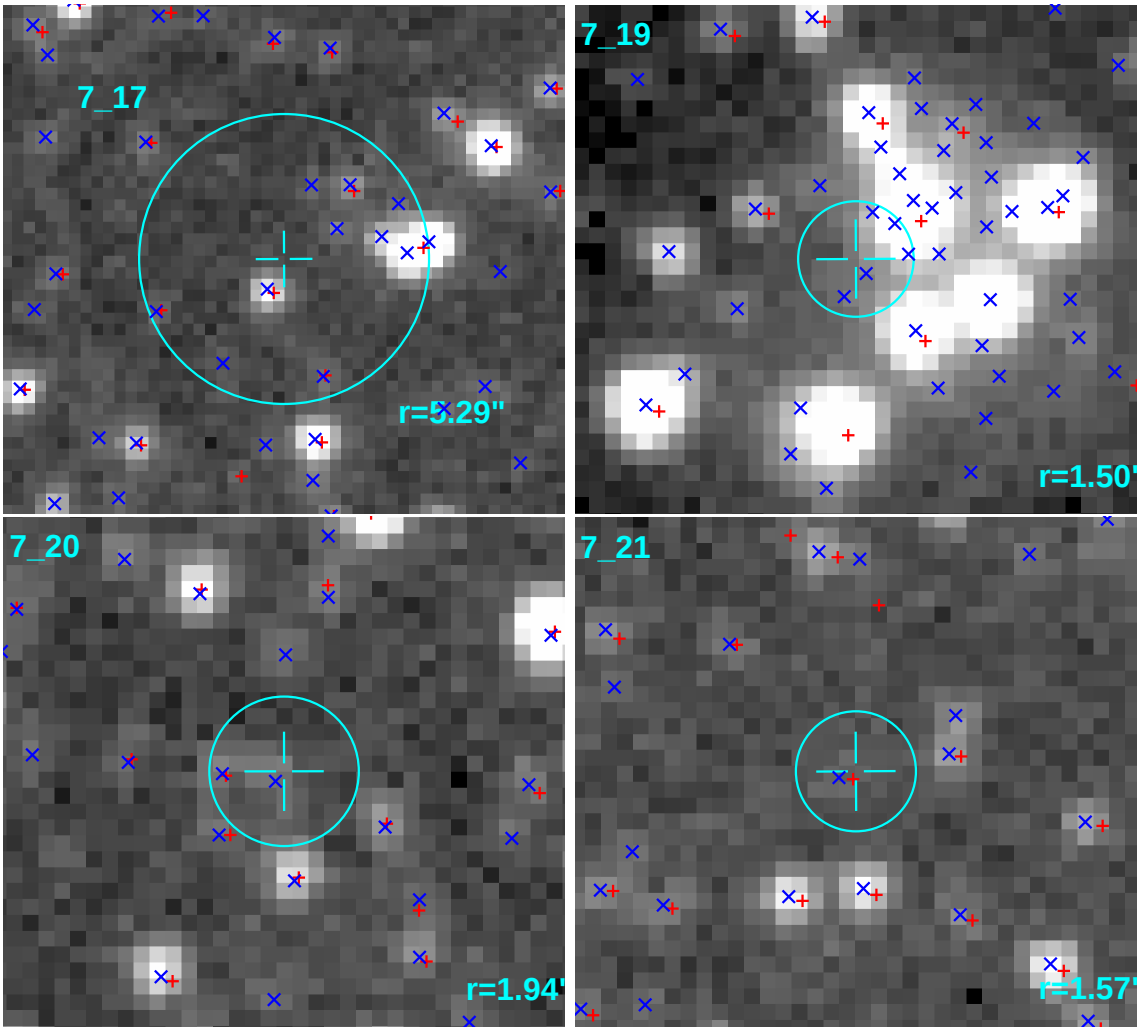
7_17
r=5.29"
7_19
r=1.50"
7_20
r=1.94"
7_21
r=1.57"

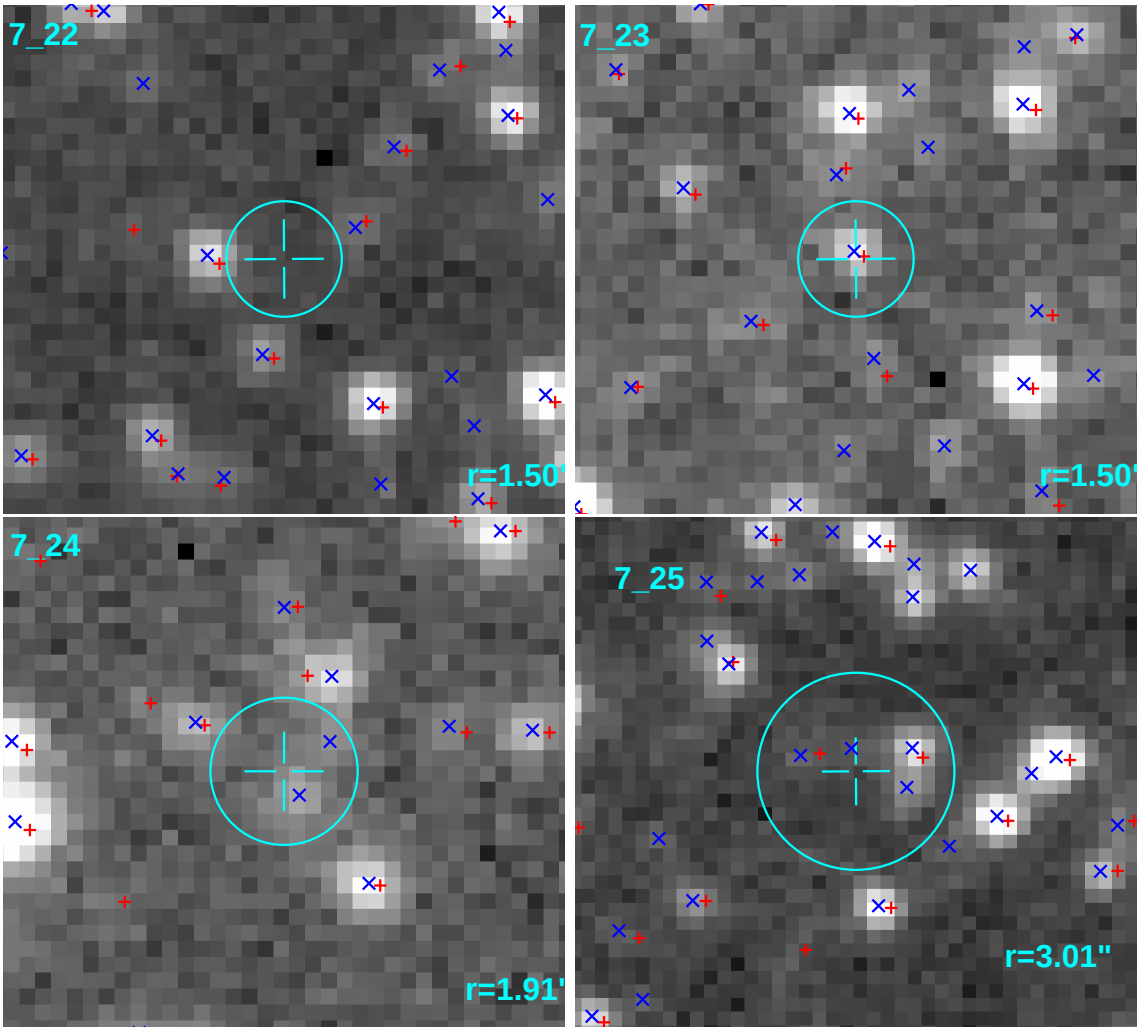
7_22
r=1.50"
7_23
r=1.50"
7_24
r=1.91"
7_25
r=3.01"

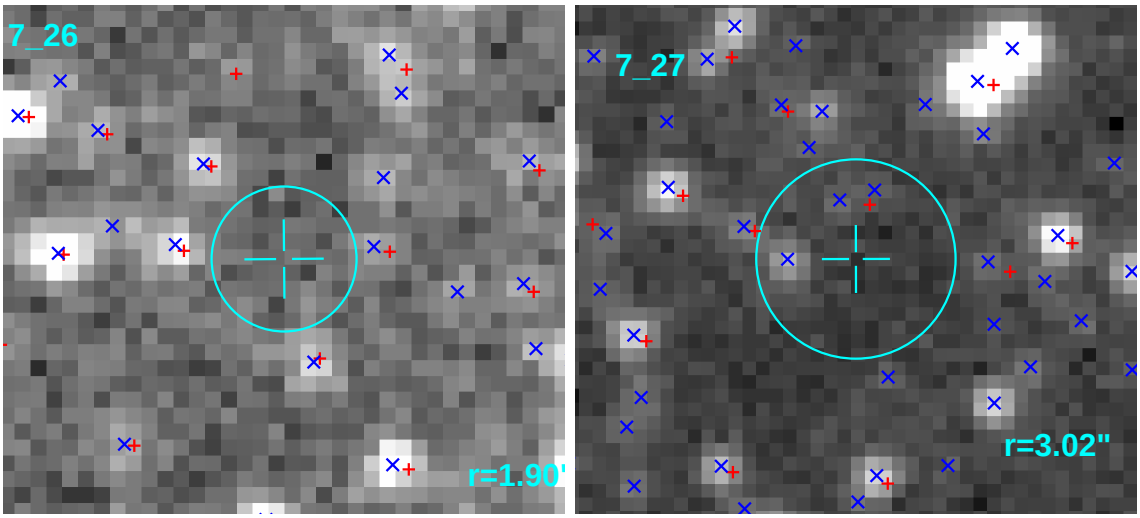
7_26
r=1.90"
7_27
r=3.02"

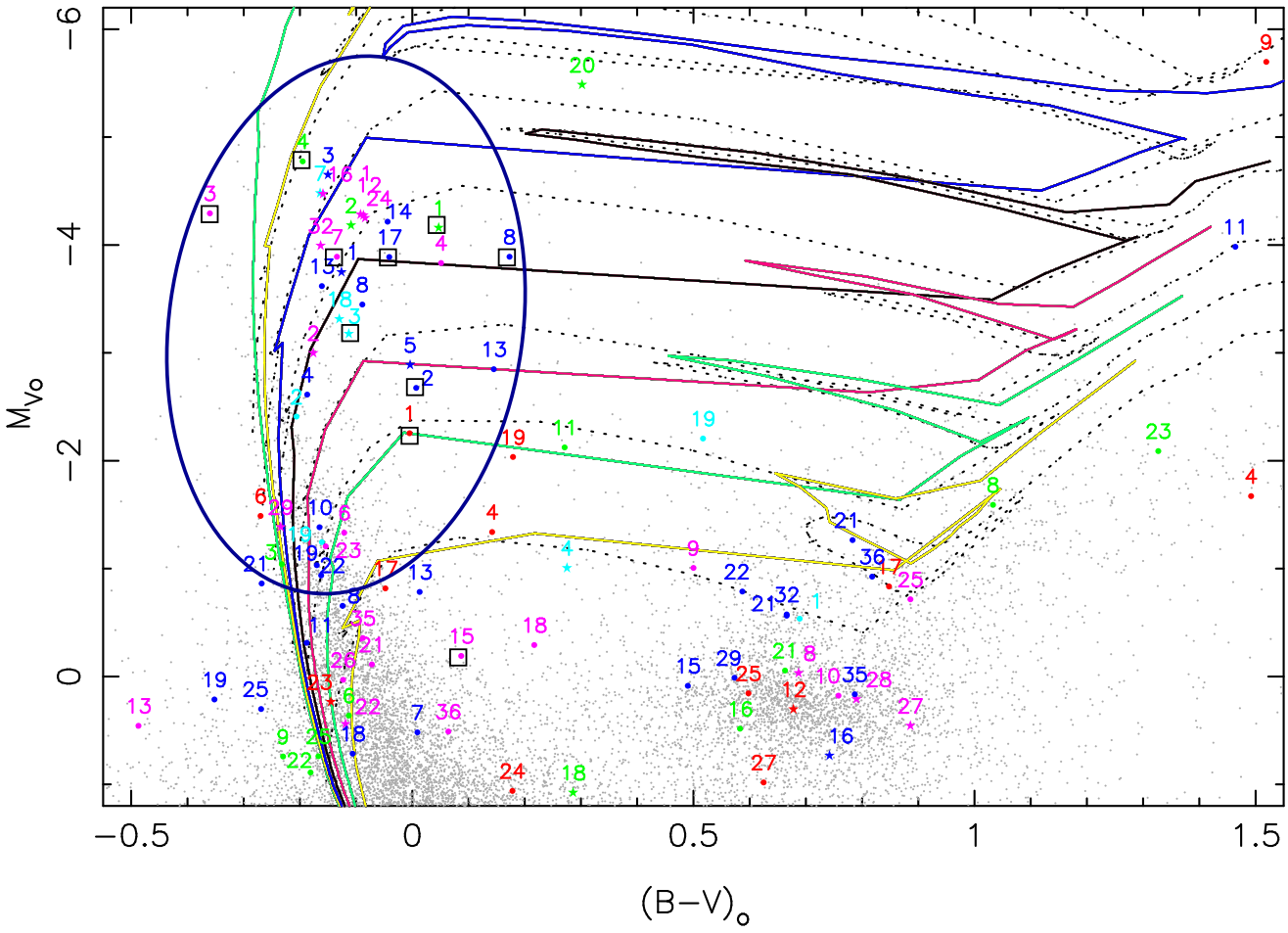

Fig. 7.— CMD of all single and the brightest of multiple matches of our *Chandra* sources. We present the M_{V_o} vs. $(B-V)_o$ CMD of all single matches (asterisk) and the brightest source of those with multiple matches (open circle) of our *Chandra* sources (which are indicated in bold face in Tables 2-6). The optical sources are color coded as, *Chandra* field 3: cyan; 4: blue; 5: magenta; 6: green; 7: red; while the OGLE-II stars that lie in our *Chandra* field 4 are indicated in gray small dots. Part of the MS, the red giant branch and the red clump loci are clearly visible. With black squares we present the 10 candidate Be stars of Mennickent et al. (2002) that we have identified as optical counterparts. Overlaid are the isochrones (solid lines) and stellar evolutionary tracks (dotted lines) from Geneva database (Lejeune & Schaerer 2001) for ages of 8.7 Myr, 15.5 Myr, 27.5 Myr, 49.0 Myr, 87.1 Myr, 154.9 Myr and 275.4 Myr and initial stellar masses of 12 $M_\odot$, 9 $M_\odot$, 7 $M_\odot$, 5 $M_\odot$, 4 $M_\odot$ and 3 $M_\odot$ stars (from top to bottom).

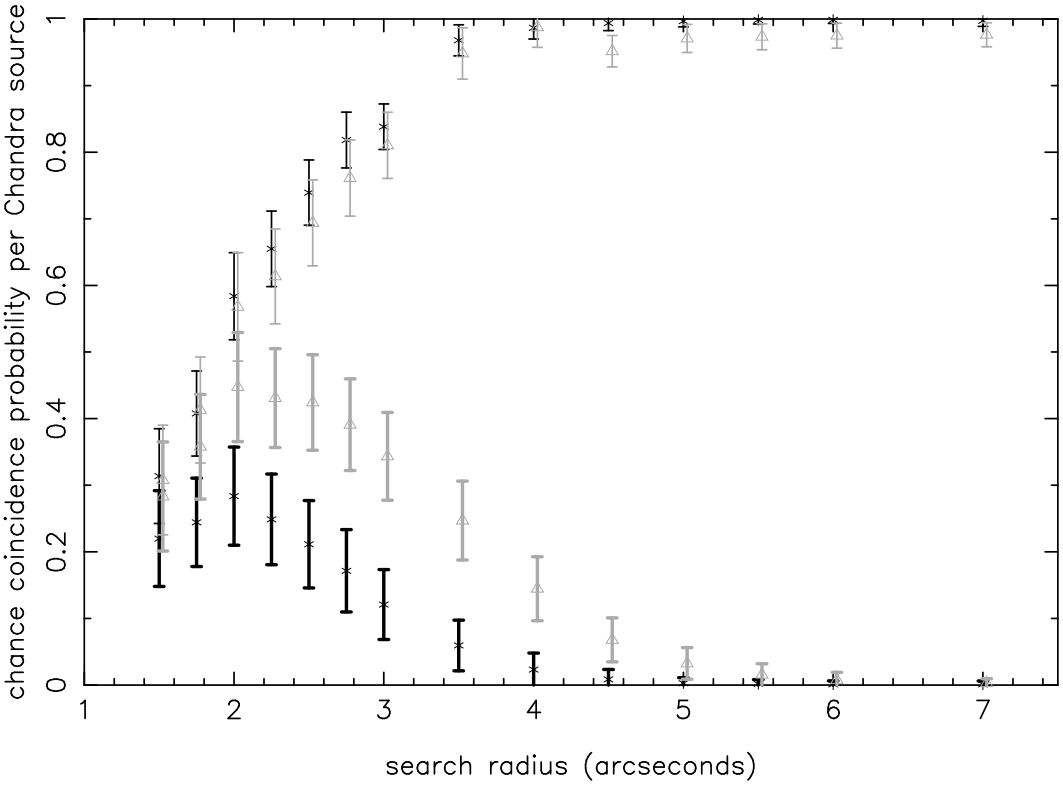

Fig. 8.— Normalized chance coincidence probability (matches per source) as a function of the search radius around the *Chandra* sources. The estimated chance coincidence probability for each X-ray source is shown in black (asterisks) for the OGLE-II data and in gray (open triangles) for data from the MCPS catalog (for clarity a small offset in the MCPS data has been applied). The thick lines represent the estimated probability of detecting by chance one source for a single match, while the thin lines indicate the probability of detecting one or more spurious matches for a source with one or more associations (i.e. total number of matches).

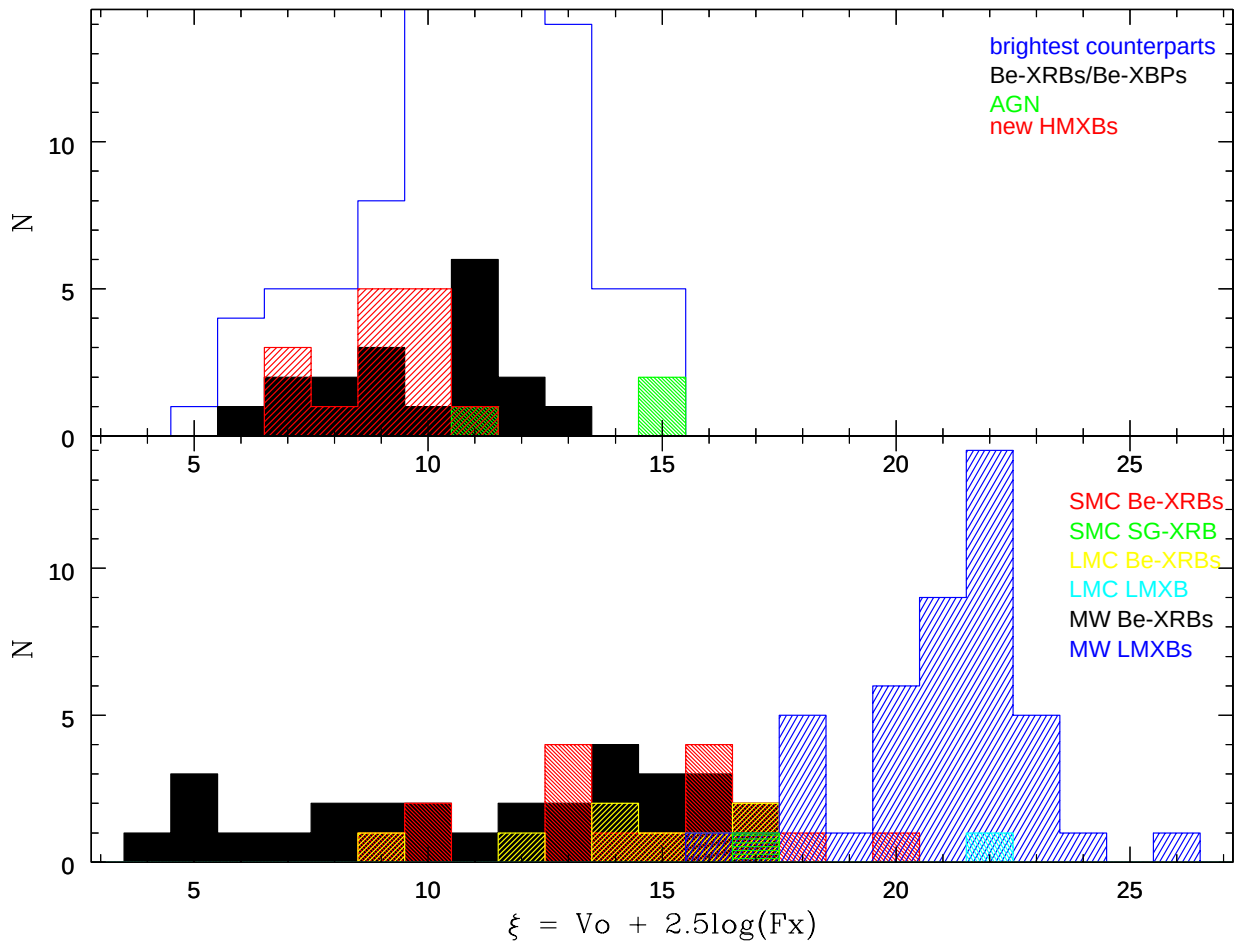

Fig. 9.— Histogram of ξ parameter values. **(a)** *Lower panel*: MCs Be-XRBs (SMC in red; LMC in yellow) and SMC SG-XRBs (in green) are taken from Liu et al. (2005). Milky Way Be-XRBs are taken from Liu et al. (2006; black), while the data for LMXBs (Galactic in blue; LMC in cyan) are taken from Liu et al. (2007). **(b)** *Upper panel*: The ξ values for the brightest optical counterparts of all *Chandra* sources (indicated in bold face in Tables 2-6) are shown with an open histogram (in blue). Identified AGN (shown in green) and known Be-XRBs and Be-XBPs (shown in black) are also included. New HMXBs (including new candidate Be-XRBs) from this work are over-plotted (shown in red). More details are given in §8.1.

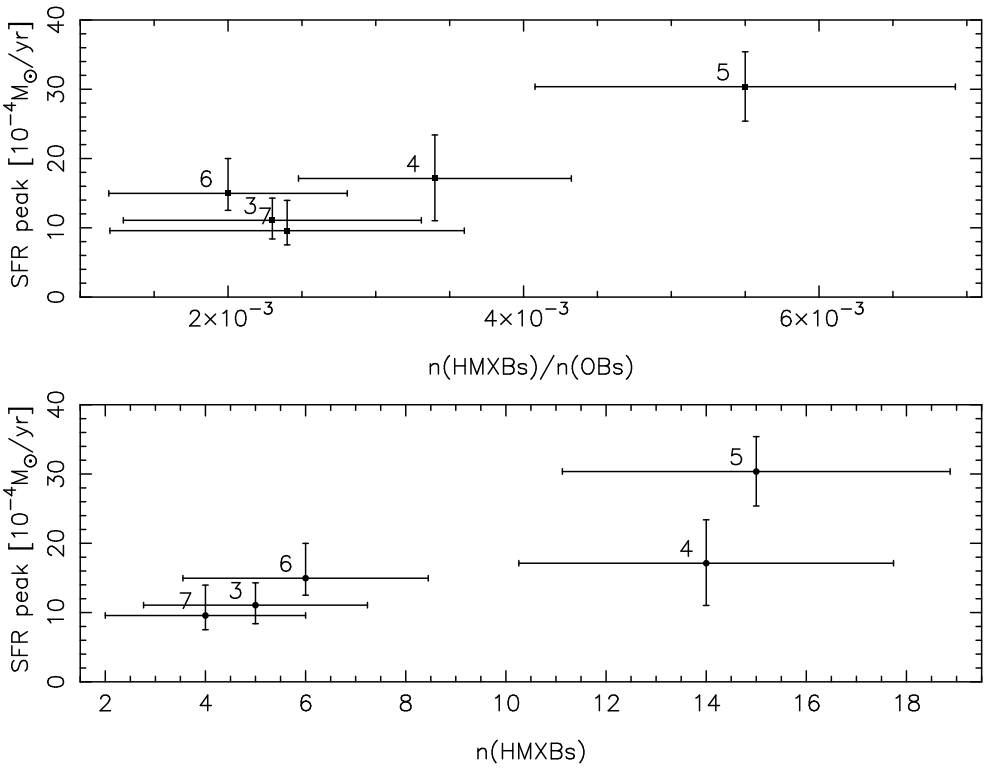

Fig. 10.— **(a)** *Lower panel*: The star-formation rate at the age of $\sim$ 42 Myr versus the number of HMXBs in each *Chandra* field. **(b)** *Upper panel*: The star-formation rate at the age of $\sim$ 42 Myr versus the ratio of the number of HMXBs to the number of OB spectral type stars in each field. The error bars in the x-axis were derived assuming Poisson statistics. In the y-axis error bars indicate lower and upper limits of the mean SF rate in each *Chandra* field.